MECHANICAL SUPPORT DESIGN OF ANALYZER FOR A DIFFRACTION ENHANCED X-RAY IMAGING (DEI) SYSTEM

A Thesis

Submitted to the College of Graduate Studies and Research

in Partial Fulfillment of the Requirements

for the Degree of

Master of Science

in the

Division of Biomedical Engineering

University of Saskatchewan

Saskatoon, Saskatchewan

Canada

By

Nagarajan Alagarsamy

PERMISSION TO USE

In presenting this thesis in partial fulfillment of the requirements for a Master's degree from the University of Saskatchewan, the author has agreed that the Libraries of this University may make it freely available for inspection. The author further agrees that permission for copying of this thesis in any manner, in whole or in part, for scholarly purposes may be granted by the professors who supervised this thesis work or, in their absence, by the Head of the Division or the Dean of the College in which this thesis work was done. It is understood that any copying or publication or use of this thesis or parts thereof for financial gain shall not be allowed without the author's written permission. It is also understood that due recognition shall be given to the author and to the University of Saskatchewan in any scholarly use which may be made of any material in this thesis.

Requests for permission to copy or to make other use of material in this thesis in whole or part should be addressed to:

Head of the Division of Biomedical Engineering

University of Saskatchewan

Saskatoon, Saskatchewan, Canada S7N 5A9

ABSTRACT

Diffraction Enhanced X-ray Imaging (DEI) uses synchrotron X-ray beams prepared and analyzed by perfect single crystals to achieve imaging contrast from a number of phenomena taking place in an object under investigation. The crystals used in DEI for imaging requires high precision positioning due to a narrow rocking curve. Typically, the angular precision required should be on the order of tens of nanoradians.

One of the problems associated with DEI is the inability to control, set, and fix the angle of the analyzer crystal in relation to the beam exiting the monochromator in the system. This angle is used to interpret the images acquired with an object present and the usual approach is to determine where the image was taken "after the fact". If the angle is not correct, then the image is wasted and has to be retaken. If time or dose is not an issue, then retaking the image is not a serious problem. However, since the technique is to be developed for live animal or eventually human imaging, the lost images are no longer acceptable from either X-ray exposure or time perspectives.

Therefore, a mechanical positioning system for the DEI system should be developed that allows a precise setting and measurement of the analyzer crystal angles. In this thesis, the fundamental principles of the DEI method, the DEI system at the National Synchrotron Light Source (NSLS) and the sensitivity of the DEI system to vibration and temperature has been briefly studied to gain a better understanding of the problem. The DEI design at the NSLS was analyzed using finite element analysis software (ANSYS) to determine the defects in the current design which were making the system dimensionally unstable. Using the results of this analysis, the new analyzer support was designed aiming to eliminate the problems with the current design. The new design is much stiffer with the natural frequency spectrum raised about eight times.

This new design will improve the performance of the system at the National Synchrotron Light Source (NSLS) of Brookhaven National Laboratory, New York, USA and should assist in the

development of a new DEI system for the Bio-Medical Imaging and Therapy (BMIT) beamline at the Canadian Light Source (CLS), Saskatoon, CANADA.

ACKNOWLEDGEMENTS

Knowledge cannot be effectively pursued or ascertained by individuals operating in a relational vacuum. Rather, it is a communal process that is profoundly impacted by those around us. Thus, this research has been molded and influenced by many individuals and organizations. It is here that I attempt to recognize their contribution and express my deepest gratitude.

The singular individual who has had the most profound impact on this work is one of my supervisors, Professor Dean Chapman. He not only provided extensive insight and wisdom for this project, but helped in many other ways. He extended freedom for me to pursue the projects that most interested me. Prof. Chapman sacrificed some of his funding to provide me a research assistantship and equipment when I needed it most, and attend many professional conferences. He has invested substantial time – over 20% of his office hours in these two years – in mentoring me and helping me grow as an effective researcher and an engineer. I have really enjoyed the moments I worked with him. I am deeply grateful for his influence on this work and my life. Once again I would like to express my greatest gratitude and thanks to Prof. Chapman, for being such a supporting mentor to me. I would like to thank my other supervisor, Dr. Walerian Szyszkowski, for his guidance, insight and near-infinite patience. As my advisor he gave a challenging and rewarding project to do, and taught me a lot of the nuances of mechanical engineering that aren't found in a textbook and how to look beyond the obvious results for the real essence of a problem. I would like to thank him for teaching me the courses related to this research through an independent study. Without his help I would not have understood mechanics and finite element methods nearly as well as I do today. I am really blessed to have two great minds as my supervisors.

I would also like to thank Dr. Christopher Parham and Dr. Zhong Zhong for giving me the details of the DEI analyzer assembly at the NSLS. I would like to thank the Engineering Shops supervisor, Mr. Henry Berg, for his help in the selection of the bearing for my system and to the

Mechanical Engineering department assistant, Mr. Doug V. Bitner for his suggestions in the selection of the pneumatic system.

Many thanks to Dr. Reza Fotouhi and Dr. Chris Zhang for their comments and help in proofreading this thesis.

DEDICATION

This thesis is dedicated to

My loving brother

&

My supervisors, Dr. Chapman and Dr. Szyszkowski

TABLE OF CONTENTS

LIST OF TABLES

LIST OF FIGURES

NOMENCLATURE

Roman

a_0	Cubic cell dimension [nm]
A	Atomic mass [amu]
B	Breadth [mm]
C	Viscous damping coefficient [N.s/mm]
D	Wire diameter [mm]
d_{hkl}	d-spacing of silicon crystal in the (h k l) lattice planes [nm]
D	Mean diameter of the spring [mm]
D_B	Bore diameter of the cylinder [mm]
E	Young's modulus of aluminum [N/m^2]
E_d	Disturbance energy [N.m]
E_K	Maximum kinetic energy [N.m]
E_{smin}	Minimum pitch diameter of the threads [mm]
f_0	Atomic form factor
f_n	Natural frequency [Hz]
F	Load acting on the spring [N]
F_H	Structure factor for H plane
F_{HKL}	Structure factor for HKL plane
F_P	Preload applied to the fastener [N]
G	Shear modulus of the material [N/m^2]
H	Height [mm]
I	Measured intensity after deflection
I_0	Incident intensity of the beam

I_C	Coherent scattering intensity
I_D	Intensity of the diffracted beam
I_H	Beam intensity on the higher side (θ_H) of the rocking curve
I_I	Incoherent scattering intensity
I_L	Beam intensity on the lower side (θ_L) of the rocking curve
I_N	Recorded intensity of X-rays after passing through an object,
I_R	Refracted portion of the incident beam
I_{YY}	Moment of area for the fixed post about Y- axis [m^4]
J	Geometric torsion [m^4]
k	Spring stiffness [N/m]
K	Stiffness of the system [N/m]
L	Length of the fixed post [mm]
M	Mass of the components in the system [kg]
N	Number of coils
P	Pitch of the threads [mm]
R	Mean radius of the spring [mm]
r_e	Classical electron radius [cm]
r_n	Effective radius of contact between the nut and joint surface [mm]
r_t	Effective contact radius of the threads [mm]
R (θ)	Analyzer reflectivity function at angle (θ)
R_1	Reflectivity of the first crystal
R_2	Reflectivity of the second crystal
$S_{\Delta\theta}$	Angular sensitivity due to vibration [μradian]
$S_{\Delta\theta max}$	Maximum sensitivity due to vibration [μradian]
$S_{\Delta T}$	Sensitivity due to change in temperature [/°K]

$S_{\Delta Tmax}$	Maximum sensitivity due to thermal effects [/°K]
$S_{\Delta T}$	Angular sensitivity due to change in temperature [μradian]
t	Period of motion [sec]
T	Thickness [mm]
T_s	Torque in the spring [N.mm]
T_{in}	Torque applied to the fastener [N.m]
V_C	Unit cell volume for the crystal, [nm^3]
W_a	Weight of the analyzer mount box with crystal, [N]
x	Displacement vector [mm]
$\ddot{x}(t)$	Acceleration vector [$m.s^{-2}$]
x_0	Amplitude of displacement or geometrical deflection [mm]
x_1	Velocity of the system [m/sec]
$\bar{y}$	Centroid [mm]
Z	Atomic number

Greek

α	Linear thermal expansion coefficient [/°K]
α_1	Maximum angle obtained using motorized actuators [degrees]
α_{max}	Maximum angle of rotation of the analyzer mount box [degrees]
β	Half-angle of the threads [degrees]
δ	phase of oscillation
$\Delta\theta_Z$	Vertical component of the refracted X-rays
ζ	Damping ratio
θ	Angle of the crystal [radians]
θ_B	Bragg angle for the lattice planes

λ	X-ray wavelength [nm]
μ	Microns
μ_n	Coefficient of friction between the face of nut and the upper surface of joint
μ_t	Coefficient of friction between nut and bolt threads
ρ	Density of silicon [kg/m^3]
τ	Shear stress acting on the helical compression spring [N/m^2]
τ_{direct}	Shear stress due to direct compressive force [N/m^2]
$\tau_{torsion}$	Shear stress due to torsion [N/m^2]
υ	Volume of the material [m^3]
φ_i	Eigenvalue vector representing the i^{th} natural frequency
ω_D	Darwin width of the analyzer crystal [μradian]
ω_i	i^{th} natural angular frequency [rad/sec]
ω_n	Angular frequency of an undamped elastic system [rad/sec]

Abbreviations

ACR	American College of Radiology
BMIT	Bio-Medical Imaging and Therapy
CLS	Canadian Light Source, Saskatoon, Saskatchewan, CANADA.
DEI	Diffraction Enhanced X-ray Imaging
FEA	Finite Element Analysis
FWHM	Full Width at Half Maximum
NSLS	National Synchrotron Light Source, Brookhaven National Laboratory, New York, USA
PZT	Lead zirconate titanate
RF	Radio Frequency

CHAPTER – 1. BACKGROUND

1.1 X-ray interaction

X-ray imaging of an object under investigation involves three kinds of contrast mechanisms which are absorption, refraction and scattering [1]. Absorption contrast is due to the differential absorption of two regions that have different materials. Refraction contrast arises from the density of electrons present in the media [1]. The scattering contrast is due to rejection or acceptance of small angle scattering from the sample [1]. X-ray scattering includes small angle scattering [2] (less than milliradians) which carries information about the structure of the object at micron scale [3]. In most of the available conventional imaging techniques, this information is lost because of the small angle nature of this type of contrast. In addition to small angle scattering, the refraction of X-rays inside the object is also not detectable in most of the imaging methods [3]. Due to scattering, small features at different depths within the object may be superimposed which in turn causes blurring of the image by adding unwanted signals to the background [4].

A novel X-ray imaging method, Diffraction Enhanced Imaging (DEI) introduced by Chapman et al. [5], overcomes these difficulties. The DEI uses a synchrotron light source which provides an intense, tunable and bright source of X-rays from a few electron volts to tens of kilo electron volts. Even with the current approach there are some drawbacks and limitations to successfully extract information from the images. The drawbacks of the DEI technique come from the theoretical approximations and behavior of the analyzer crystal. Specifically the DEI has three main drawbacks. These can be summarized as three special cases, as follows:

1. Locating the analyzer crystal on the rocking curve;
2. Limited linearity range;

3. Scattering effects on the images.

1.1.1 Locating the analyzer crystal on the rocking curve

In DEI it is nearly impossible to set the analyzer crystal on both sides of the rocking curve at same intensity values. Due to drifting of the crystal which causes intensity changes, there is no guarantee that the analyzer will stay at a particular point on the high or low angle side of the rocking curve [7]. For achieving a high level of precision, the crystal needs to be stable over time and different environmental conditions (temperature, stress, etc). According to Paquin [6], dimensional instabilities are classified as temporal instabilities, thermal mechanical cycle instabilities, thermal instabilities, and hysteresis. These dimensional instabilities are from the applied external forces as in bending to shape and changes in residual stress.

1.1.2 Limited linearity range

The range in which images can be taken with DEI is defined by the width and shape of the rocking curve. Figure 1.1 shows the rocking curve for a Silicon crystal with (3 3 3) lattice plane. The (3 3 3) refers to the miller indices [33] which identify the orientation and interplanar spacing of lattice planes within the crystal.

The linear range of the rocking curve is expected to be on the order of the Full Width at Half Maximum (FWHM) or the Darwin width [4] [27] (the Darwin width is the intrinsic width of the rocking curve of the Bragg reflection for the perfect crystal within an incident plane wave). If the angular range is over this limit then it will create errors, as the rocking curve might be in the wing region or over the top of the curve. Drifting of the crystal due to mechanical and thermal effects makes it difficult to set the analyzer at half intensity points on the rocking curve. When the monochromator comes to thermal equilibrium, these drifts are small, but at higher energies they become more disturbing as the width becomes narrower [7].

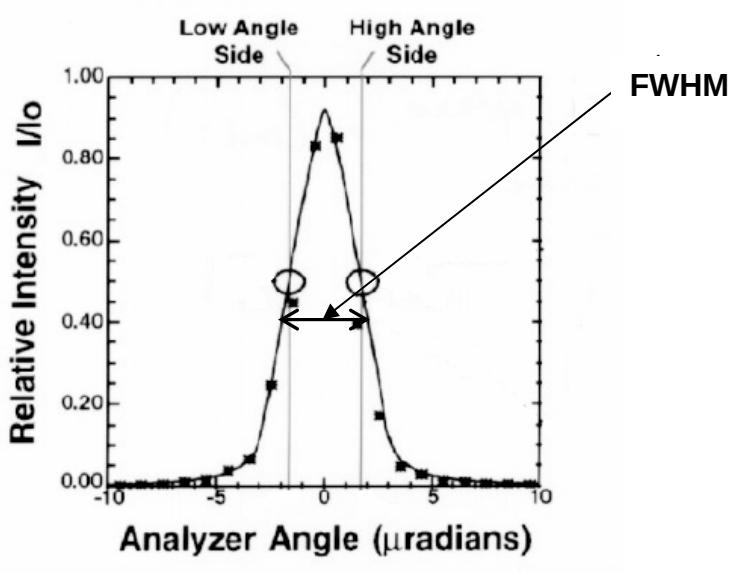

Figure – 1.1 Linear range of a Si (3 3 3) rocking curve [4]

1.1.3 Scattering effects on the images

With the currently available DEI technique, it is difficult to pull off the scattering effects from apparent absorption and refraction, because of the degradation effects which were not considered by the equations that provide the final images [4]. The information present in the object is suppressed due to the presence of extinction effects which are due to the problems with set points on the rocking curve [7]. Therefore, the DEI images are informative only to a certain level. However, it should be taken into account that these limitations are acceptable with DEI because they still produce good quality images when compared to conventional techniques. For the present method to be effective, the analyzer crystal should be positioned very precisely [7].

1.2 Objectives

The objectives of the thesis are described below

1. To increase the dimensional stability of the system in order to set, fix and locate the angle of the analyzer crystal precisely by increasing the lowest natural frequency of the system. This can be done in two ways, either by increasing the stiffness or by decreasing the mass of the system. Both the methods have been employed in increasing the lowest natural frequency of the system.

2. To find an effective way to automatically make the larger angular adjustments of the analyzer crystal. This is done in the current set up manually, which makes the imaging process in the current system more time consuming.
3. To keep the analyzer crystal inside an enclosure, so that the crystal can be isolated from the environmental conditions.

1.3 Thesis outline

This thesis will outline the possible ways of overcoming the limitations in using the DEI method at NSLS (Figure – 1.2) and CLS (Figure – 1.3). It is focused on reducing the vibrations of the analyzer crystal by designing a thermally and mechanically stable support system. This thesis is organized as follows.

Chapter 2 presents the fundamental principles of the DEI method, the DEI system at the NSLS, and the sensitivity of the DEI system to vibration and temperature.

Chapter 3 discusses the natural frequency analysis of the analyzer assembly which was done using ANSYS. The problems which make the system too flexible were identified.

Chapter 4 discusses the new analyzer support design.

Chapter 5 describes in detail the control system for making the analyzer angle adjustments.

Chapter 6 discusses the frequency analysis of the new analyzer support system.

Chapter 7 presents the conclusion of this thesis and the future work.

Figure – 1.2 National Synchrotron Light Source [25]

Figure – 1.3 Canadian Light Source [26]

CHAPTER – 2. DIFFRACTION ENHANCED IMAGING

2.1 Introduction

The Diffraction Enhanced X-ray Imaging (DEI) technique is an analyzer-based technique introduced by Förster et al. [9]. This principle was applied to synchrotron radiation by Chapman et al. which is called Diffraction Enhanced Imaging. The name "Diffraction Enhanced Imaging" used in this thesis refers to an image-processing method which permits the extraction of the refraction contrast from the absorption contrast of the specimen [4].

The DEI takes advantage of the unique atomic structure of perfect crystals used to prepare (monochromator) and analyze the X-ray imaging beam. This produces higher contrast in the images due to the monochromatic X-rays which come from the synchrotron light source which has high intensity and inherent vertical collimation [5]. Figure – 2.1 explains how DEI works. A polychromatic white beam from the synchrotron is converted into a monochromatic beam by diffracting it with the monochromator crystals. This monochromatic beam is then passed through the object under investigation as in conventional imaging methods. However, in DEI a matching crystal called the analyzer crystal, is placed parallel to the monochromator crystals after the object, between the detector and the object.

The X-rays are not only reflected but are also absorbed by the crystal. However, at one specific angle the X-rays are reflected rather than absorbed which is called "Bragg condition". When this condition is met, the diffraction of the X-rays is over a narrow range of the incident angles. As the crystal is rotated about the axes parallel to the lattice planes, the crystal will go through the Bragg diffraction condition and this diffracted intensity will trace out a profile called the rocking curve [10]. Figure – 2.2 shows how the rocking curve is generated. If the angle of cryst-

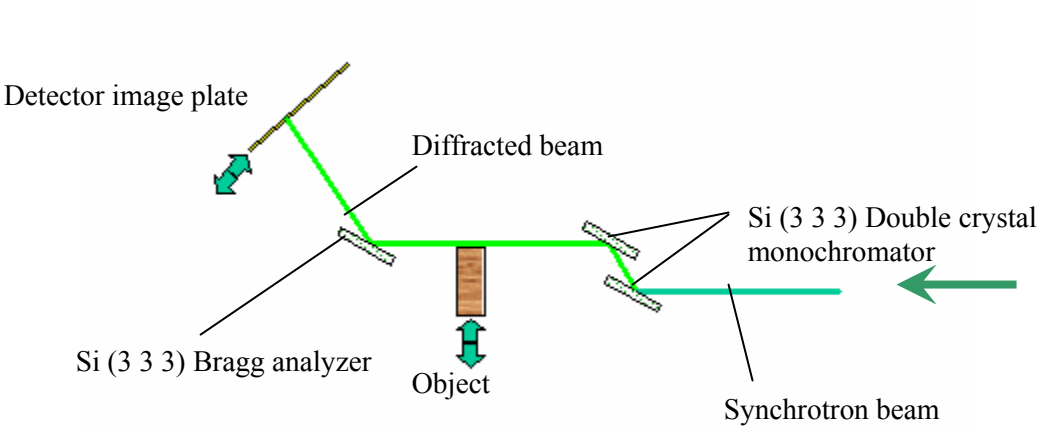

Figure – 2.1 DEI experimental setup

al (θ) where the beam hits is plotted against the reflectivity (R_1 , R_2) for a plane wave, the graph which obtained will be of rectangular shape. In DEI rocking of the analyzer crystal against the monochromator crystals occurs, in which both of them have the same properties. This gives a roughly triangular shape which we call as the rocking curve. In the Figure – 2.2, ω_D represents the Darwin width of the crystal which corresponds to the smaller angular width on the analyzer's rocking curve.

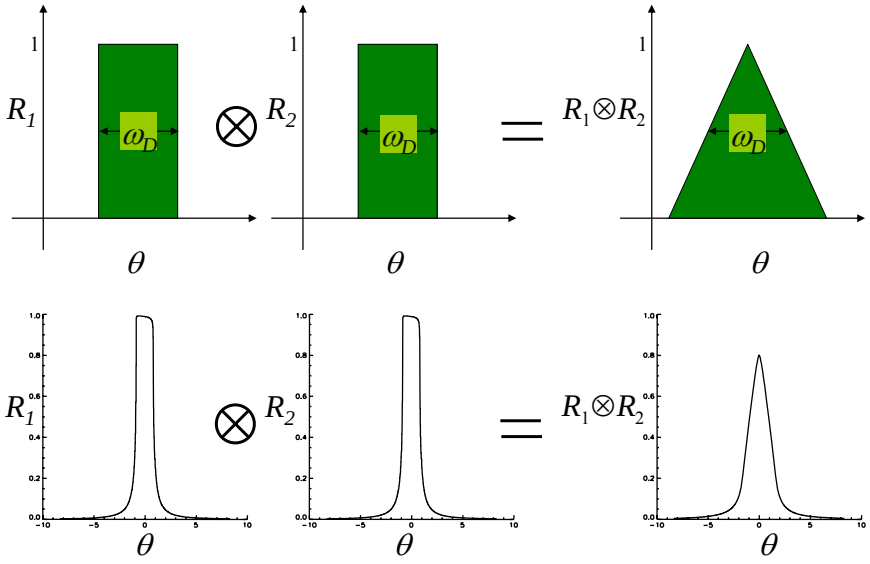

Figure – 2.2 Rocking curve (the graph on the top is the approximation and the one on the bottom is the calculated curve) [5]

2.2 Physical principles of DEI

In normal radiography, the recorded intensity of X-rays after passing through an object, I_N, can be expressed as

$$I_N = I_R + I_D + I_C + I_I \quad (2.1)$$

where, I_C and I_I represent the coherent and incoherent scattering portions, respectively; and I_D represents the diffraction intensity which arrives at the detector along with the portion of incident beam, I_R. I_R will be separated from the other components by DEI and will show the contrast based on refraction, absorption and extinction [4]. The use of the synchrotron light and a double crystal monochromator improves the contrast and spatial resolution which may be affected due to the scattering components I_C and I_I. The use of the analyzer crystal between the object and the imaging system removes the scatter contribution to the image since only X-rays reflected at certain angles will be diffracted onto the detector. As I_C and I_I are eliminated as contributions to the image, the incident beam only has the refracted portion, I_R, which is very close to the initial beam direction [4].

In DEI, two images of the American College of Radiology (ACR) phantom are obtained one on each side of the rocking curve of the Bragg analyzer. One is the apparent absorption image, which is an actual image from direct transmission. Here the term apparent absorption is used, since the analyzer is capable of eliminating some of the ultra-small angle X-ray scattering [27] and this loss of intensity results in an increased or apparent absorption of X-rays. The other image is the refraction image, which is the gradient of the refractive index along the path of X-ray beam through the object. Figure – 2.3 shows the images of the ACR phantom obtained one at an analyzer angle that is slightly greater than the peak angle of the rocking curve (high angle side), and one at lower than the peak angle (low angle). The places which were highlighted in the images show the air bubbles present in the specimen which will not be that visible with conventional X-ray imaging methods.

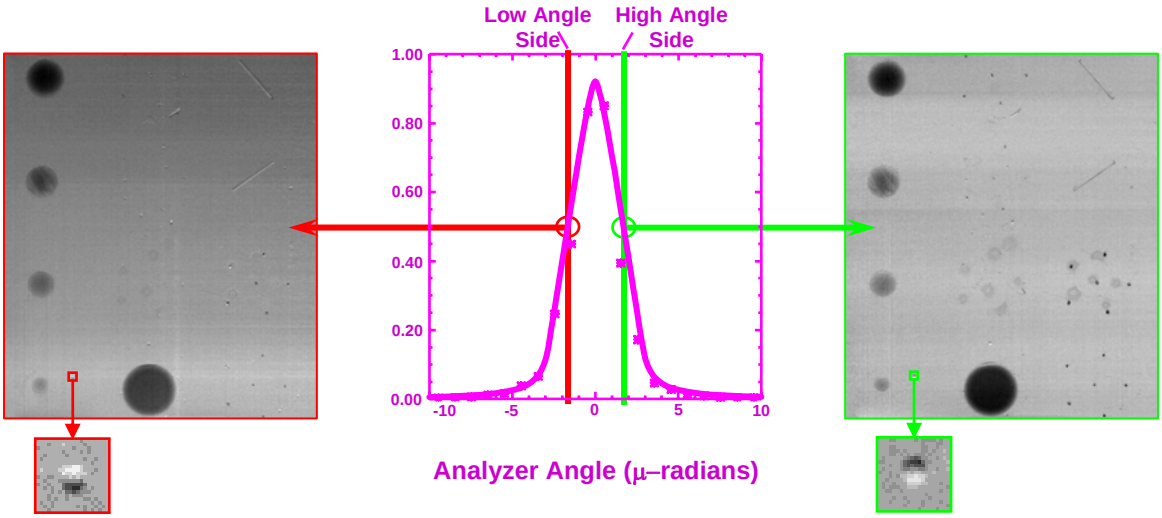

Figure – 2.3 Higher and lower side images of ACR phantom in the rocking curve [30]

Note the dark circular objects in the ACR phantom. These simulate solid tumours in breast tissue. These typically have absorption contrast values of a few percent. However, the contrast in these images is more than 20 times higher. This higher contrast is due to the rejection of the ultra-small angle X-ray scattering that these simulations possess. This is an example of the enhanced contrast present in the apparent absorption image.

The analyzer crystal is chosen to diffract the beam in the vertical plane and so the sensitivity is only to the vertical component, $\Delta\theta_Z$, of the refracted X-rays. According to Chapman et al. [4], the intensity diffracted by the analyzer is set as a relative angle, θ, from the Bragg angle, θ_B, where $\theta_B + \theta$ is the angle between the incident beam and the diffraction planes and is given by

$$I_i = I_R\, R\,(\theta_B \pm \theta) \qquad (2.2)$$

where I_i is the intensity at relative angle, θ, from Bragg angle, θ_B, and R (θ) is the analyzer reflectivity function at angle, θ. The analyzer reflectivity function, R (θ), is a function of the rocking curve. The intensities of the images, I_L and I_H, which are taken on the lower side (θ_L) and the higher side (θ_H) of the rocking curve, can be expressed by Taylor approximation.

$$I_L = I_R\left(R(\theta_L) + \frac{dR(\theta_L)}{d\theta}\Delta\theta_Z\right) \tag{2.3}$$

$$I_L = I_R\left(R(\theta_H) + \frac{dR(\theta_H)}{d\theta}\Delta\theta_Z\right) \tag{2.4}$$

These two equations are coupled and can be solved for I_R and $\Delta\theta_Z$. The resultant equations can be written as

$$I_R = \frac{I_L\left(\frac{dR}{d\theta}\right)(\theta_H) - I_H\left(\frac{dR}{d\theta}\right)(\theta_L)}{R(\theta_L)\left(\frac{dR}{d\theta}\right)(\theta_H) - R(\theta_H)\left(\frac{dR}{d\theta}\right)(\theta_L)} \tag{2.5}$$

$$\Delta\theta_Z = \frac{I_H R(\theta_L) - I_L R(\theta_H)}{I_L\left(\frac{dR}{d\theta}\right)(\theta_H) - I_H\left(\frac{dR}{d\theta}\right)(\theta_L)} \tag{2.6}$$

These equations can be applied on a pixel-by-pixel basis to the diffracted images from both the higher and lower angle side of the rocking curve.

2.3 DEI system sensitivity to mechanical and thermal effects

It is evident that the DEI relies on perfect crystals**.** The X-ray diffraction properties of perfect crystals make this system susceptible to mechanical and thermal effects which are vibration and thermal instabilities.

2.3.1 System sensitivity to vibration

As a result of the vibrations due to environmental conditions, there will be a change in angle of the crystal which can be represented by $\Delta\theta$. The system response is a function of change in intensity, ΔI, to the incident intensity of the beam, I_0, which can be represented by $\Delta I/I_0$. The angular sensitivity of the system due to vibration can be defined as the fractional intensity change per unit angle variation which can be obtained from the formula,

$$S_{\Delta\theta} = \frac{\Delta I}{I_0 \Delta\theta} \tag{2.7}$$

Now $I(\theta)=I_0 R(\theta)$ where $R(\theta)$ is the rocking curve (2.8)

$$dI=I_0 \frac{dR(\theta)}{d\theta} d\theta \text{ or} \tag{2.9}$$

$$S_{\Delta\theta}=\frac{dI}{I_0\, d\theta}=\frac{dR(\theta)}{d\theta} \tag{2.10}$$

As an example, the low angle side of the rocking curve ($-\omega_D \leq \theta \leq 0$) can be modeled as a straight line as,

$$I(\theta) \cong \frac{I_0}{\omega_D}(\theta + \omega_D)$$

Therefore, $\Delta I \cong \frac{I_0}{\omega_D}(\Delta\theta)$

Substituting in (2.7), $S_{\Delta\theta max} \cong \frac{1}{\omega_D}$ (2.11)

This equation shows that the sensitivity is dependant on the Darwin width of the crystal.

In Figure – 2.4, note that higher order reflections have higher angular sensitivity and also that all reflections become more angular sensitive as the imaging energy increases. For example, the commonly used Si (3 3 3) at 40 keV has an angular sensitivity of ~ 0.8 /μradian. This means that, an angular change of 1 μradian will drop the reflected intensity by 80% from the peak intensity. Typically the intensity changes should be below 1% for good imaging conditions. Thus a tolerable angular change would be ~ 13 nanoradians. ($\Delta I/I_0 = 0.01 = S_{\Delta\theta} . \Delta\theta$ or $\Delta\theta = 0.01/ (0.801/\mu\text{radian}) = 0.0125$ μradian. A similar condition for the Si (5 5 5) at 40 keV leads to a tolerance angle change of ~ $\Delta\theta = 0.01/ (2.7/\mu\text{radian}) = 3.7$ nanoradians. Thus the angular tolerance of the order of few nanoradians is a requirement for the analyzer system.

Figure – 2.4 shows the angular sensitivity of the silicon analyzer crystal for various X-ray energies and the table represents the Darwin widths of the silicon crystal for different lattice planes which were calculated using the formulas above.

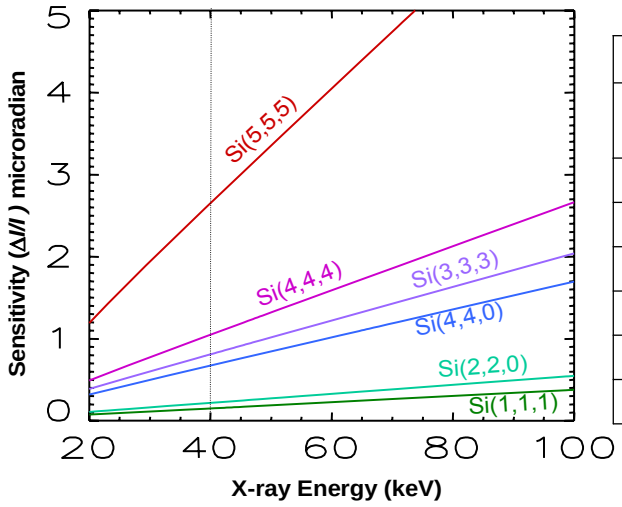

Darwin Widths at 40keV	
Reflection	Darwin Width (μ radian)
Si (5,5,5)	0.377
Si (4,4,4)	0.955
Si (3,3,3)	1.24
Si (4,4,0)	1.49
Si (2,2,0)	4.59
Si (1,1,1)	6.65

Figure – 2.4 Vibration sensitivity vs. energy for various reflections [30]

2.3.2 System sensitivity to thermal effects

As a result of the thermal changes in the system due to environmental conditions, there will be a change in angle of the crystal which can be represented by $\Delta\theta$. The system response is a function of change in intensity, ΔI, to the incident intensity of the system, I_0, which can be represented by $\Delta I / I_0$. The angular sensitivity of the system due to a change in temperature can be described as the fractional change in intensity per unit temperature variation which is

$$S_{\Delta T} = \frac{\Delta I}{I_0 \, \Delta T} \tag{2.12}$$

Temperature change will affect the lattice parameter,

$$\frac{\Delta d}{d} = \alpha \, \Delta T \quad \text{where } \alpha \text{ is the linear thermal expansion coefficient.} \tag{2.13}$$

This can be converted to a change in Bragg angle,

Starting with: $\lambda = 2d_{hkl}\sin\theta$ then (2.14)

$d\left(\lambda = 2d_{hkl}\sin\theta\right) = d(2d_{hkl}\sin\theta)$ or (2.15)

$0 = 2dd_{hkl}\sin\theta - 2d_{hkl}\cos\theta \, d\theta$ or (2.16)

$$\frac{dd_{hkl}}{d_{hkl}} = \cot\theta\, d\theta \quad \text{or} \quad \frac{\Delta d_{hkl}}{d_{hkl}} = \cot\theta\, \Delta\theta \tag{2.17}$$

Now $I(\theta) = I_0 R(\theta)$ where $R(\theta)$ is the rocking curve,

$$dI = I_0 \frac{dR(\theta)}{d\theta} d\theta \quad \text{or}$$

$$S_{\Delta T} = \frac{dI}{I_0\, dT} = \frac{dR(\theta)}{d\theta}\frac{d\theta}{dT} = \frac{dR}{d\theta}\alpha\tan\theta. \tag{2.18}$$

The maximum temperature sensitivity occurs at the ½ points on the rocking curve (maximum slope points)

$$S_{\Delta T\max} = \frac{dR\left(\theta_{1/2\ \text{Darwin width}}\right)}{d\theta}\alpha\tan\theta \cong \frac{\alpha\tan\theta}{\omega_D}. \tag{2.19}$$

At room temperature (25° C) for silicon, $\alpha = 2.59 \pm 0.05 \times 10^{-6}$ /°K, then

$$S_{\Delta T\max} = 2.59\text{x}10^{-6}/^{o}\text{K}\,\frac{\tan\theta}{\omega_D}$$

$$\omega_D = \frac{2d_{hkl}r_e\lambda}{\pi V_c\cos\theta}\left|F_{hkl}\right| \tag{2.20}$$

$$S_{\Delta T\max} = \alpha\frac{\tan\theta}{\omega_D} = \alpha\frac{\sin\theta}{\cos\theta}\frac{\pi V_c\cos\theta}{2d_{hkl}r_e\lambda}\frac{1}{\left|F_{hkl}\right|}$$

$$= \alpha\frac{\pi V_c\sin\theta}{2d_{hkl}r_e\lambda}\frac{1}{\left|F_{hkl}\right|} = \alpha\frac{\pi V_c}{4d_{hkl}^2 r_e}\frac{1}{\left|F_{hkl}\right|} \tag{2.21}$$

using Bragg's law to eliminate $\sin\theta/\lambda$

It should be noted that this function is energy (wavelength) independent. For a sigma polarized beam being diffracted from the (h k l) lattice planes at a wavelength λ, F_{hkl} is the structure factor, θ_B is the Bragg angle of the analyzer crystal, V_C is the unit cell volume for the crystal, r_e is the classical electron radius ($2.18\text{x}10^{-13}$cm), ρ is the density of silicon, A is the atomic mass, d_{hkl} is the d spacing of the (h k l) lattice plane and Z is the atomic number.

For a silicon structure indexed as a cubic system, the relationship between the d-spacing, d_{hkl}, Miller indices (h k l) and cubic cell dimension, a_0, is

$$d_{hkl} = \frac{a_0}{\sqrt{h^2 + k^2 + l^2}} \tag{2.22}$$

The atomic form factor, f_0, is a measure of the silicon atom's ability to scatter the X-rays at a given momentum transfer, or in DEI, (h k l) measured in electron units. In other words, the intensity scattered by an atom of silicon compared to that scattered by a single electron. Thus it has a value of Z (or 14 for silicon) at (0 0 0) or forward scattering and this value drops as the (h k l) increases. The structure factor is obtained from the atomic scattering factor and includes information where the atoms are located in the cubic unit cell's ability to scatter X-rays for a given (h k l) also in electron units [33].

Some of the relevant parameters for silicon are summarized in Table 2.1. Table – 2.2 represents the temperature sensitivity of the analyzer crystal at room temperature for various silicon lattice planes which were calculated using the equations derived above.

Table – 2.1 Diffraction properties of single crystal silicon: allowed reflections, the atomic form factor, magnitude of structure factor and d-spacings. [30]

Silicon			
Z = 14		ρ = 2330 kg/m^3	
A = 28.086 amu		a_0 = 0.54305 nm	
V_C = 0.1601 nm^3			
(h, k, l)	f_0	$\lvert F_{hkl} \rvert$	d_{hkl}
0,0,0	14.00	113.21	
1,1,1	10.63	60.993	0.3135nm
2,2,0	8.42	68.582	0.1920nm
3,1,1	7.71	44.480	0.1637nm
4,0,0	7.03	57.467	0.1358nm

3,3,1	6.76	39.108	0.1246nm
4,2,2	6.14	50.350	0.1108nm
3,3,3; 5,1,1	5.81	33.737	0.1045nm

Table – 2.2 Temperature sensitivity for a few common reflections of silicon at room temperature [30]

Temperature sensitivity for a few common reflections for silicon at room temperature	
Reflection	Sensitivity (/°K)
Si (5,5,5)	1.750
Si (4,4,4)	0.547
Si (3,3,3)	0.314
Si (4,4,0)	0.285
Si (2,2,0)	0.0457
Si (1,1,1)	0.0193

As noted earlier, the temperature sensitivity is energy independent. Again for the commonly used Si (3 3 3) reflection, the temperature sensitivity is 0.314 /°K. A temperature change of the crystal of 1 °K will drop the peak intensity of the reflected beam by more than 30%. The intensity changes required should be or below 1%, this implies temperature stability at or below $\Delta T = 0.01/(0.314\ /°K) = 0.032$ °K. Thus the analyzer must be in temperature controlled environment. In this study provisions will be made to isolate the crystal from thermal effects.

2.4 DEI experimental set up at the NSLS

X15A is a bending–magnet beamline at the NSLS. The X-ray storage ring operates at 2.80 GeV energy and the X-ray beam is 16.3 m from the source and is 130 mm wide at the entrance to the experimental hutch. The DEI set up contains a granite table which is 0.375 m x 0.3 m x 2.1 m on which the analyzer and the monochromator crystals were fixed. To reduce the vibrations of the floor

from affecting the granite table, rubber pads and vibration insulating composite plates were placed under the legs of the table which supports the whole structure [5]. Figure – 2.5 shows a schematic diagram of the DEI image acquisition system at X15A. For restricting the vibrations from the object in reaching the crystals, the object scanning stage and shutter are isolated from the granite table and were supported by a second steel frame which is directly fixed to the floor. The DEI experimental setup consists of three main parts which are the

1. Monochromator,
2. Analyzer and
3. Detector.

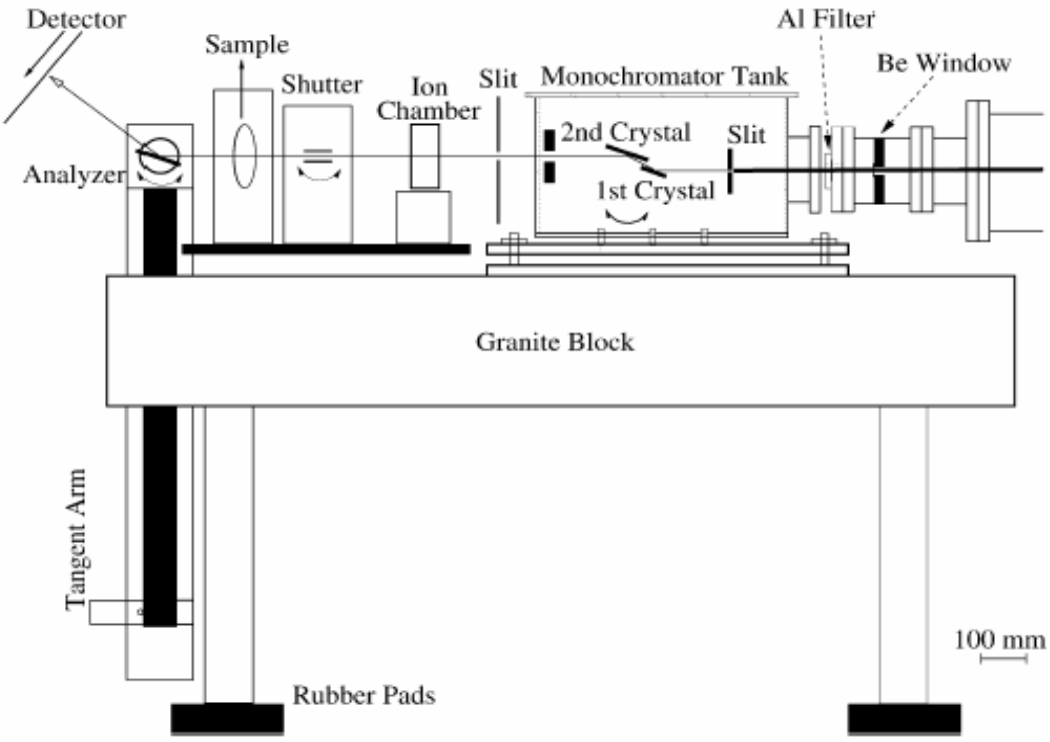

Figure – 2.5 Schematic diagram of a DEI setup NSLS [5]

2.4.1 Monochromator

The Bragg angle of the monochromator selects the wavelength of the X-rays to be used from the white synchrotron radiation beam. The ideal monochromator for the DEI would be a

channel-cut device; because of the extreme width requirement of images and the difficulty in fabrication, an alternative channel-cut system is used at X15A. Figure – 2.6 shows the drawing of the monochromator assembly. The monochromator consists of two parallel Bragg crystals which are made of perfect float-zone silicon. As the surface is parallel to the (1 1 1) planes, these crystals can be used in the symmetric Bragg mode with (n n n) depending on the angular resolution required [5]. The monochromator crystals are enclosed in a box-type design with a fixed offset of 1 cm between them and mounted on the bottom and top plates of the box. For the adjustment of the Bragg and azimuthal angle the crystals are fixed to a kinematic mount. To accommodate the energy changes of the beam, the box is mounted in such a way that the middle of the crystal's surface is at the center of rotation. The box is designed in such a way that the top plate can slide along the direction of the incident beam in 12.7 mm steps to change the distance between the crystals [5].

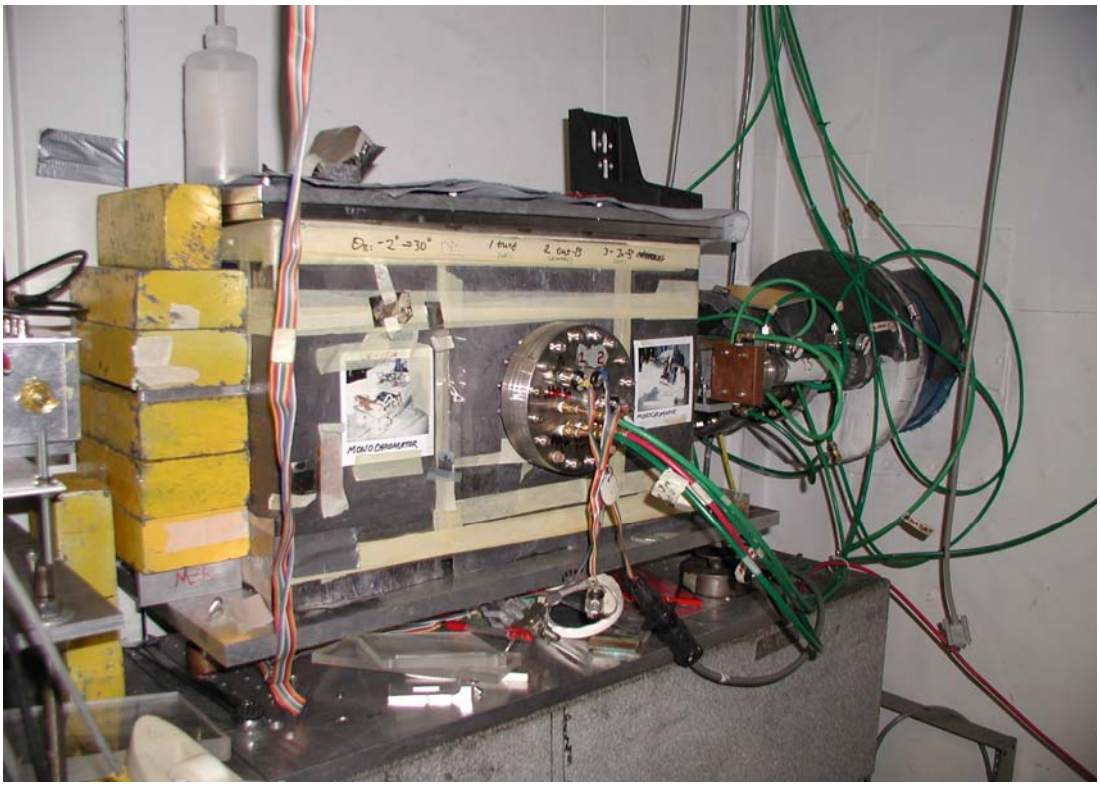

Figure – 2.6 Monochromator assembly [29]

Due to the vibrational resistance and mechanical stability of this design, the intensity modulation of the monochromatic beam is less than 1% peak-to-peak for the crystals diffracting in (3 3 3) mode at 18 keV. For preventing the monochromator assembly from the corrosion caused by ozone, the assembly is enclosed by a stainless-steel tank into which helium at atmospheric pressure flows at 50 cm^3 per minute. For beam entrance and exit, windows made of 100 μm thick Kapton were used as they do not absorb much of the X-ray beam. The crystals are 10 mm thick and 150 mm wide and they have strain relief cuts (2 mm wide and 8 mm deep) on the top at 10 mm from its ends. The lengths are 60 mm and 90 mm long respectively.

There is no need to change the distance between the crystals as the length of the second crystal permits large change in energy range. The crystals are supported on their back side by three balls placed under the strain relief region and by clamping on the other side. As the X-ray beam coming from the synchrotron hits the first crystal, heat will be generated on the surface and within the crystal as the beam is absorbed. To reduce the thermal effects, the first crystal is thermally coupled to a gravity water cooled copper block and the gap between them is filled with a gallium-indium eutectic. Three piezo-driven screws (resolution 0.03 μm) were used to adjust the Bragg and azimuthal angle adjustment of the second crystal and for making it parallel to the first crystal [5].

2.4.2 Analyzer

The analyzer crystal in the DEI experimental setup and the second crystal of the monochromator are the same. A single crystal silicon (3 3 3) is used because of its properties like high thermal conductivity, low thermal expansion co-efficient, good polishability, chemical inertness, high stiffness and good stability [6]. A 1 m long tangent arm driven by a linear actuator with a resolution of 0.1 μm is used to adjust the angle of the analyzer in which an angular resolution of 0.1 μradian can be obtained. This resolution is sufficient for positioning the analyzer at any point of the rocking curve. The azimuthal angle of the analyzer is adjusted by a motorized kinematic

mount. The analyzer crystal is fixed on the same table or granite block where the monochromator is mounted [5].

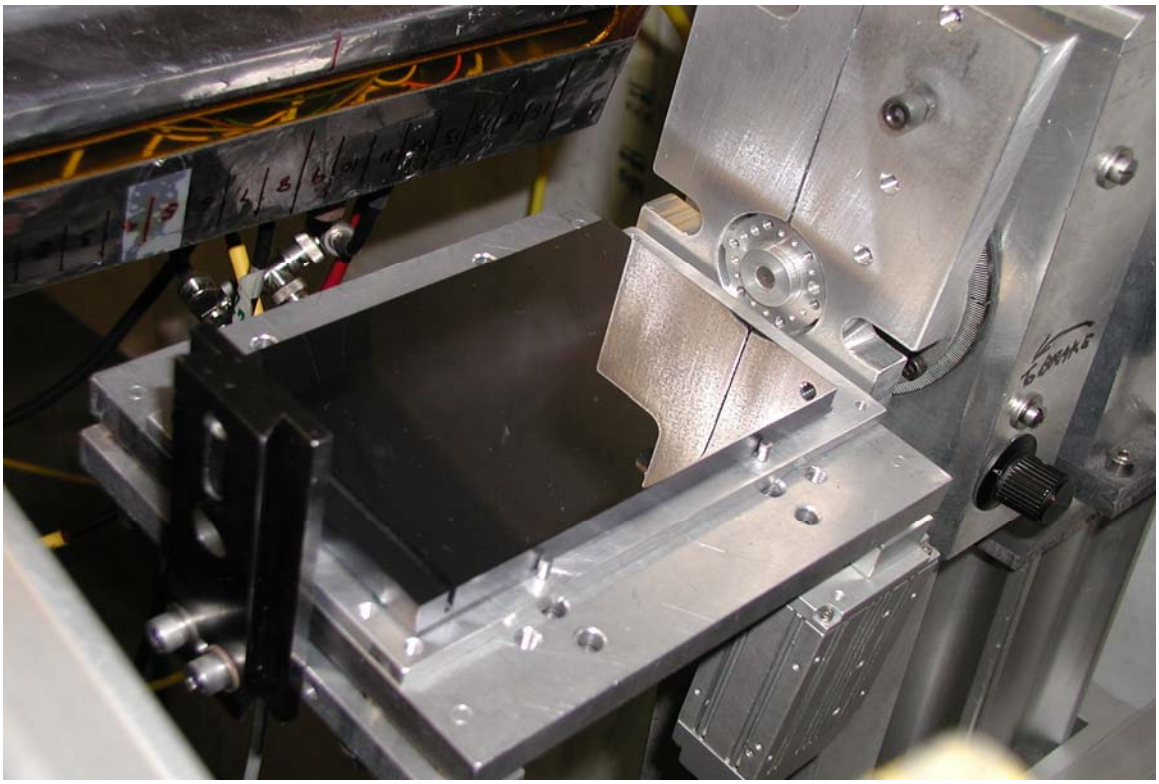

Figure – 2.7 Analyzer crystal [29]

2.4.3 Detector

At the X15A beamline, most of experiments are carried out using image plate readers (Fuji Medical Systems, model BAS2000). Blurring in the images was avoided by scanning the plate in the direction opposite to the sample's scan direction as the analyzer inverts the X-ray beam like a mirror. As shown in the Figure – 2.8 the image plate scanner is perpendicular to the beam diffracted by the analyzer, by tilting the image plate to an angle of $2\theta_B$ from the vertical direction. This tilting avoids the blurring of the image due to the height and the tilting of the diffracted beam [5].

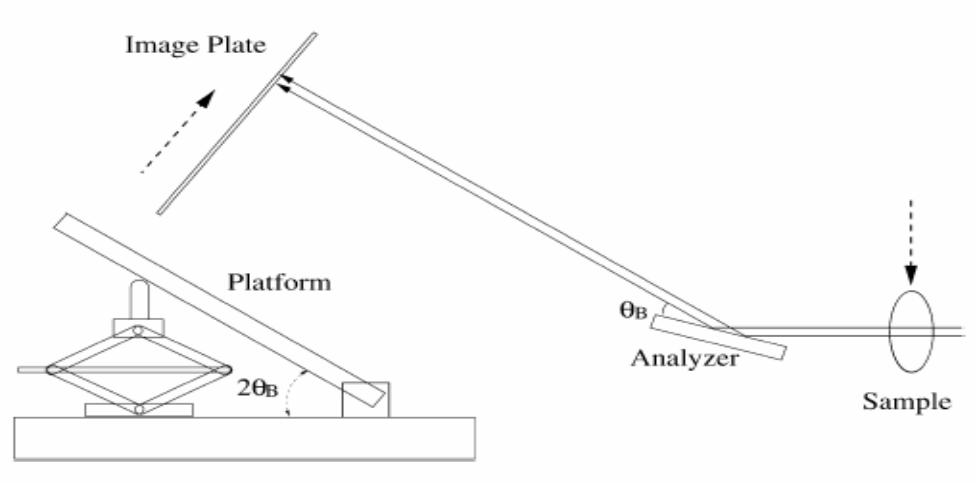

Figure – 2.8 Scanning of the image plate [5]

2.5 Summary

In this chapter the fundamental principles of the DEI method was presented and the complete design of the experimental setup and the working of the different parts in the DEI system were discussed. Moreover, the DEI system sensitivity to factors like vibration and temperature were derived to know how important they are to control the drifting of the analyzer crystal. Next chapter will discuss in detail about the measures implemented to obtain mechanical stability at the NSLS. The factors which cause this system to vibrate even after taking the stability measures will be discussed with the help of the finite element analysis results obtained from the ANSYS software.

CHAPTER – 3. VIBRATION ANALYSIS

3.1 Introduction

If there is no external force applied to an elastic system, the system will experience free vibration and the motion of the system will depend on disturbances exciting the system. Furthermore, if the resistance to motion or damping in the system is small, the oscillatory motion will continue for a very long time. With one dominating frequency such a system can be modeled as a simple mass-spring-dashpot system shown in Figure – 3.1. Assume that the disturbance is characterized by energy E_d.

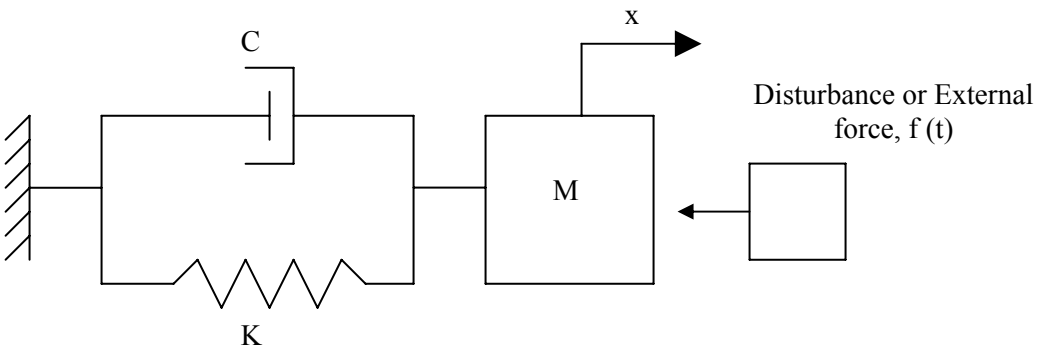

Figure – 3.1 Spring-mass-dashpot system

The equation of motion for a simple spring mass damper system which can be obtained from Newton's second law is [32]

$$M\ddot{x} + C\dot{x} + Kx = f(t) \qquad (3.1)$$

where M is the mass, C is the viscous damping, K is the stiffness, x is the displacement vector, $\ddot{x}(t)$ is the acceleration vector and f (t) is the external force. Here this force is assumed random coming from some external disturbances, which are characterized by energy, E_d, delivered to the system.

In the absence of an external force, eqn.(3.1) can be written as

$$M\ddot{x} + C\dot{x} + Kx = 0 \quad \text{or} \tag{3.2}$$

$$\ddot{x} + 2\zeta\omega_n\dot{x} + \omega_n^2 x = 0 \tag{3.3}$$

where $\omega_n = \sqrt{\frac{K}{M}}$; $\zeta = \frac{C}{2\sqrt{KM}}$

ω_n is the angular frequency for an undamped elastic system and ζ is the damping ratio

By assuming a solution of the form, $x = e^{st}$ (3.4)

where s is a constant. Upon substitution into the differential equation,

$$(s^2 + 2\zeta\omega_n s + \omega_n^2)e^{st} = 0 \tag{3.5}$$

which is satisfied for all values of t when

$$s^2 + 2\zeta\omega_n s + \omega_n^2 = 0$$

The roots of this second order polynomial equation are [32]

$$s_{1,2} = -\zeta\omega_n \pm i\omega_n\sqrt{1-\zeta^2} \tag{3.6}$$

where $\omega_n\sqrt{1-\zeta^2} \cong \omega_d$ which is the damped natural frequency.

Substituting in eqn.(3.4), yields

$$x = x_0\ e^{-\zeta\omega_n t}\ \sin(\omega_n t + \delta) \tag{3.7}$$

where x_0 is the amplitude of displacement or geometrical deflection and δ is the phase which can be determined by initial conditions.

If $\zeta < 0.2$, then $\omega_n \cong \omega_d$. For one cycle, the vibration or displacement can be approximated by

$$x = x_0\ \sin\omega_n t \tag{3.8}$$

Velocity is determined as,

$$x_1 = x_0\omega_n\ \cos\omega_n t \tag{3.9}$$

Therefore, the maximum kinetic energy is

$$E_k = \frac{1}{2}\omega_n{}^2 x_0^2 M \tag{3.10}$$

It was assumed that this energy comes from the disturbance energy, E_d. Thus

$$E_d = \frac{1}{2}\omega_n{}^2 x_0^2 M \tag{3.11}$$

Consequently , one obtains

$$x_0 = \frac{1}{\omega_n}\sqrt{\frac{2E_d}{M}} \tag{3.12}$$

As can be seen from above, the displacements due to disturbances are inversely proportional to the system frequency. From this one can infer that if the angular frequency of the system is higher, then any (random) environmental disturbances will have smaller effects. For this reason, when designing this mechanical support system, one has to make sure that the natural frequency of vibration of this system is as high as possible. Generally, it can be achieved by reducing the mass of the components in the system (smaller M) and by making the design stiffer (greater K).

3.2 Measures implemented to obtain precise positioning

The DEI system implemented at the X15A beam line at the National Synchrotron Light Source employs a number of steps to improve the geometrical stability requirements [5]. Some of the steps are:

1. The use of vibration isolated granite block on which the crystals (a double crystal monochromator and analyzer) are mounted,
2. Mechanically stiff mounts for the crystal assemblies,
3. Temperature control of the crystal environment, and
4. Mechanical isolation of all scanning and monitoring systems from the granite block.

Even after implementing these measures the geometrical stability of the system is still an is-

sue. The vibration measurements taken at the NSLS showed that the analyzer assembly vibrates with the frequency between 15-25 Hz. In this chapter, the DEI system has been analyzed for the natural frequency of vibration using the finite element software and by hand calculations.

3.3 Natural frequency analysis of analyzer assembly

As mentioned before, the higher natural frequency means smaller deformations caused by disturbances or that the system is stiffer. Therefore, the natural frequency can be considered as a measure of the stiffness [13].

ANSYS is a finite element software package which has been used by design engineers for structural, thermal, fluid, and electrical analyses. In this thesis work, it was used as a computational tool for analyzing the old and new designs of the analyzer assembly system for DEI.

The natural frequency analysis of the analyzer assembly is an eigenvalue problem which is described below. As the free vibration is assumed in this finite element modal analysis, the force applied is zero.

The undamped vibration of a mechanical system can be written as [32]

$$M\ddot{x} + K x = 0 \tag{3.13}$$

where M and K are the mass and stiffness matrix respectively and x is the vector of DOF's

The displacement of the system free of forces will have the form,

$$x_i = \varphi_i \cos \omega_i t \tag{3.14}$$

where φ_i is the eigenvalue vector representing the i^{th} natural frequency and ω_i is the i^{th} natural frequency.

By substituting eqn.(3.14) into eqn.(3.13) yields

$$(K - \omega_i^2 M)\varphi_i = 0 \tag{3.15}$$

This equation represents an eigenvalue problem, which can be solved for eigenvalues (ω_i^2) and eigenvectors (φ_i). The eigenvalues are found from:

$$\left|K - \omega_i^2 M\right| = 0 \quad \rightarrow \omega_1^2, \omega_2^2, \omega_3^2 \ldots\ldots\ldots\ldots \tag{3.16}$$

Substituting back to eqn.(3.14), the corresponding eigenvectors are determined. Note that because of (3.14), any φ_i can be multiplied by an arbitrary value. It should be noted that for graphical purposes, the modal deflections determined are M-normalized that is $\varphi_i{}^T M \varphi_i = 1$; therefore the numerical values of displacements have no physical meanings. The subspace iteration method [15] is used to perform modal analysis.

3.3.1 Modeling and simulation of analyzer assembly using ANSYS

In this section, the numerical results for the analyzer assembly obtained with the help of ANSYS are presented. Figure – 3.2 shows the schematic representation of the analyzer assembly with the parts (members).

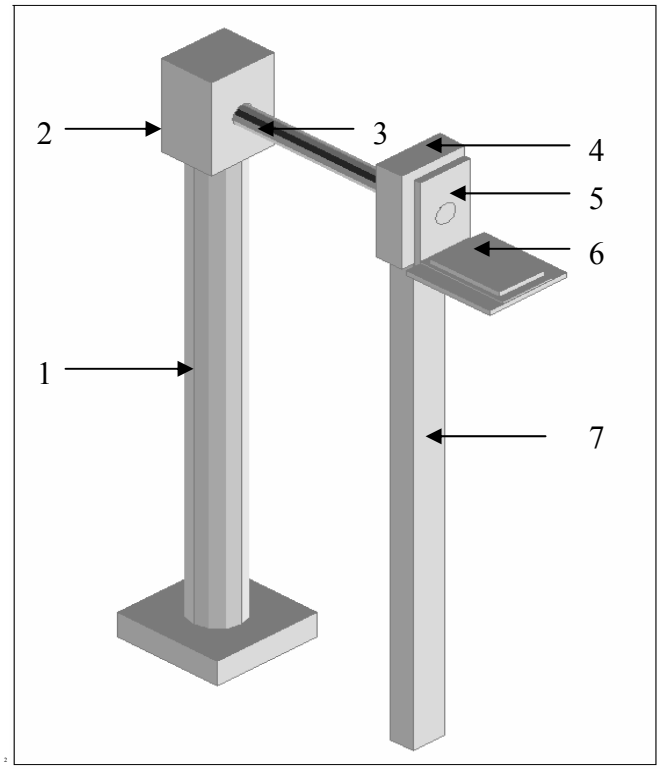

Figure – 3.2 Analyzer assembly, 1&2 - Fixed post, 3 - Shaft, 4 - Tangent bar head, 5 - Tangent bar leg, 6 - Connection assembly, 7 - Crystal and support assembly.

Also, some simplified by-hand calculations are included to verify the finite element analysis results. The development of the finite element model for the DEI assembly involves the following steps:

3.3.1.1 Design of geometry

In order to model the assembly, the element types Beam 4 and Shell 63 have been chosen from the library of ANSYS. Beam 4 is a 3D elastic beam type with tension, compression, torsion and bending capabilities [14]. This element can be represented by two nodes and six degrees of freedom at each node, which are the translations along the nodal X, Y and Z directions and rotations about the X, Y and Z axes (Figure – 3.3). Such an element is chosen because the analyzer assembly members mostly behave like beams or shafts. The whole assembly looks like a cantilever beam which is fixed at one end and has a crystal supported by plates hanging on the other end. So the element chosen should have all the properties needed for analyzing this type of structures.

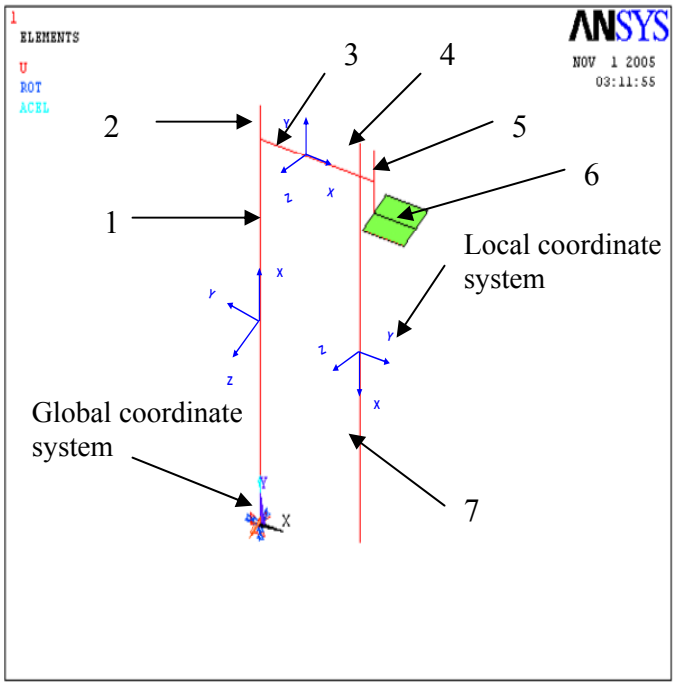

Figure – 3.3 FEA model showing the axis for different planes

Shell 63 is chosen to model the analyzer crystal and the holding plate. It has four nodes and six degrees of freedom at each node [15]. The input data needed for the shell 63 are only the

thicknesses while for beam 4 elements the inputs required are the area, moments of inertia about the Y and Z directions and torsional moment of inertia about the X direction in the local coordinate system. The formulas and the calculations are included in Appendix – A (Section A.1).

3.3.1.2. Material properties

The analyzer assembly is made of aluminum, steel and silicon. Only steel and aluminum members are modeled and the weight of silicon has been calculated and added to the weight of aluminum as the crystal and the base plate were assumed as one piece in this analysis. So only the properties of two materials were given as inputs. The material properties like density, modulus of elasticity and Poisson ratio should also be given as the inputs for the analysis.

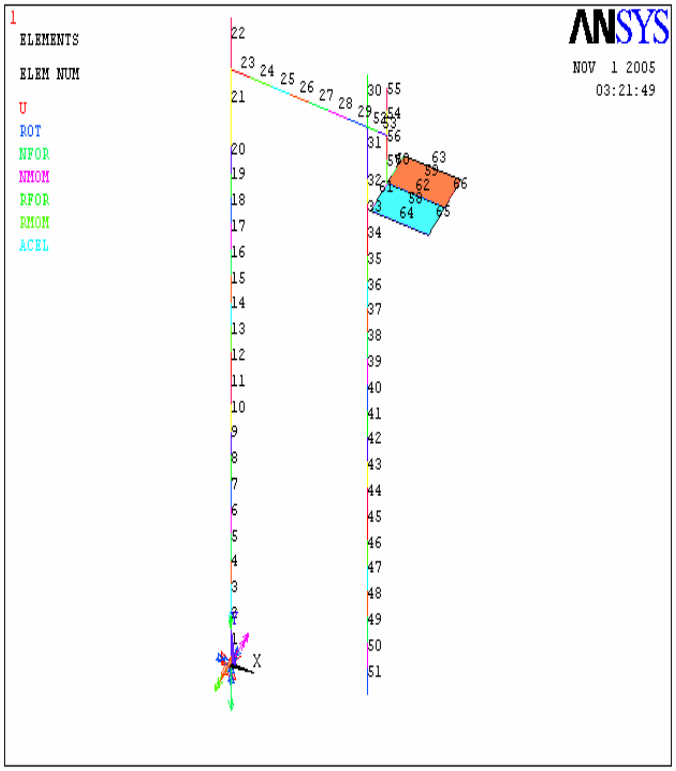

Figure – 3.4 Numbering of elements

3.3.1.3 Meshing

The nodal points are shown in Figure – 3.4. Each beam element is represented by a line connecting the nodal point. For a graphical representation, the shapes of the elements can be drawn

as shown in the Figure – 3.5. The size of the elements secures accurate results of the modal analysis. A mesh refinement study was done with a lesser and greater number of elements, which has not changed the natural frequency values nor the vibration modes.

3.3.1.4. Boundary conditions

In this analysis, for the bottommost element of the fixed post (point A) the displacement is kept zero for all the six degrees of freedom and for the bottom most element of the tangent bar (point-B), the displacement in the X and Y directions in the global coordinate system was kept zero. The shaft and the tangent bar should be free to independently rotate at C which requires using the so called coupling degrees of freedom. The green symbol in the Figure – 3.5 represents this coupling condition.

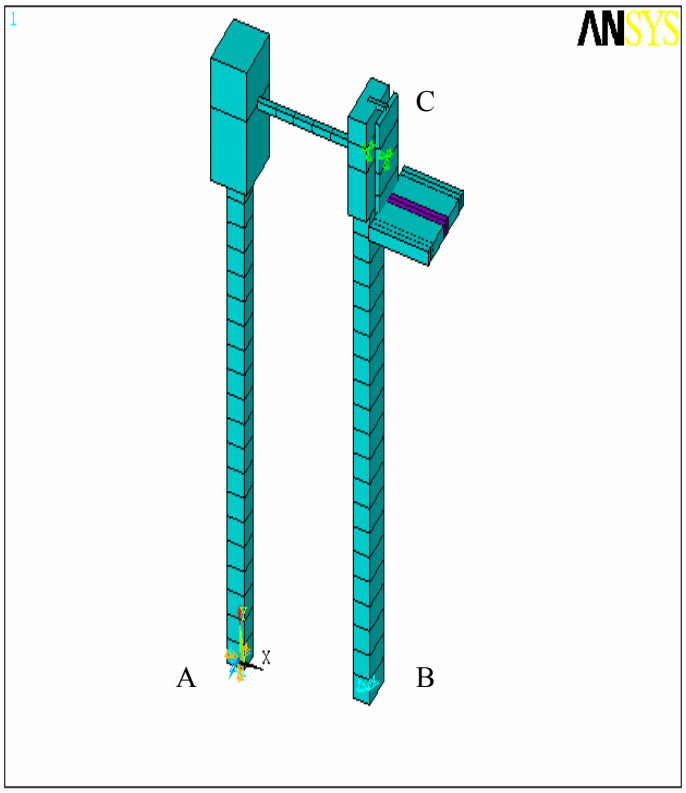

Figure – 3.5 FEA model of analyzer assembly

3.3.1.5. Computer outputs and results

After the application of boundary conditions, a modal analysis is performed by ANSYS to determine the frequencies and the modal shapes. The frequencies (in Hz) are ordered from the lowest/fundamental frequency to the highest. Eventhough only the lowest natural frequency is the required data; the first six modes are calculated to make a comparison of the frequencies and to reduce the computational time. The increase in number of modes will make simulation process time consuming. As the aim of this project is to increase the lowest natural frequency system by increasing the stiffness of the system, only the modal analysis was done. The results of this analysis are discussed next, mode by mode.

3.3.1.5.1 Vibration mode – 1, Frequency f_1 = 17.9 Hz

In the Figure – 3.6, isometric (1), top (2), front (3) and side (4) views of the analyzer assembly are shown to give a better idea of the first mode of vibration. In this mode, the structure of the analyzer assembly is mainly affected by the deflection of fixed post about the Y axis. While going through the animations it was also observed that the system is also affected by the shaft which causes bending due to smaller diameter. This frequency can be raised by making the post stiffer for rotation and by reducing the mass of the other parts hanging on the post. Also, by increasing the shaft diameter this frequency will increase.

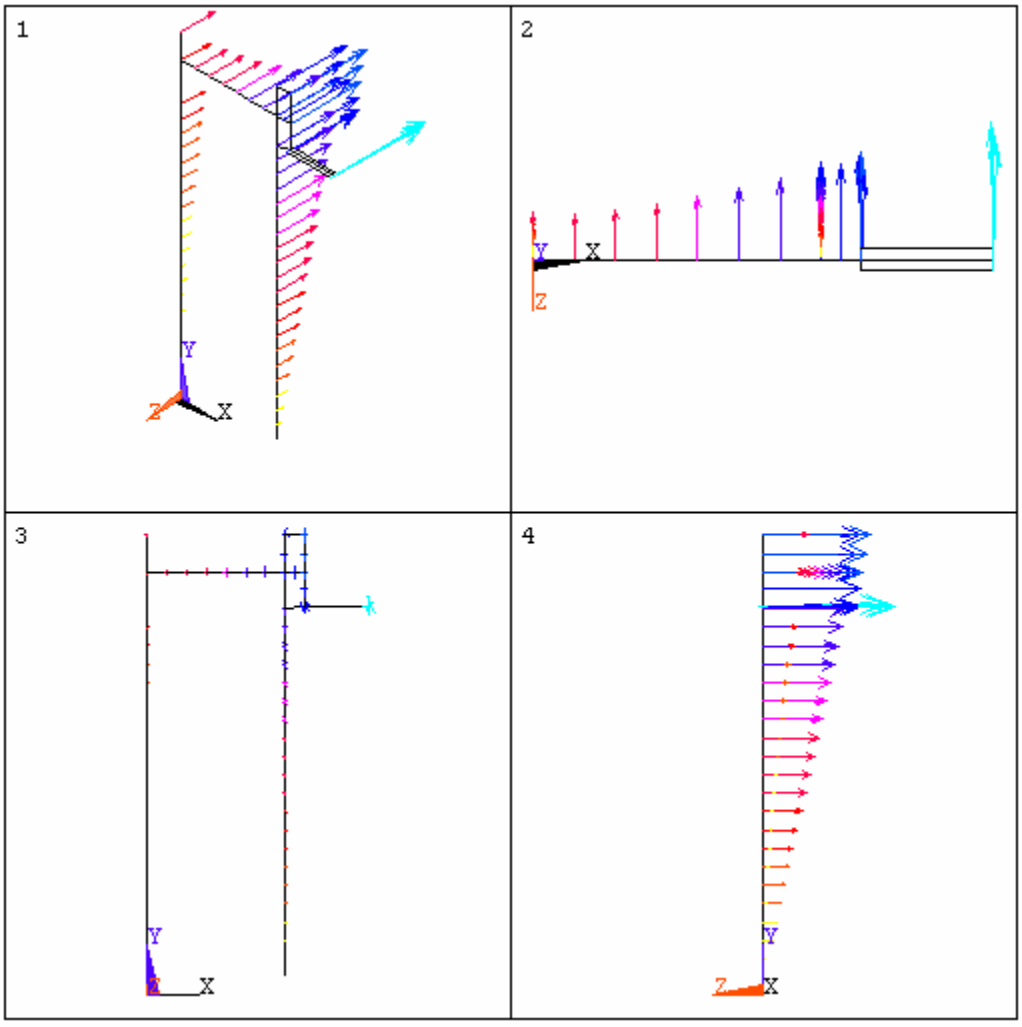

Figure – 3.6 Vibration mode – 1

3.3.1.5.2 Vibration mode – 2, Frequency f_2 = 23.5 Hz

The second lowest of the natural frequencies of vibration is shown in the Figure – 3.7. In this mode, the structure of the analyzer assembly is mainly affected by the bending of the fixed post about the rotational Z axes. The simulation results showed that this bending may also be due to the high weight of the parts hanging on this post or the flexible shaft which is not stiff enough to hold the mass of crystal and the connection assembly. This frequency can be raised by reducing the mass of the other parts hanging on the post or by increasing the bending stiffness of the fixed post.

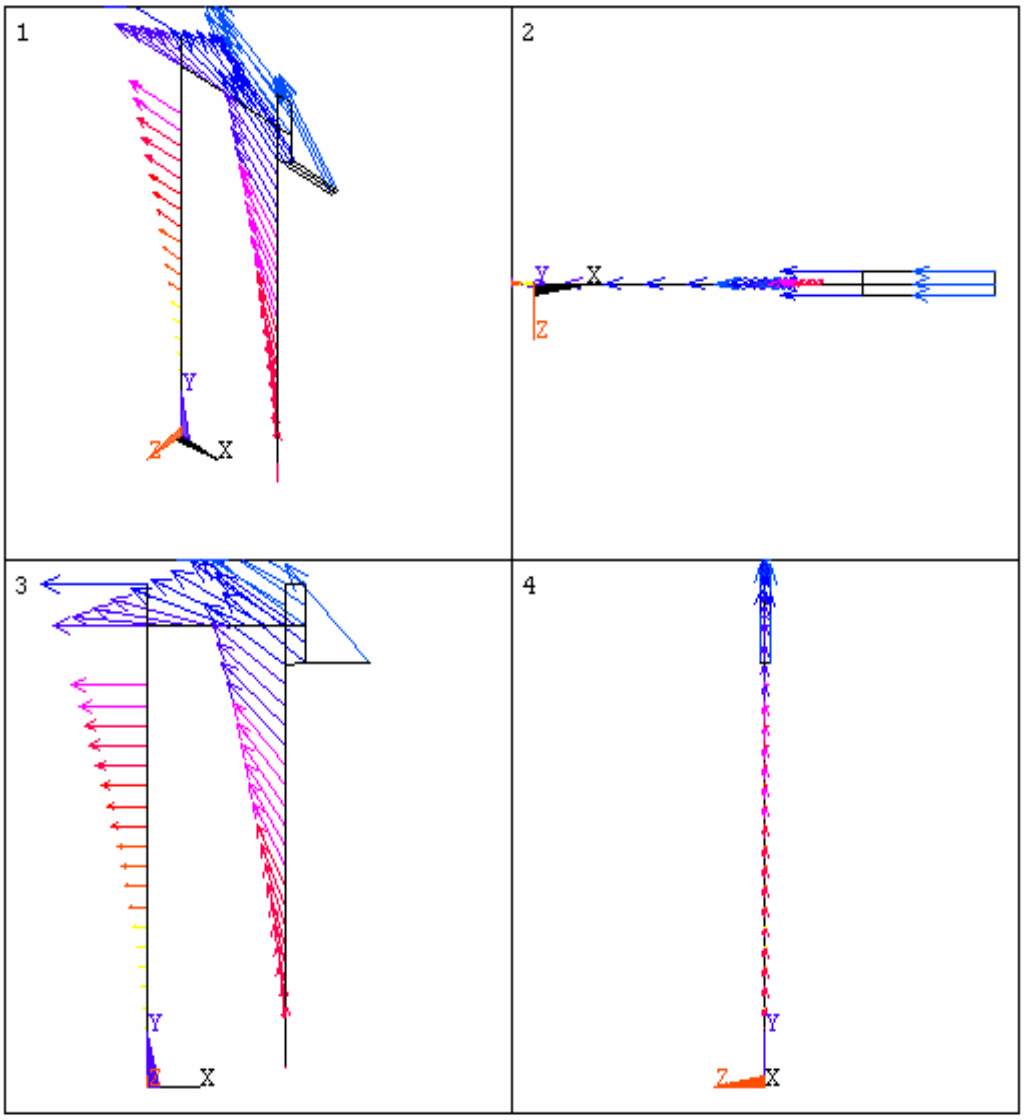

Figure – 3.7 Vibration mode – 2

3.3.1.5.3 Vibration mode – 3, Frequency f_3 = 42 Hz

In this mode shown in Figure – 3.8, the structure of the analyzer assembly is mainly affected by the rotation of the crystal assembly about the Z-axis . This is due to an ineffective connection assembly which connects the shaft and the crystal assembly. This mode can be raised by increasing the stiffness of the connection assembly which acts as an interlink between the shaft and the crystal assembly.

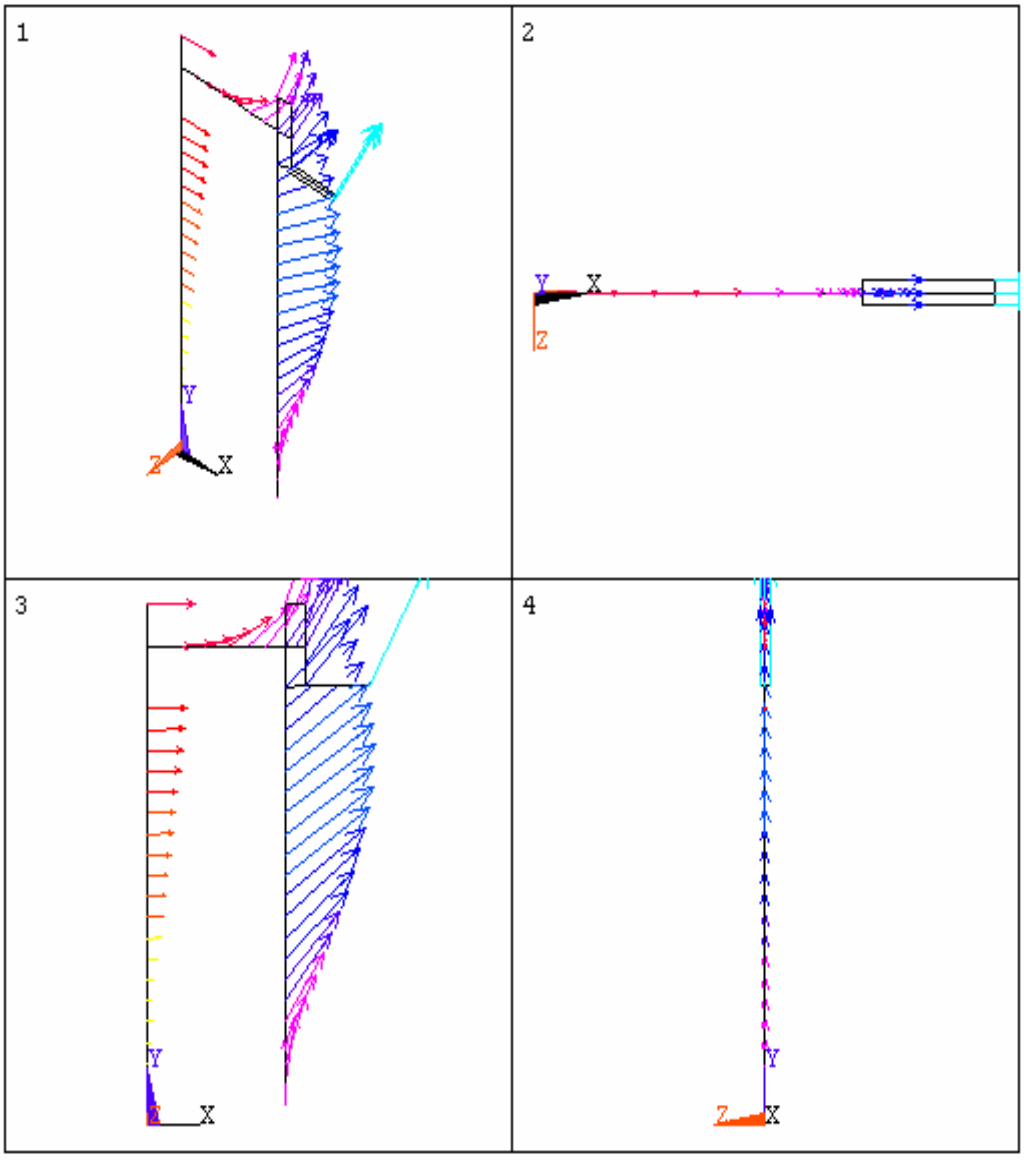

Figure – 3.8 Vibration mode – 3

3.3.1.5.4 Vibration mode – 4, Frequency f_4 = 62 Hz

In this mode shown in Figure – 3.9, the vibration of the analyzer assembly is mainly due to the deflection of the post in the X-Z plane. This frequency can be increased by stiffening the post in the X-Z plane.

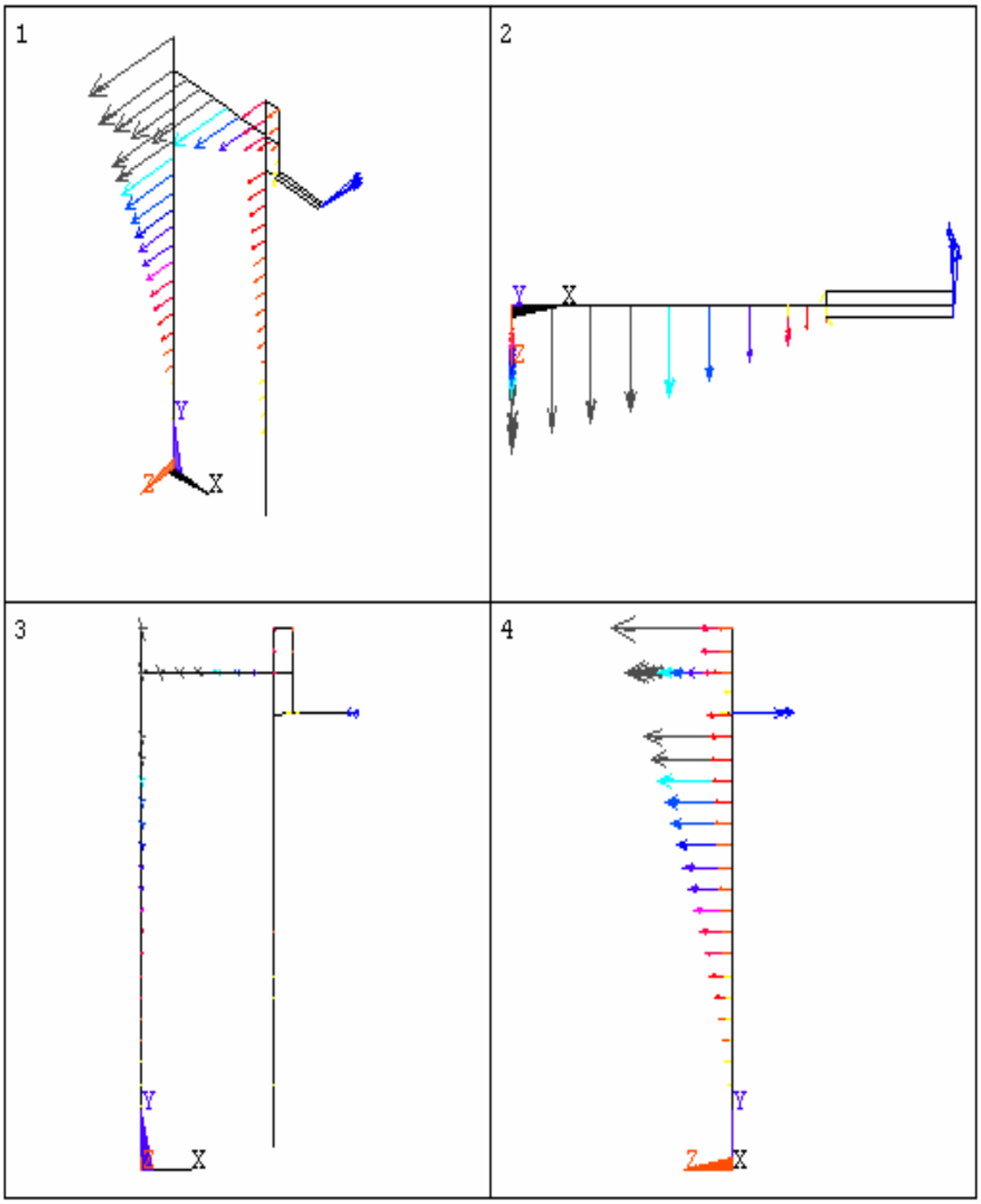

Figure – 3.9 Vibration mode – 4

3.3.1.5.5 Vibration mode – 5, Frequency f_5 = 178 Hz

In this mode shown in Figure – 3.10, the structure of the analyzer assembly is mainly affected by the deflection of the tangent bar in the X-Y plane. This frequency can be raised by having a holder which is stiff enough to hold the tangent bar or by reducing the height of the tangent bar.

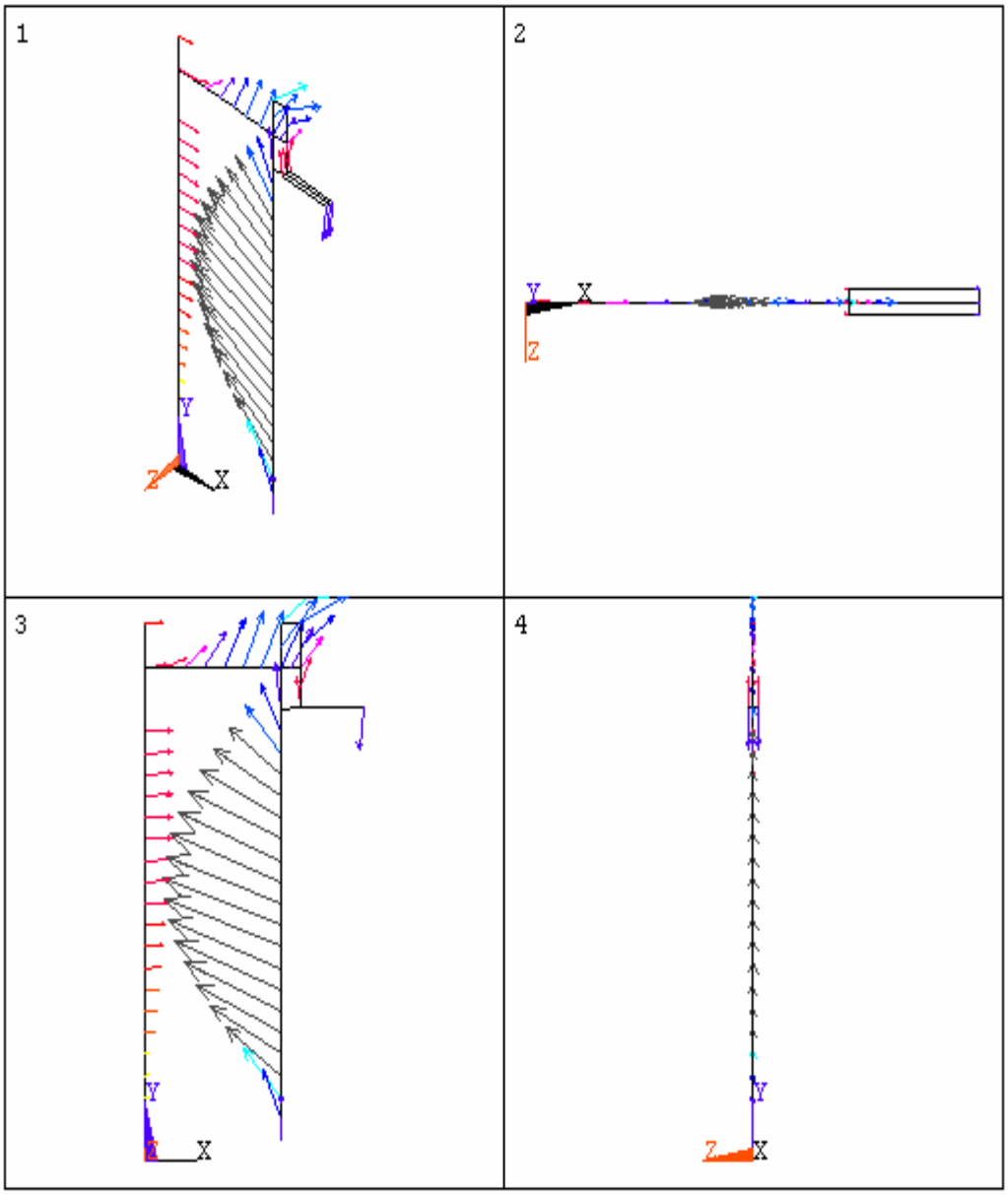

Figure – 3.10 Vibration mode – 5

3.3.1.5.6 Vibration mode – 6, Frequency f_6 = 188 Hz

In this mode shown in Figure – 3.11, the vibration of the analyzer assembly is mainly due to the bending of the tangent bar in the X-Z plane. The simulation results also show that the connecting rod which acts as an interconnection between the tangent bar and the crystal connection assembly is bent. This frequency can be raised by reducing the size of the tangent bar, or by having a holder for the tangent bar to restrict the movement along rotational X and Z axes, and by increasing the stiffness of connection assembly which connects the shaft and the crystal assembly.

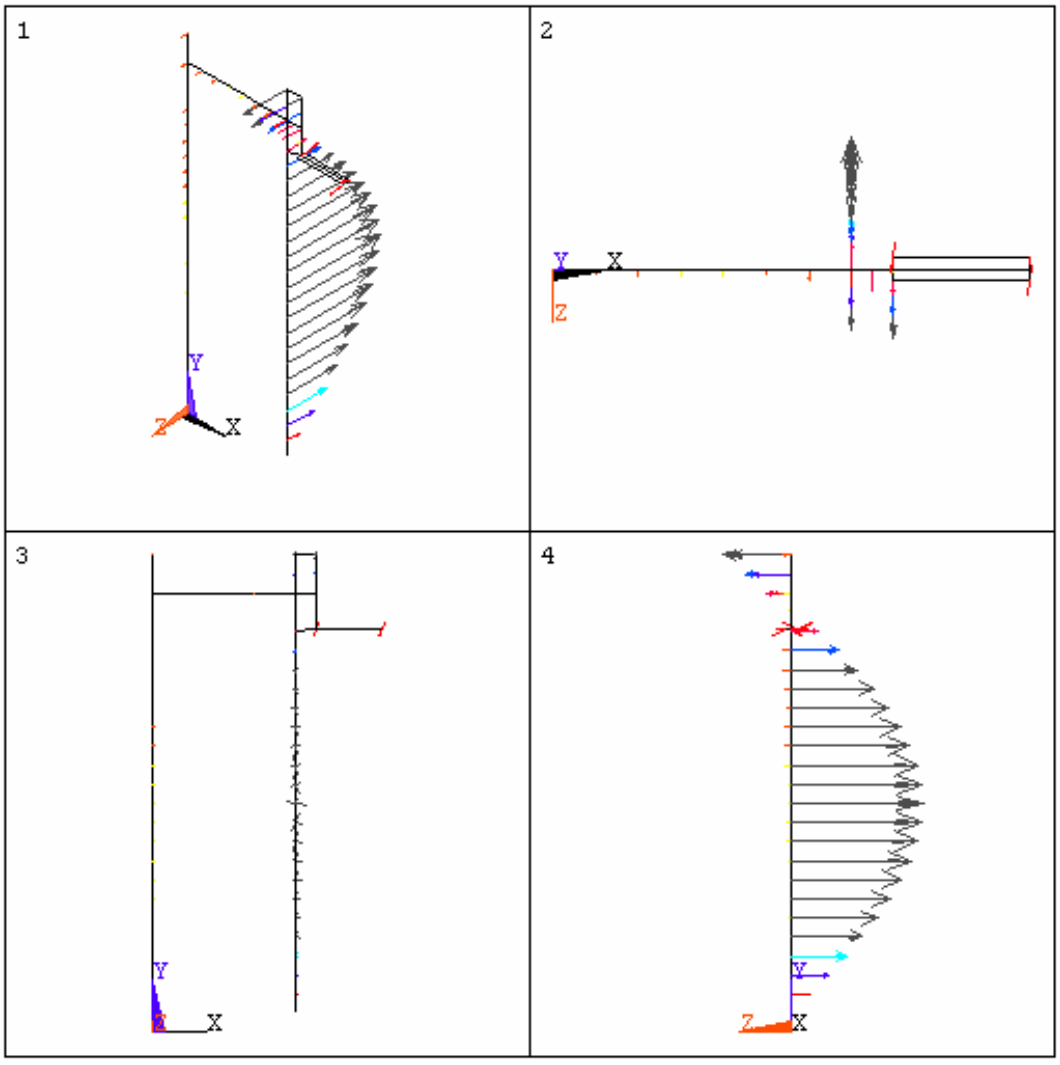

Figure – 3.11 Vibration mode – 6

Table – 3.2 shows a summary of the system mode shape frequencies from ANSYS .

Table – 3.2 Natural frequency values

MODE	FREQUENCY (Hz)
1	17.894
2	23.458
3	41.678
4	61.795
5	178.080
6	188.470

3.3.2. Approximate frequency calculation for analyzer assembly

In order to estimate the lowest frequency, it has been assumed that the whole mass of the system lies at the top end of the fixed post as shown in the Figure – 3.12 B. The real system is shown in Figure – 3.12 A. These calculations are presented to verify the analysis results obtained from ANSYS.

The following data are used:

Density of aluminum = 2710 kg/m^3 [31]

Young's Modulus of aluminum, E = $70*10^9$ N/m^2 [31]

Moment of area for the fixed post (See Appendix A, Table – A.1) I_{ZZ} =$1.99*10^{-6}$ m^4

Total mass of the system hanging on the post,

M = Mass of shaft + Mass of crystal assembly + Mass of tangent bar assembly

= 4.0086 + 2.95 + 2.922

M = 9.8806 kg

Length of fixed post (from Figure – 3.12(A)), L = 1.19 m

$$\text{Circular frequency } \omega = \sqrt{\frac{3EI}{ML^3}} = 158.43 \text{ rad/sec} \tag{3.16}$$

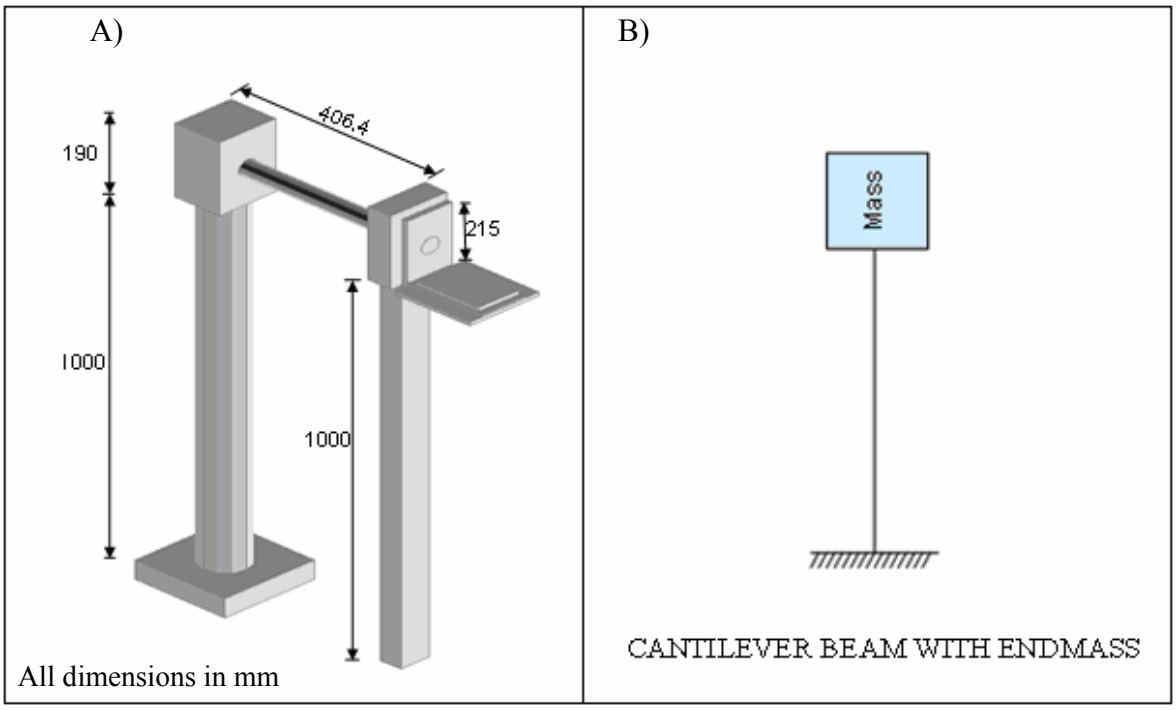

Figure – 3.12 Cantilever beam with end loading

$$\text{Natural frequency, } f_n = \frac{\omega}{2\pi} = 25.21 \text{ Hz} \tag{3.17}$$

This result is sufficiently close to f_2.

3.4 Summary

Frequency observed by measurements of the analyzer assembly at the NSLS = 15 – 25 Hz

Natural Frequency by mechanical calculations = 25.21 Hz

Two lowest frequencies by ANSYS $f_1 = 17.9$ Hz & $f_2 = 23.5$ Hz

The two lowest natural frequencies obtained by using ANSYS compare closely to those obtained from the vibration measurements. The natural frequency needs to be raised to make the system more resistant to environmental disturbances. This will be discussed in the next chapter.

CHAPTER – 4. MODIFIED DESIGN OF THE ANALYZER ASSEMBLY

4.1 Introduction

In this chapter, modifications to the NSLS analyzer design will be briefly described. By increasing the dynamic stiffness of the system, the new system should be able to

1. Reduce analyzer assembly oscillations due to random disturbances;
2. Drive the analyzer more precisely to the required angle on the rocking curve; and
3. Keep the analyzer dimensionally stable for the required time until the image is taken.

4.2. Reducing the analyzer assembly oscillations

After examining the current DEI system by using the finite element method, it was found that the low frequencies are mainly due to the heavy weight of all the parts in the assembly and a cantilever beam set up. The whole weight of the analyzer crystal in the existing system is positioned at the end of the beam. This problem could be rectified by supporting the analyzer's weight at both ends (a simply supported beam instead of a cantilever beam) which considerably stiffens the system (about 8 times). Also, the weight of the analyzer assembly will be reduced by using aluminum instead of steel for every part other than the crystal and the shaft. Another reason for using aluminum is that it does not oxidize quickly. Non-aluminum parts used were galvanized to have corrosion resistance. A magnetic kinematic base is added to hold the crystal in the new setup which reduces the wear and tear and allows for the easy positioning of the analyzer crystal. An additional magnet is also used to hold the tangent bar with the tip of the motorized actuators so that the tangent bar can be stiffened.

4.3 Driving the analyzer to the required angle on the rocking curve

During imaging in a DEI system, images at different points on the rocking curve are taken, which is achieved by rolling the analyzer through increments of micro radians. In the current setup at the NSLS, this is achieved by using only the tangent bar assembly. As adjusting the angle of analyzer by the tangent assembly is quite effective, the same principle is used for adjusting the angle of the analyzer box as a whole in the new design. A motorized linear actuator is used instead of the stepper motor in the new design, because the stepper motor at the end of the tangent bar may excite some vibrations due to the rotary motion. In the DEI assembly, the crystal position may change during imaging, this can be additionally adjusted more precisely by employing piezo-electric actuators. Displacements of such actuators driven by applied voltages cause the crystal to rotate in the range of micro radians. The voltages correspond to the required rotation of the crystal. A control system is being designed to help the piezo-electric actuators act according to the crystal position. The new design also has motorized linear actuators on the bottom of the piezo-electric actuators; these actuators will be used to adjust the Bragg and azimuthal angle of the analyzer crystal in addition to the tangent bar. The crystal is held only by a helical compression spring. In order to prevent the crystal from sliding while making larger angular adjustments; stopper pins covered with rubber are placed on the sides of the crystal.

4.4 Keeping the analyzer stable at the required analyzer angle

Because of the thermal drifts caused by the environmental conditions, the analyzer angle may change while the image is actually taken. To protect the assembly from environmental conditions, the analyzer crystal is fully enclosed by a box type design made of aluminum plates. The light beam enters and exits the box via a kapton filter which absorbs negligible amounts of the beam's energy coming from the monochromator.

4.5 Working principle of the precise positioning system

During the imaging process, the angle of the analyzer crystal needs to be adjusted to take i-

mages on various points of the rocking curve. In the system, a 1 m long tangent bar is used to adjust the angle of the analyzer. This is done using a motorized actuator which is fixed at the bottom end of the tangent bar. The top of this tangent bar is clamped to the shaft using a pneumatic cylinder. While adjusting the angle of the analyzer, this pneumatic cylinder will be engaged. The linear movement of the actuator is converted into a rotary motion of the shaft using the tangent bar. The linear range which can be obtained from this actuator is 12 mm and the change in angle that can be obtained is 0.01 microradians (Figure – 4.1). If there is any need to make more angular changes, the shaft is clamped at the adjusted angle using the shaft holder on both sides of the tangent bar head

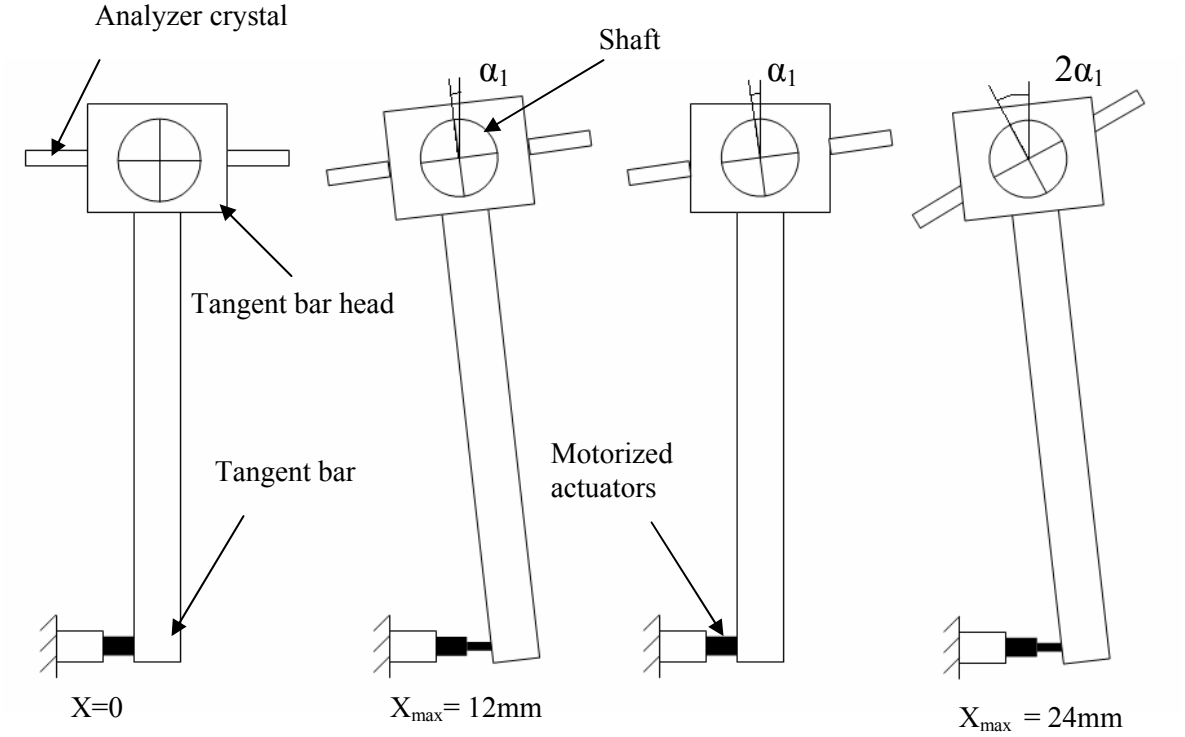

Figure – 4.1 Micrometer positions

which were controlled by the pneumatic cylinders. Then the tangent bar is unclamped from the shaft and returns to its initial position by disengaging the other pneumatic cylinder. Then the whole process repeats again for the angular adjustment of the analyzer. The tangent bar motion in the Z axis is restricted by two metal pieces called tangent bar holders placed on both sides of tangent bar as shown in Figure – 4.2. The pneumatic cylinders are fixed to the corner cube using a piece of

metal this actuator rests on the magnet which is attached to the end of the tangent bar using a holder. The bearing holder is used to reduce vibration of bearings during rotary motion and for restricting the linear movement of the shaft by giving a certain preload (See 4.6.1) on both sides. This bearing holder will be fixed to both ends of the granite block so that the crystal stays inline with the beam.

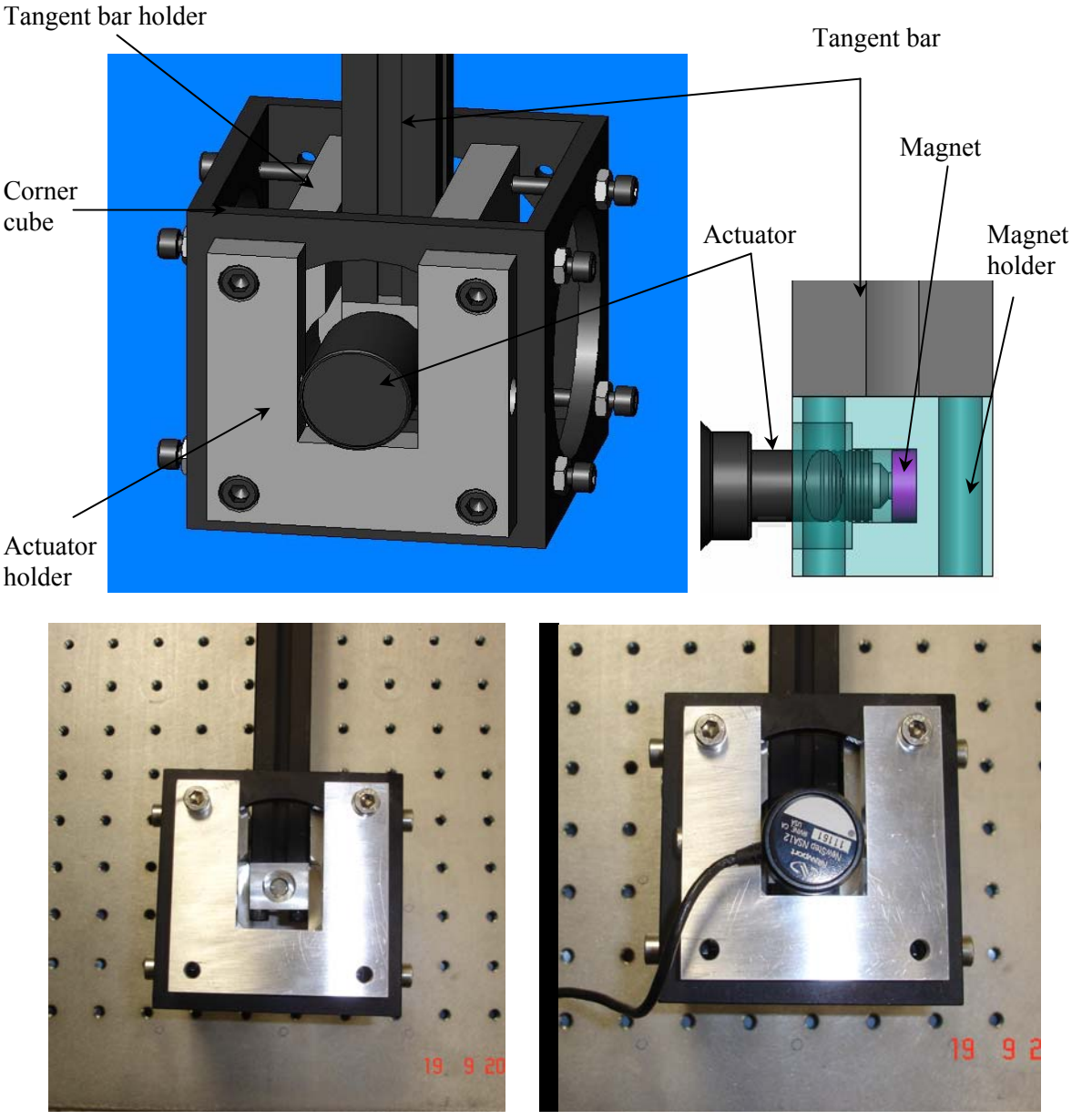

Figure – 4.2 Tangent bar, actuator and magnet holder

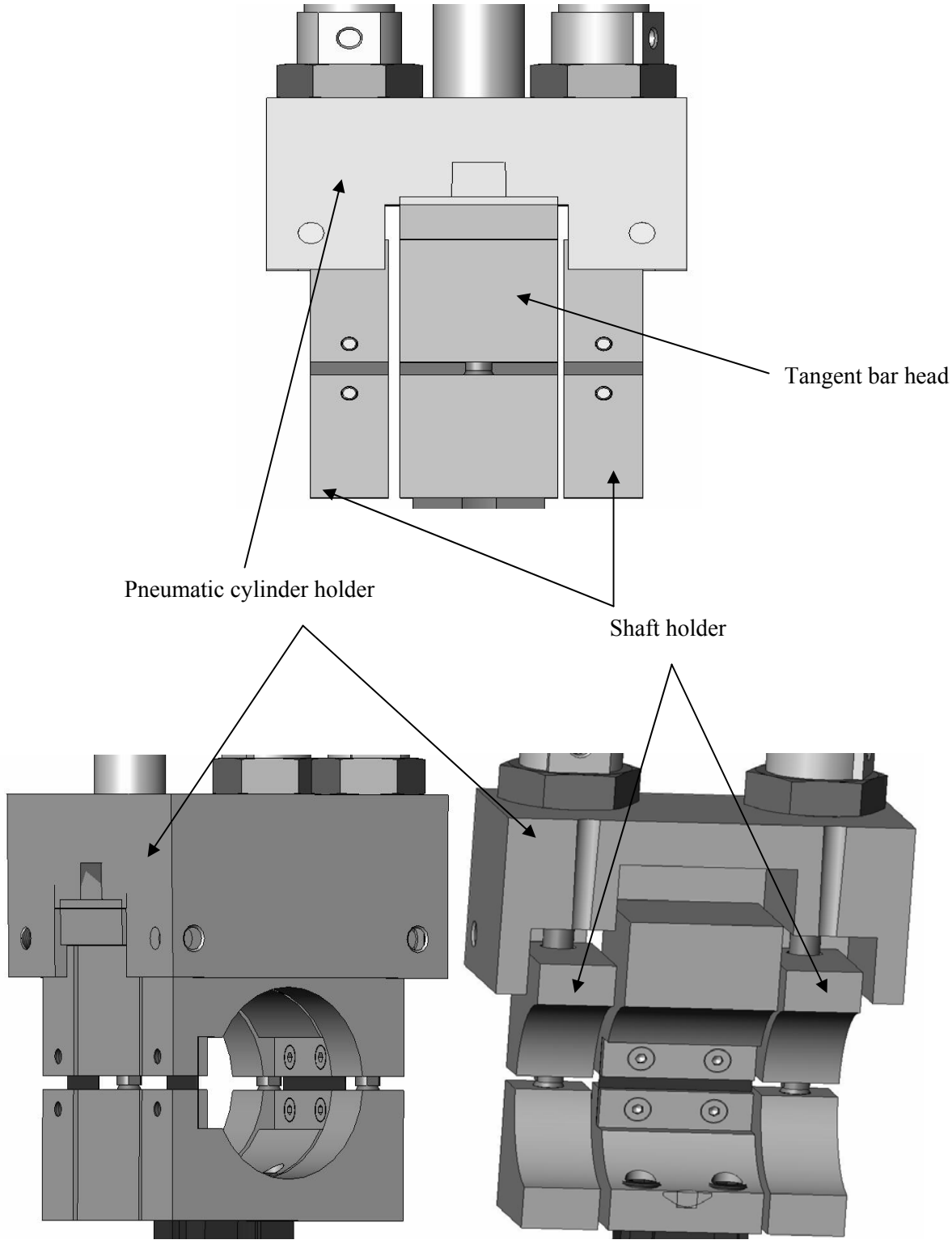

Figure – 4.3 Shaft and the pneumatic holder

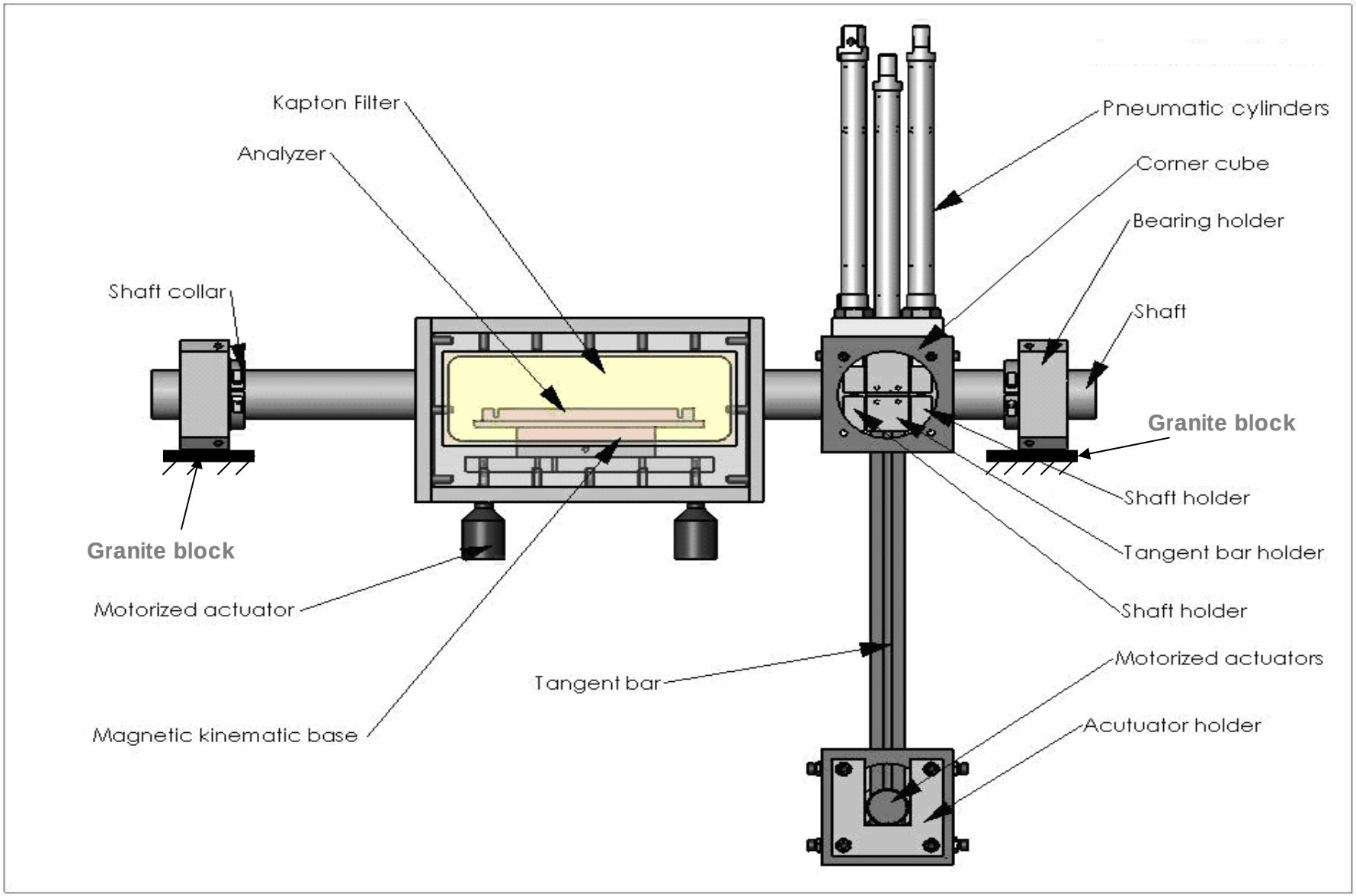

Figure – 4.4 Front view of DEI analyzer assembly

Figure – 4.5 DEI analyzer assembly

The shaft collars are used on both sides of the bearings to restrict their linear movement (Figure – 4.3). For adjusting the crystal in X, Y and Z axes and to keep them inline with the beam, three motorized actuators were attached to the base-plate in which the crystal is attached. Figure – 4.4 shows the front view of the analyzer assembly with different parts indicated. In Figure – 4.4, the length of the tangent bar is reduced from 1 m to 0.15 m to give a clear picture of the assembly. The selection of particular parts for the analyzer assembly shown in Figure – 4.5 will be discussed next.

4.6 Selection of bearing

During imaging, the change in angle required to rotate the analyzer crystal is in the order of micro-radians, so bearings with high precision called high precision single row angular contact bearings made by SKF bearings were used in this analyzer assembly. These angular contact bearings are used in this system on both shafts at one of the ends so that the analyzer angle can be changed precisely. These bearings produce minimal beating during the rotation and also have the least friction torque than any other bearings available. These bearings are designed in such a way that they can support combined radial and thrust loads or heavy thrust loads depending on the contact angle magnitude. The other advantage of this kind of bearing is that the axial movement of the bearings can be prevented by applying a certain amount of preload (See 4.6.1). These bearings are required to be sealed, which prevents foreign matter to enter the bearing area.

Figure – 4.6 shows this type of bearing and the places where they are used in the analyzer assembly. To stiffen the assembly in the axial direction, these bearings can be preloaded.

4.6.1 Preload

For the angular contact ball bearings, a certain amount of preload should be applied so that it will not have movements in the axial direction when the shaft is rotated [17]. The amount of preload recommended by the bearing manufacturer is 60 N. As shown in Figure – 4.6, two bearings were used in this system; they should be preloaded in the opposite direction so that the motion of

the shaft in the axial direction can be restricted. For giving the preload, the inner race of the bearings will be restricted from moving by the use of the shaft collars shown in Figure – 4.7, designed especially for fitting the inner race of these high precision angular contact bearings. For giving the preload to these bearings a special cage is designed in such a way that the preload can be applied by pressing the bolts against the outer race of the bearings. Figure – 4.8 shows the bearings in the experimental setup. For restricting the movements of the outer race after the preloading, M6 threaded holes were made on the cage for tightening them on the diagonal positions. Figures – 4.9 & 4.10 shows the sectional view of the bearing cage with preloading given on the outer race of the bearing.

In this new design, the 4 mm threaded holes which were on the front face will be used for preloading according to the requirements and the 6 mm threaded holes on the edges will be used for fixing the bearing outer race from moving after the preload has been given.

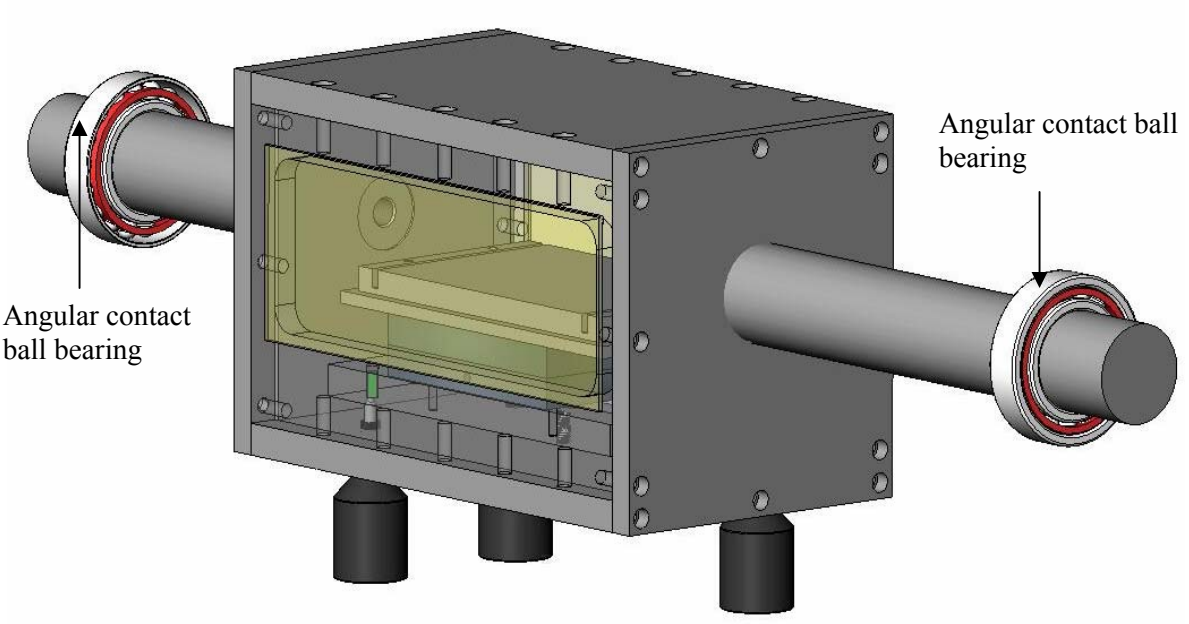

Figure – 4.6 High precision single row angular contact ball bearing

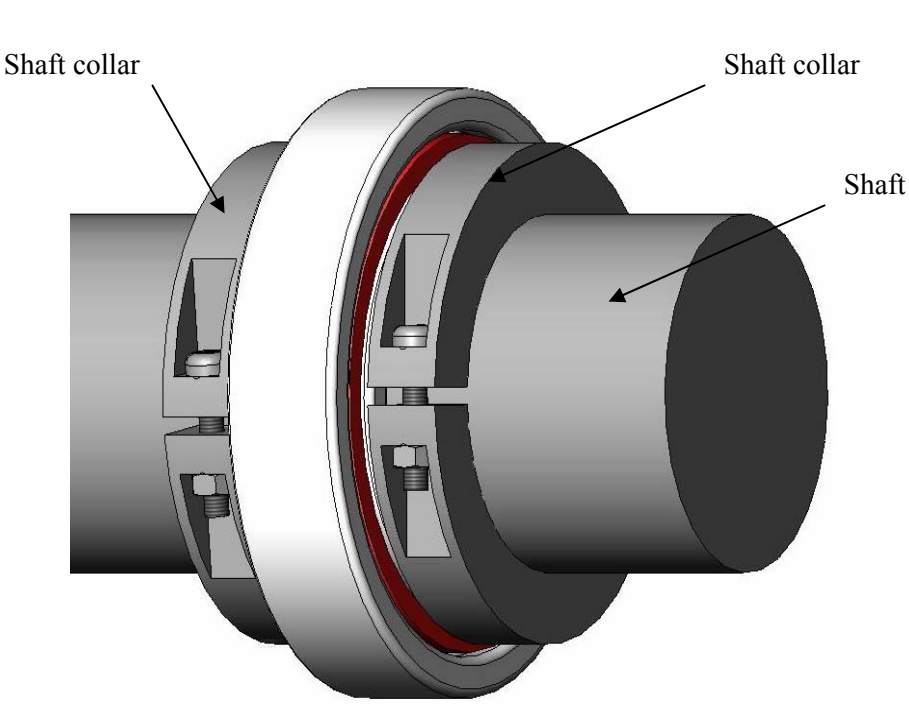

Figure – 4.7 Bearing with collar

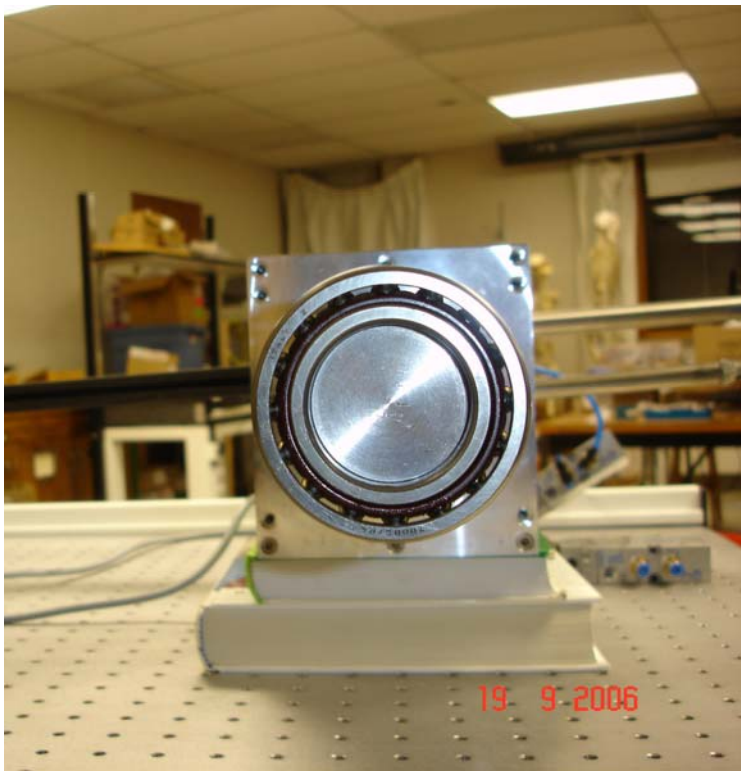

Figure – 4.8 Bearing with collar (experimental setup)

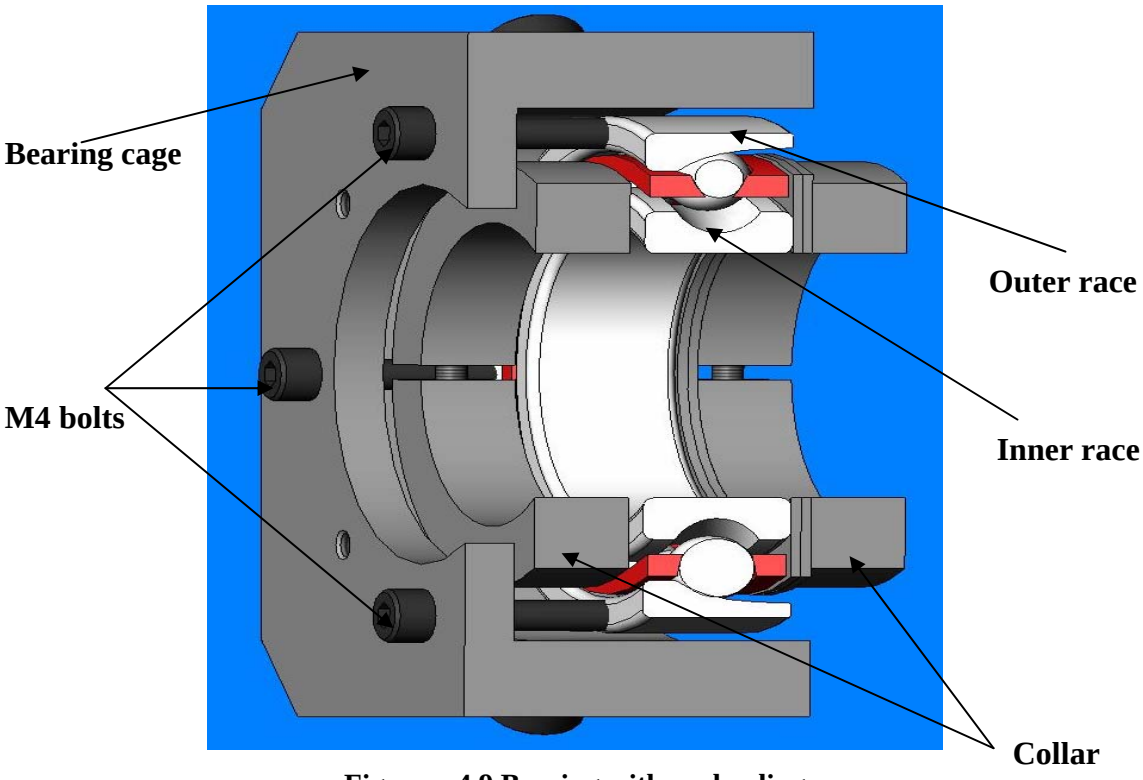

Figure – 4.9 Bearing with preloading

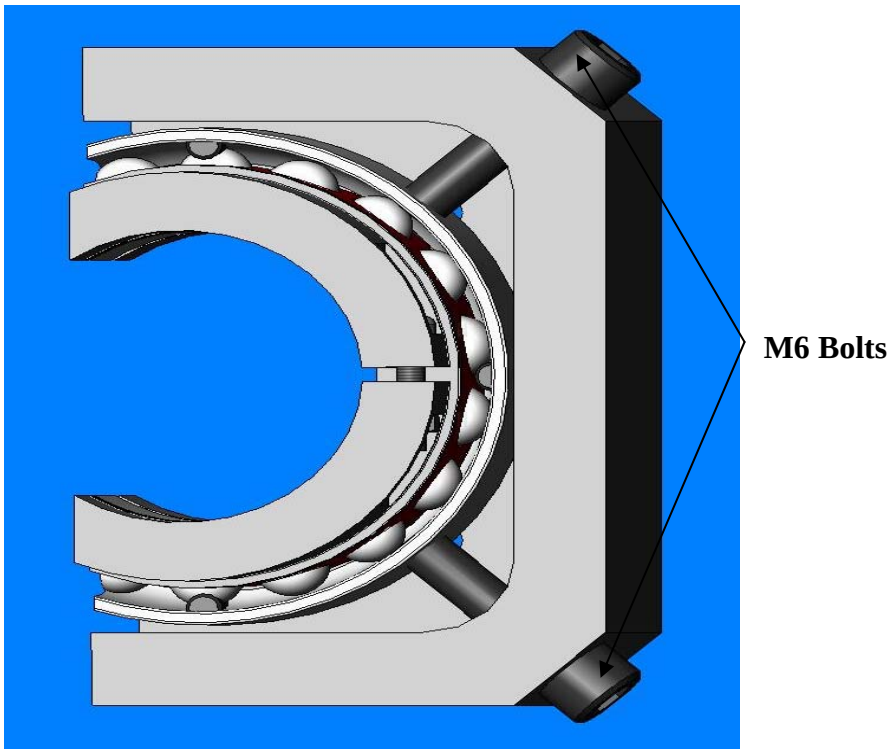

Figure – 4.10 Bearing with preloading

Then the bearing cage will be moved to the required position and the preloading will be applied by using the M4 bolts made of steel along the outer race of the bearings. After the required preload is given, M6 bolts will be tightened against the top face of the bearing outer race so that the bearing will not move during the angular adjustments of the analyzer assembly.

4.6.1.1 Calculation of the torque required to generate a desired preload

The torque required to generate a desired preload is according to Motosh [18]

$$T_{in} = F_P \times \left(\frac{P}{2\pi} \times \frac{\mu_r r_t}{\cos\beta} + \mu_n r_n \right) \tag{4.1}$$

Where T_{in} – torque applied to the fastener, N.mm

Preload created in the fastener, $F_P = 60$ N

Pitch of the threads, P = 0.7 mm

Coefficient of friction between nut and bolt threads, $\mu_t = 0.1$ (Assumed)

$$\text{Effective contact radius of the threads, } r_t = \frac{D + E_{smin}}{4} = \frac{4 + 3.33}{4} = 1.825 \text{ mm} \tag{4.2}$$

Half-angle of the threads, $\beta = 30^o$

Coefficient of friction between the face of nut and the upper surface of joint, $\mu_t = 0.1$(Assumed)

Effective radius of contact between the nut and joint surface, $r_n = 0.6 \times D = 0.6 \times 4 = 2.4$ mm

Therefore,

$$T_{in} = 60 \times \left(\frac{0.7}{2\pi} \times \frac{0.1 \times 1.825}{\cos 30^\circ} + (0.1 \times 2.4) \right) = 33.6 \text{ N.mm}$$

Thus the desired preload of 60 N can be generated by applying a torque of 33.6 N.mm using a calibrated torque wrench.

4.6.2 Piezo-electric actuator

Actuators made of piezoelectric material are used in the new analyzer assembly. In this system for controlling the angle of the crystal which is inside the analyzer box, piezo-electric

actuators are used. These are positioned at three places in a diagonal above the micrometer motor, so that the Bragg angle and the azimuthal angle can be adjusted accurately in some tens of micro-radians. At a maximum voltage of 150 V or the maximum clamping force of 425 N, the maximum displacement that can be obtained for this actuator is 17.4±2 µm. The sole purpose of using the piezoelectric actuator here is to enable automatic position sensing and keep the analyzer crystal stable when there are any changes in angle due to vibration.

The piezo-electric actuator made by Thorlabs Inc. already available in the lab was used in this system. This actuator consists of multiple layers of piezoelectric sheets. The model name of the actuator is AE0505D16 (see Figure – 4.11). A piezo-electric material possesses a crystalline structure of lead zirconate titanate PbZrO3-PbTiO3 (PZT), which is the primary component of the piezoelectric material [19]. The crystalline structure of the PZT controls the behavior of the Piezo-electric material. The forces that will be acting on the piezoelectric actuators were calculated to make sure that the actuators serve the purpose.

In the Figure – 4.12 the points A, B and C represent the positions of piezo-electric actuators. The weight of the crystal, crystal base plate, magnetic kinematic base and the plate with piezo resting on the piezo-electric actuators are 0.326 kg, 0.387 kg, 0.707 kg and 0.619 kg respectively.

Figure – 4.11 Piezo-electric actuator [21]

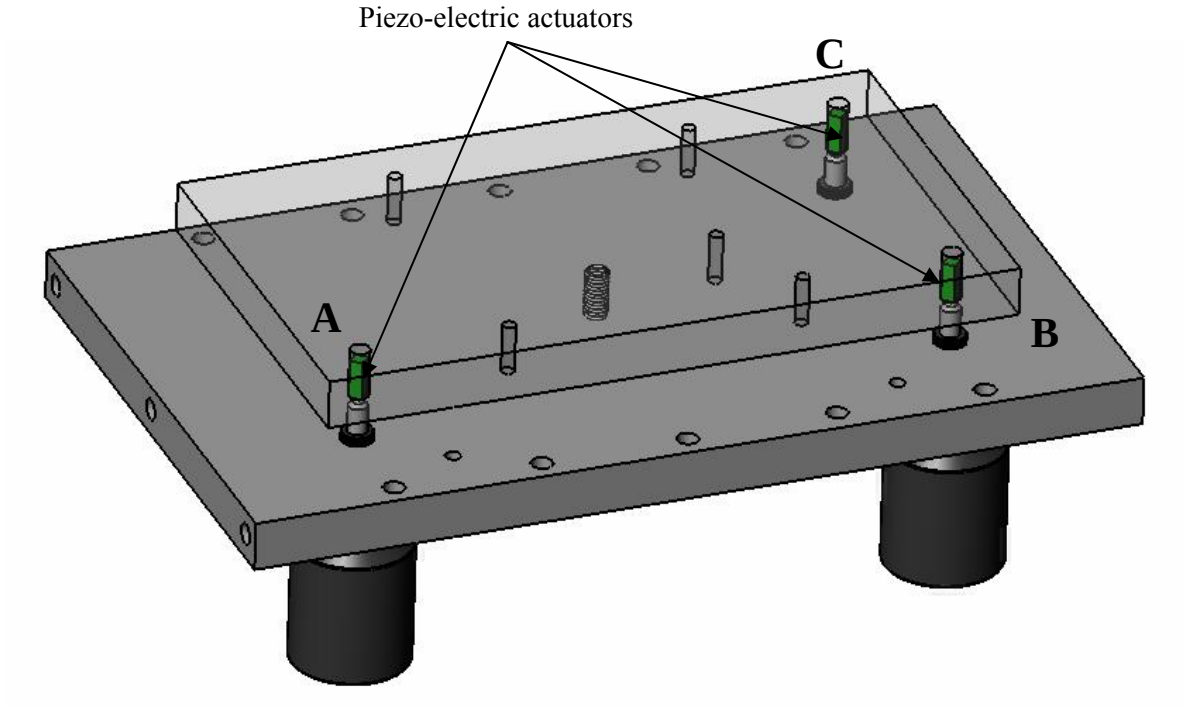

Figure – 4.12 Positioning of piezo-electric actuators

The total mass resting on the piezo electric actuators is 0.326 + 0.387 + 0.707 + 0.619 = 2.039 kg or a weight of 19.98 N. As A and C are in diagonal to each other, and the forces acting on each of the piezo-electric actuator are $F_A = 9.99$ N, $F_B = 0$ and $F_C = 9.99$ N.

The maximum load which a piezoelectric actuator can carry is 425 N and the force which it holds is 9.99 N, so the actuators should be able to control the movement of up to about 17 μm.

4.6.3 Motorized actuators

Four motorized actuators were used in this analyzer assembly, out of which three actuators were attached to the bottom of the analyzer box for adjusting the Bragg and azimuthal angle of the analyzer crystal. The remaining actuator is used for adjusting the angle of the analyzer box as a whole. Figures – 4.13 & 4.14 shows the positions where these actuators were attached.

Newport's motorized actuator and controller are used in this new DEI assembly. These actuators are compact in size (only 60 mm long x 30 mm diameter). The actuator and controller have been designed for remote adjustment of optical mounts which can be influenced by the compr-

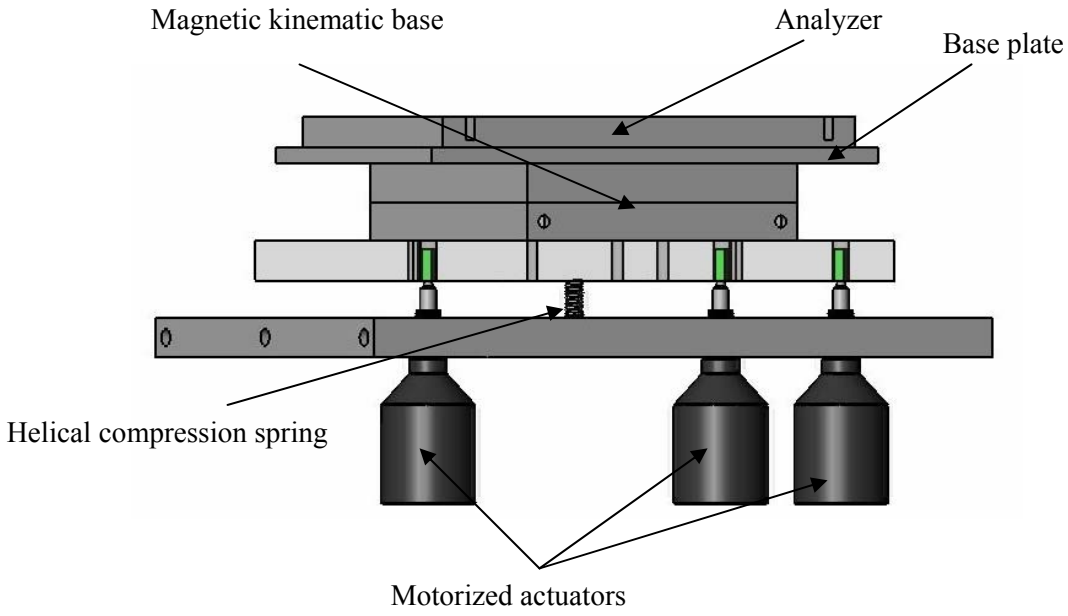

Figure – 4.13 Motorized actuators for crystal adjustment

Figure – 4.14 Motorized actuators for crystal adjustment

essive and torsional forces imposed by manual adjustment micrometers. These actuators can also be automated using LabVIEW or other software by sending commands to the controller.

These actuators can be used for loads up to 28 N and they have a reliable open-loop stepper motor which provides 12mm travel with a sub-micron level minimum incremental motion. For protecting the equipment damage from over-travel, these actuators are fixed with an integrated minimum travel optical limit switch. To avoid the periodic motion variations which may occur in rotating actuators, these are equipped with a non-rotating tip which also prevents wear [28].

The important feature of these actuators is that they incorporate a novel spring mechanism that virtually eliminates backlash which is critical in adjusting the angle of the analyzer. The actuator at the bottom end of the tangent bar was held tightly with a holder as shown in Figure – 4.2, to stop any vibrations. The holder is bolted to the corner cube which is fixed to the granite block.

4.6.4 Selection of spring

In order to make the Bragg and azimuthal angle adjustments of the analyzer crystal easier, a helical compression spring (See Figure – 4.13) is used in DEI system to keep together the analyzer crystal, base plate and the magnetic kinematic base in contact with the tip of the motorized actuators. This spring supports the crystal, crystal base plate and the magnetic kinematic base whose total weight is nearly 19.99 N. A helical compression spring which can support a weight of 100 N is used in this system. Assuming that the material used is stainless steel, the maximum shear stress value is taken as 500 MPa. As already assumed the maximum force as 100 N, a selection of wire, mean diameter and the number of coils of the helix can be calculated from spring stiffness.

$$\tau = \tau_{torsion} + \tau_{direct} = T_s\, r/J + F/A \qquad (4.3)$$

$$= (FD/2)\,(d/2)/\,(\pi d^4/32) + F/\,(\pi d^2/4) = (1 + 0.5d/D)\; 8\, FD/\pi d^3$$

$$\text{Spring stiffness, } k = Gd^4 / 8nD^3 \qquad (4.4)$$

where τ_{direct} is the shear stress due to direct compressive force [N/m^2], $\tau_{torsion}$ is the shear stress due to torsion [N/m^2], T_s is the torsion in the spring, F is the force on the spring, A is the area, D is the mean diameter of the spring, r is the radius, G is the shear modulus and n is the number of coils in the spring.

4.6.5 Magnetic kinematic base

In the existing analyzer assembly, there is no easy way to adjust the crystal position because the crystal is clamped to the base plate using bolts. In the new design of the analyzer assembly, a magnetic kinematic base from Thorlabs shown in Figure – 4.15 is used for holding the crystal and the base plate. With this magnetic kinematic base, the crystal can be held tightly and the crystal adjustments can be made easily.

Figure – 4.15 shows the magnetic kinematic base where the crystal supported by a base plate can be fixed in the analyzer assembly. This kinematic base consists of two plates: a top mounting plate and a bottom base plate. The two plates are magnetically coupled using two pairs of high strength magnets. The top plate can be removed and replaced, automatically repositioning to an exact location with the repeatability of a micro-radian. The bottom plate can be fastened to an optical bench using two M6 clearance slots. These mounting slots can also be accessed with the top plate in place. The main advantage of using this type of magnetic kinematic base is that it is stiff enough and also the crystal can be clamped at any place as there were 18 holes on the top plate along this mount. This reduces the wear and tear of the crystal, as there is no need to make any threaded holes to change the position of mounting and also saves the time.

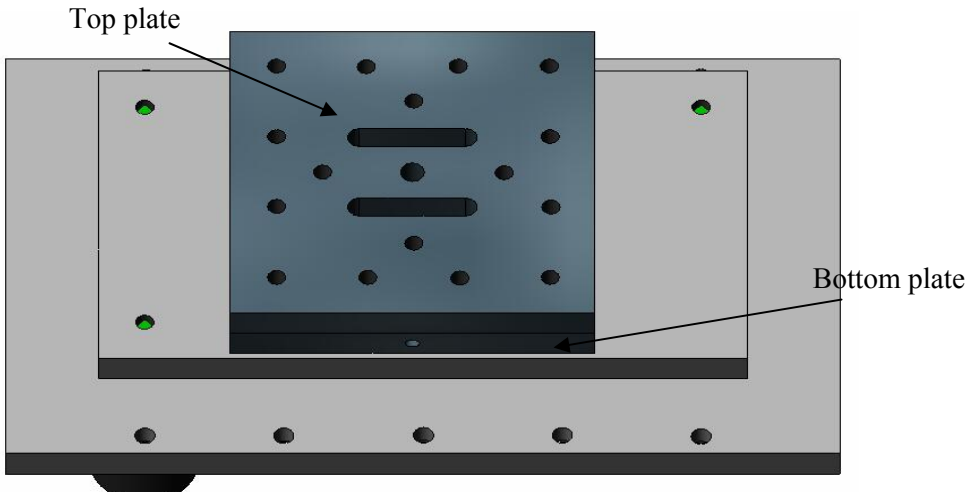

Figure – 4.15 Magnetic kinematic base

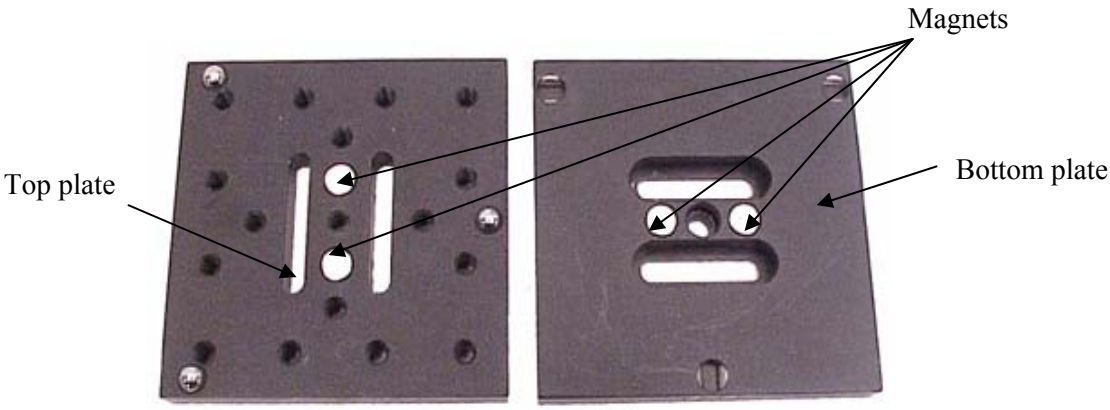

Figure – 4.16 Magnetic kinematic base [21]

4.7 Summary

In this chapter, the measures taken to reduce the vibrations due to the internal factors and environmental conditions were discussed and then the steps on how to keep the crystal stable for taking images on the rocking curve during experiments in the new DEI assembly were described. Finally, this chapter described in detail about the selection and design of various parts for the new DEI analyzer assembly. Next chapter will discuss about the pneumatic system which will be used for adjusting the angle of the analyzer crystal.

CHAPTER – 5. DESIGN OF A SYSTEM FOR LARGER ANALYZER ANGLE ADJUSTMENTS

5.1 Introduction

With the DEI system, the angular adjustment of the analyzer crystal is very critical as the images are taken at different points on the rocking curve which is in the range of some tens of nano-radians. This is achieved in the current setup by using a tangent bar arrangement which is driven by a stepper motor. The linear motion of the stepper motor is converted into the rotary motion of the crystal which is attached to the shaft by using the tangent bar. As the micrometer motor has only a limited displacement range (which is 12 mm), the analyzer angle that can be changed is also limited. If there is any need to make more angular adjustments, it is done in the current system manually by locking the rotation of the shaft using a set screw and disengaging the connection between the shaft and the tangent bar and taking the tangent bar back to the original position it was before. This was explained in Chapter – 4 (see Figure – 4.1). With such a method of changing the angles manually, there is a possibility to miss some points on the rocking curve. This also makes the imaging process more time consuming. To make the angular adjustments more precisely and make this process easy, a control system with pneumatic locks is being used in the new setup. This chapter will discuss in detail the pneumatic system which will be used in the new setup.

5.2 Working of a pneumatic lock system for an analyzer assembly

The new DEI assembly has three pneumatic cylinders in which one cylinder will be used to disengage the tangent bar (Figures – 5.1 & 5.4) from the shaft and the other two will be used to holdthe shaft precisely at the same angle of rotation. In the new design (Figure – 5.1), the tangent bar and the shaft are compressed together tightly by using a piston rod of the cylinder on the tangent

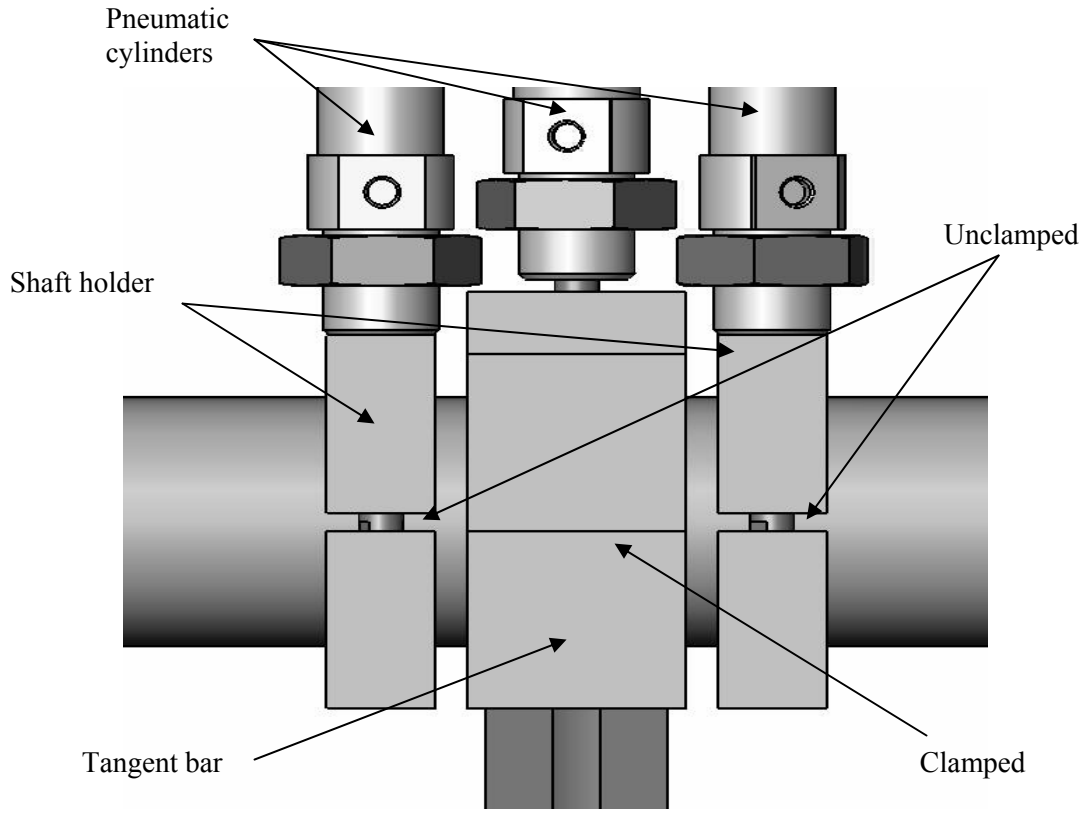

Figure – 5.1 To drive the shaft for angular adjustments

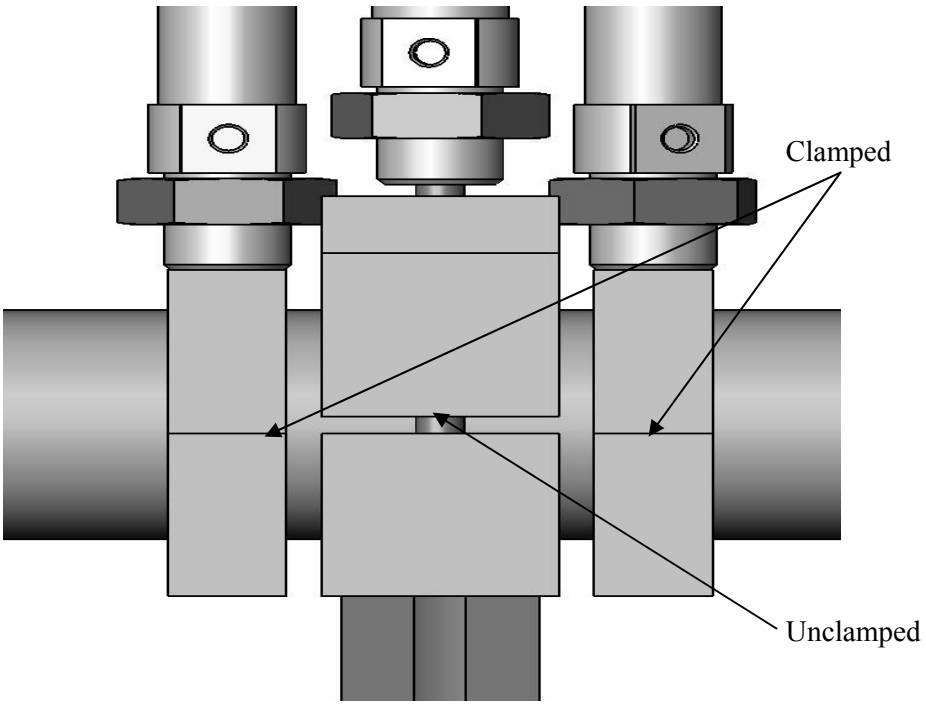

Figure – 5.2 To hold the shaft for large angular adjustments

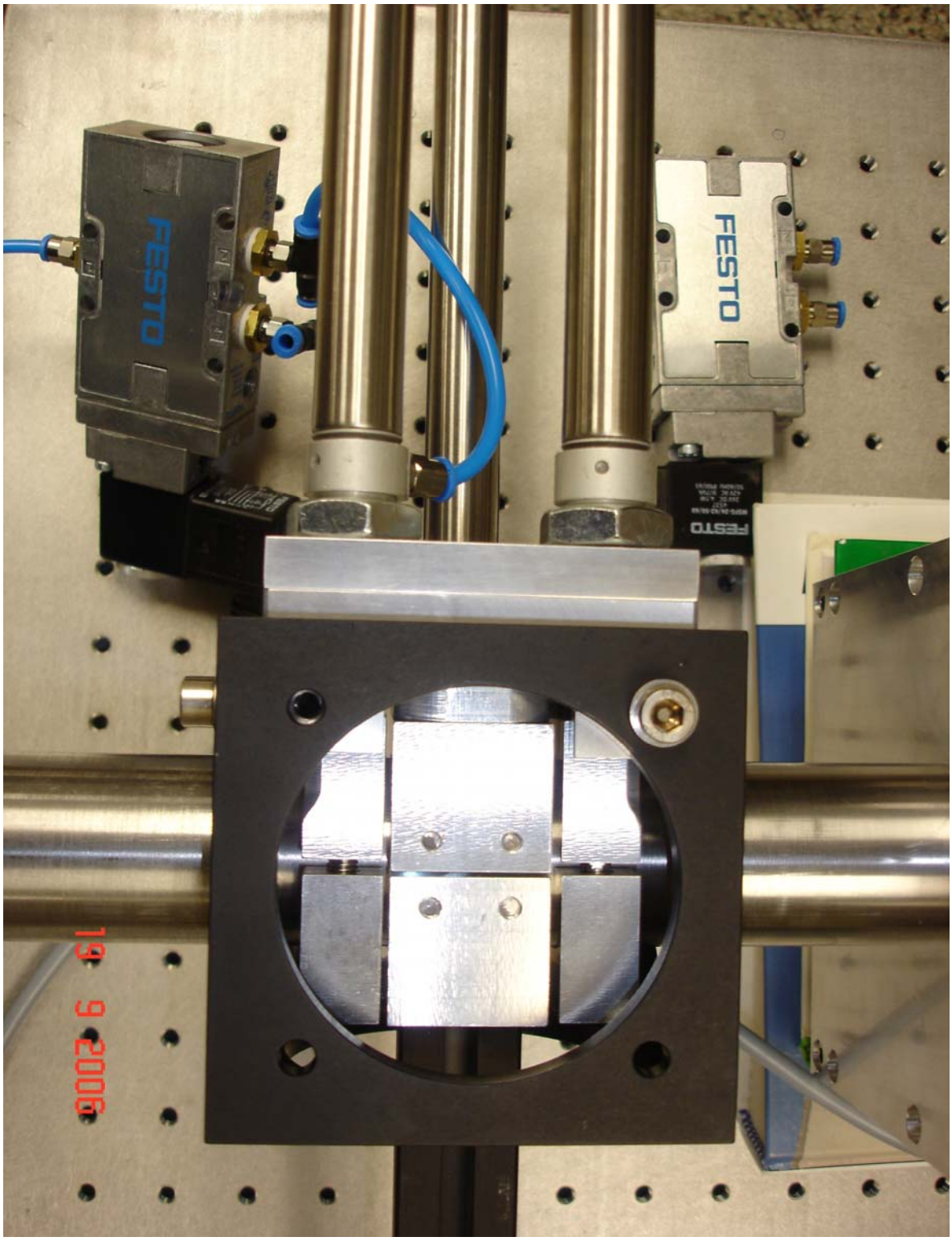

Figure – 5.3 Pneumatic lock system (experimental setup)

bar head. When there is a requirement for making larger angular changes of the analyzer, two of the pneumatic cylinders will be used to hold the shaft firmly in its position first (Figure – 5.2) and then the tangent bar will be disengaged from the shaft using the other pneumatic cylinder. As the air supply is only required for fractions of seconds to make larger angular adjustments if required, this system is not prone to oscillations due to air supply.

In keeping the tangent bar effectively in contact with the shaft, the contact area plays an important role. To increase the contact area, the tangent bar head was designed in such a way that there will be some gap between tangent head faces which connects the tangent bar with shaft .While applying the axial force to keep the tangent bar head in contact with the shaft, there were some chances that plastic deformation will occur on the central part of opposite side of the tangent bar head. So in this setup, the tangent bar head is made of two pieces of aluminum and are connected together by a sheet metal plate made of spring steel on the opposite side where axial force is applied by the cylinder. The diameter of the hole in the tangent bar head is kept as 42 mm instead of the shaft size of 40 mm, as the contact could be made with the shaft exactly at the centre. The tangent bar holder is shown in the Figure – 5.4. The same principle is used in the design of the shaft holder too (Figure – 5.5), except that the shaft holder will be fixed to the pneumatic cylinder holder which is connected to the corner cube fixed on the optic table.

5.2.1 Selection of pneumatic cylinder

A certain amount of torque should be applied in order to rotate the shaft with the analyzer mount box. This torque can be calculated from (see Figure – 5.6) [22],

$$T = W_a \times a \times \sin\alpha_{max} \tag{5.1}$$

where W_a – weight of the analyzer mount box with crystal

a – distance between the centre of shaft and centre of gravity of analyzer mount box

α_{max} – maximum angle of rotation of the analyzer mount box

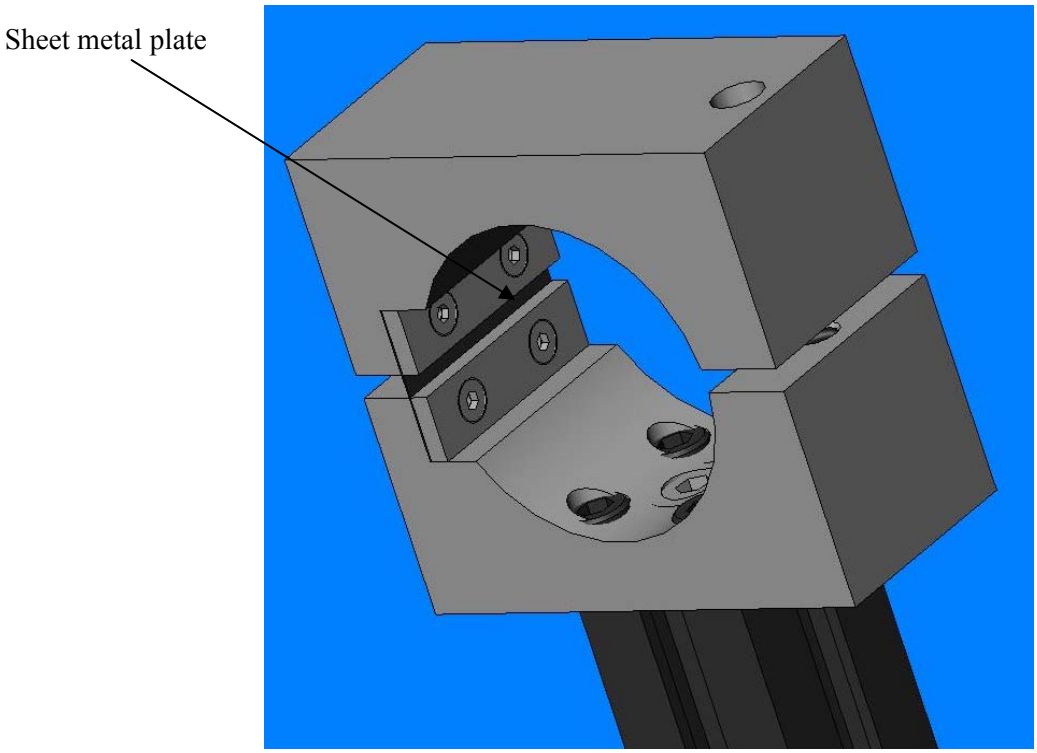

Figure – 5.4 Tangent bar head

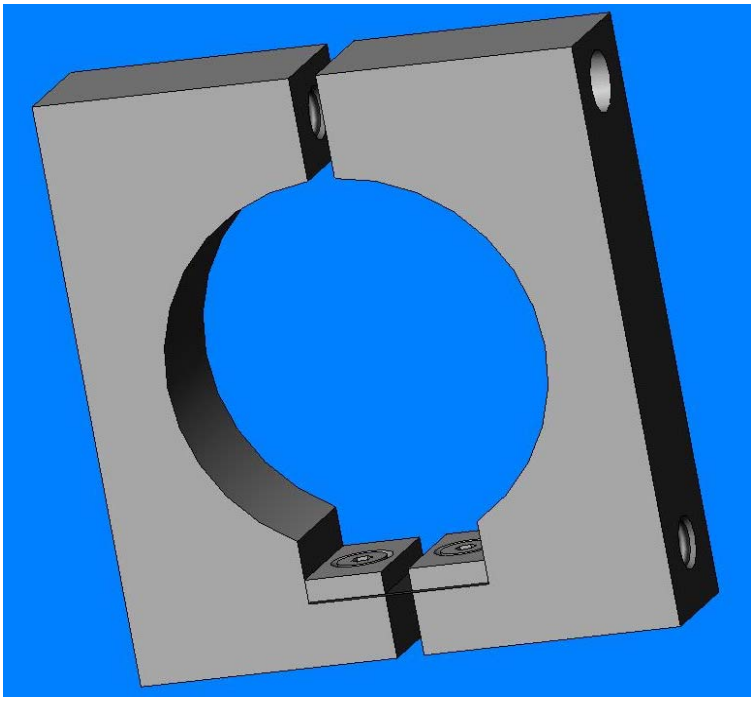

Figure – 5.5 Shaft holder

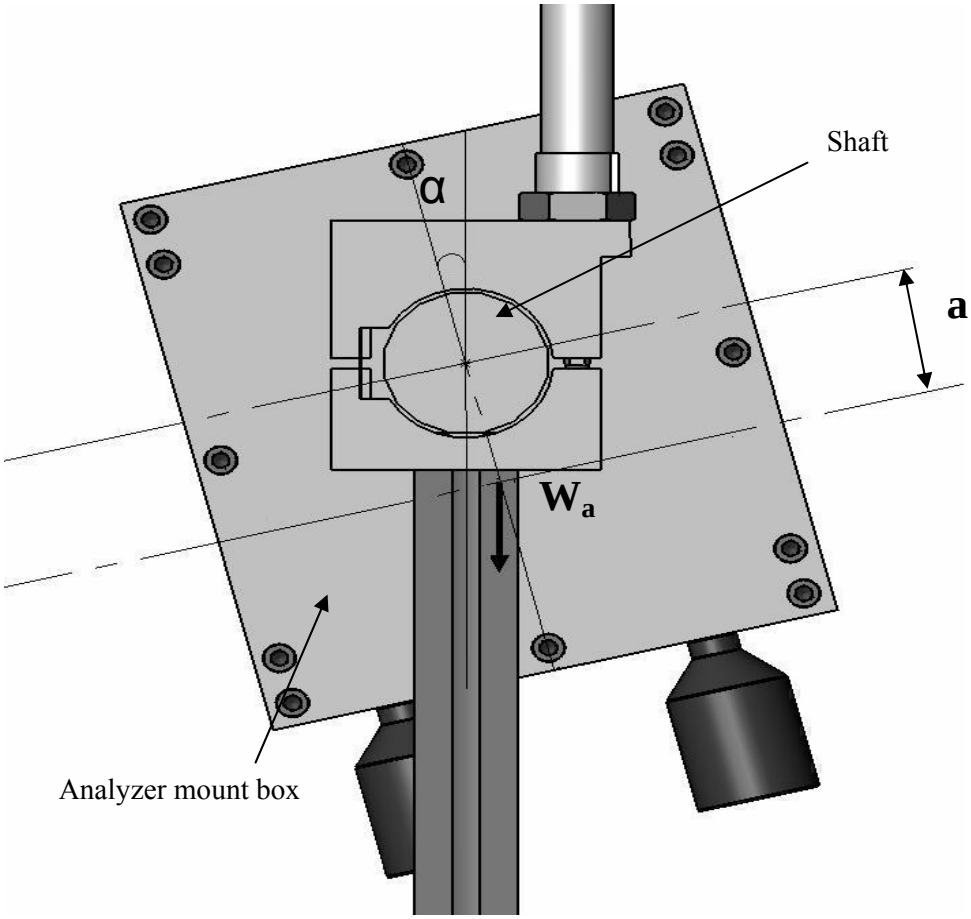

Figure – 5.6 Torque required to rotate the mount box

The above equation defines the torque to be generated by this motorized actuator at the efficiency of the tangent bar and then transmitted by this shaft holder.

5.2.2 Calculation of the centre of mass for analyzer mount box

To find the centre of gravity of the analyzer mount box, the bottom area of the cross plate is considered as the reference axis and the centroid for every part is calculated based on this reference axis (see Figure – 5.7). The mass and the centre of mass for each of the parts in this assembly are given in Table – 5.1

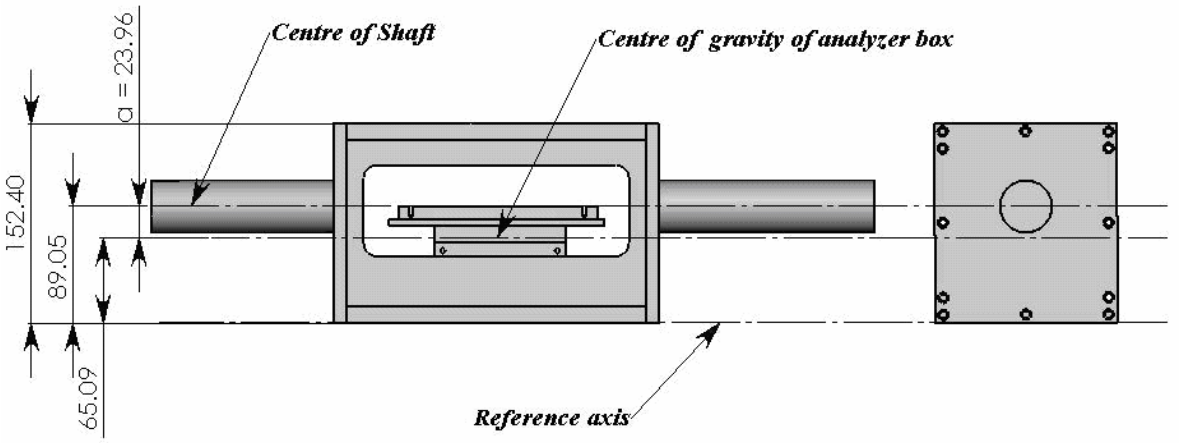

Figure – 5.7 Diagram showing the centre of gravity (all dimensions are in mm)

Table – 5.1 Calculation of the centre of gravity of analyzer mount box from shaft axis

No	Part name	Volume (V)×10^3 mm^3	Mass (m)kg	Centroid $\bar{y}$ mm	$\bar{y} \times m$ kg.mm
1	Silicon crystal	126.00	0.29	71.2	20.90
2	Crystal support plate 1	82.50	0.22	63.7	14.01
3	Kinematic base	262.19	0.71	48.5	34.44
4	Crystal support plate 2	82.50	0.62	30.2	18.72
5	Micrometer motor	-	0.40	15.1	6.04
6	Cross plate (Top)	405.58	1.09	146.05	160.51
7	Cross plate (Bottom)	405.58	1.09	6.35	6.98
8	Face plate (Front)	188.40	0.51	76.05	38.79
9	Face plate (Back)	188.40	0.51	76.05	38.79
10	End plate (Left)	270.39	0.73	76.2	55.93
11	End plate (Right)	270.39	0.73	76.2	55.93
			∑m =6.93		$\sum \bar{y} \times m = 451.04$

The centre of mass for every part in the analyzer assembly has been calculated in the Appendix.

$$\text{Centroid : } \bar{y} = \frac{\Sigma \bar{y} \times m}{\Sigma m} = \frac{451.04}{6.931} = 65.09 \text{ mm} \qquad (5.2)$$

Centre of the shaft = 89.05 mm

Distance between shaft axis and centroid of analyzer box = a = 89.05 − 65.09 = 23.96 mm

From (5.1), $T = W_a \times a \times \sin\alpha_{max} = 6.931 \times 9.81 \times 23.96 \times \sin 90^o = 1629.11$ N.mm

It is evident that this torque must be transmitted by the friction between the shaft and the shaft holder. The holder will be preloaded with the force F generated by this pneumatic cylinders. The relationship between this force and the torque can be derived by using the diagram of forces shown in the Figure – 5.8

$$\text{Torque} = 2 \times \mu \times F \times 2 \times R \qquad (5.3)$$

We have

Radius of the shaft, R = 20 mm

Mass of the crystal assembly = 6.93 kg

Substituting the values into the equation (5.1),

$1629.11 = F \times 2 \times 0.25 \times 2 \times 20$

$F = 81.46$ N

Therefore, the preload force required to engage the tangent bar to shaft, F = 81.46 N

For selecting the bore of the cylinder we already have the sufficient details about the force required. The normal pressure used in the design of the pneumatic cylinders is 4 bar (4×10^5 N/m^2), but for adjusting the angle of the analyzer assembly the maximum pressure of P = 10 bar is chosen.

Maximum pressure the cylinder can withstand = 10 bar.

$$\text{Since } F = P \times \frac{\pi}{4} \times D_B^2 \qquad (5.4)$$

$$10 \times 10^5 = \frac{81.46}{\frac{\pi}{4} \times D_B^2}$$

Required bore diameter of the cylinder, $D_B = 10.187$ mm .

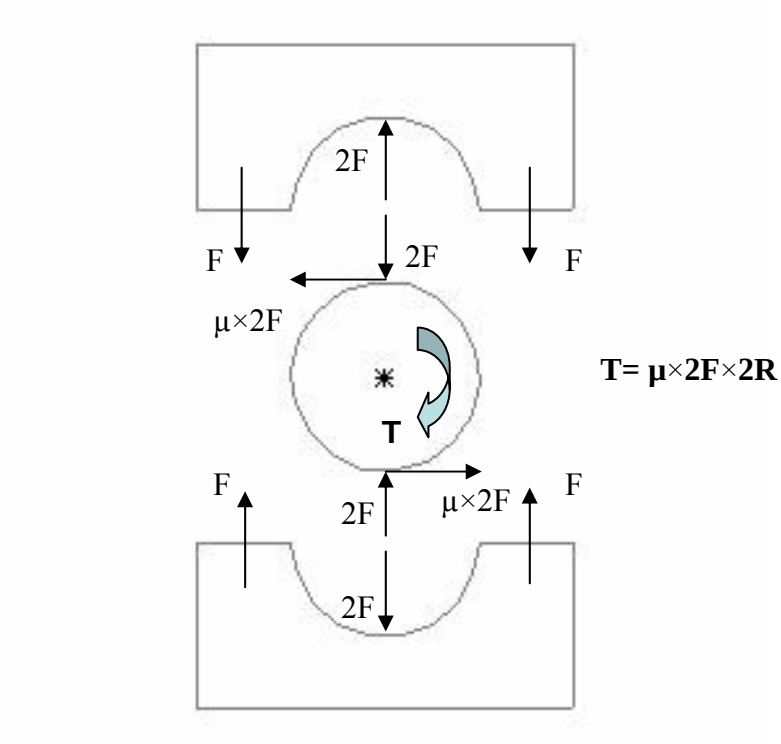

Figure – 5.8 Diagram of forces for the holder-shaft connection

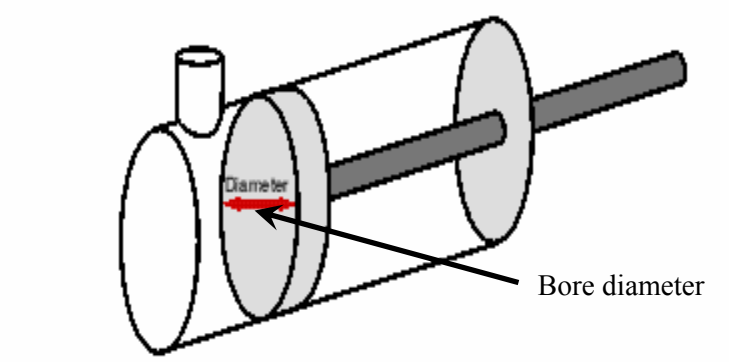

Figure – 5.9 Bore diameter [24]

To provide some margin for the proper operation of the system, the cylinder bore of 16 mm is chosen. With this bore diameter (Figure – 5.9), the force F = 81.86 N will be obtained approximately at 4 bar. The single end double acting cylinders manufactured by FESTO (Figure – 5.10) were chosen for this system.

Figure – 5.10 FESTO pneumatic cylinder [24]

This type of cylinder has two air connections. When compressed air is applied to one connector, the other connector will allow the air to exhaust to atmosphere and at this stage, the piston is driven to one end of the cylinder. When air is applied to the second connector, the first connector will allow the air to exhaust to atmosphere and the piston will return back to its initial position. In this type of cylinder, the piston is effectively locked in position at both ends of its stroke. Three cylinders used were of standard double acting cylinder type. Double acting means that the pressure can be applied on both sides of the cylinder for controlling the piston movement [24]. The theoretical force that can be obtained at 6 bar compressor pressure for advancing movement is 121 N and for retracting movement is 104 N [24]. The stroke length of the cylinders chosen were 160 mm as because the shaft and the tangent bar holder heads were 30 mm length and the pneumatic cylinder holder is also 60 mm above the threaded portion of the bottom holders.

5.2.3 Compressor

The compressor provided by Thorlabs Inc. for use in optical tables is used in the new analyzer assembly. The compressor will put out approximately 10 bar before the relief valve opens. Because the compressor can produce a significant amount of vibration, vibration isolation mounts

were used in analyzer assembly design. In order for these to isolate the vibration, they were mounted to a 1/4" aluminum plate.

5.2.4 Manual and electrically controllable solenoid valve

Two position and 5 port double solenoid valves from FESTO are used for controlling the air supplied to the cylinders. In a double-acting cylinder both the instroke and outstroke are controlled by compressed air - not just the outstroke as in a single-acting cylinder. Double-acting cylinders are usually controlled by a more complicated valve called a five-port valve**.** If one pulse of the solenoid is used to make the cylinder extend, then the pulse on opposite solenoid is used to make it retract [22].

If the power is turned off in a single solenoid valve, the valve would return back to its original position and the cylinder will retract but a double solenoid valve will maintain its original position until the opposite solenoid is turned on [23]. The valve requires a minimum pressure of 1.38 bar to work. The valve comes separate from the coil and must be assembled to it. The solenoid valve is of 24V DC type because of the computer-based control system requirements. Figures – 5.10, 5.11, 5.12, 5.13 shows the solenoid valve coil and the connections used for fitting the tube to the valve and the cylinder respectively.

5.3 Summary

This chapter discussed in detail about the working principle of the double solenoid valve controlled pneumatic lock system which is used for making larger angular adjustments of the analyzer crystal in the modified DEI assembly. The selection of various components according to certain parameters like bore diameter and the piston length used in the pneumatic system were calculated. The next chapter will discuss in detail about the finite element analysis results obtained on the modified analyzer assembly design.

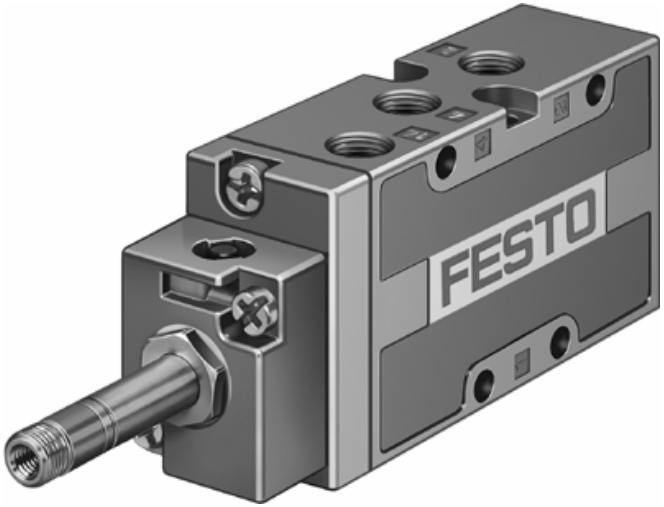

Figure – 5.11 Solenoid valve [24]

Figure – 5.12 Solenoid coil (MSFG-24DC/42AC 4527) [24]

Figure – 5.13 Reducing nipple D-M5I-1/8A 3842 [24]

Figure – 5.14 Socket connector cable 30937 KMF-1-24DC-5-LED [24]

CHAPTER – 6. VIBRATION ANALYSIS OF THE MODIFIED ANALYZER ASSEMBLY

6.1 Introduction

In this chapter, finite element analysis of the modified analyzer assembly is presented to compare the natural frequencies of the new design and the old system. The procedures and elements used were the same as the old analyzer assembly analysis. The major design changes were: the increase in shaft size, a box-type setup made of aluminum to protect the crystal from environmental conditions, and fixing of the whole setup on the top of the granite block (0.7 m above the height of the old analyzer assembly).

6.2 Modeling and simulation of new analyzer assembly

The element types chosen were the ANSYS Beam 4 and Shell 63 which were the same as those used in the analysis of the old analyzer assembly. This modified analyzer assembly looks like a simply supported beam which is fixed on both ends and has a box which encloses the crystal supported by plates hanging in the middle.

Shell 63 element is used for the analysis of the box which encloses the analyzer crystal and the other parts such as the crystal, the faceplates, cross plates and endplates. The input data needed for the Shell 63 is the thickness and for beam 4 elements the input required are the area, moment of inertia along Y and Z directions and geometric torsion along x direction which was calculated using the formulas added in the Appendix – A (Section – A.1).

The finite element model of the modified analyzer assembly is shown in the Figure – 6.1.

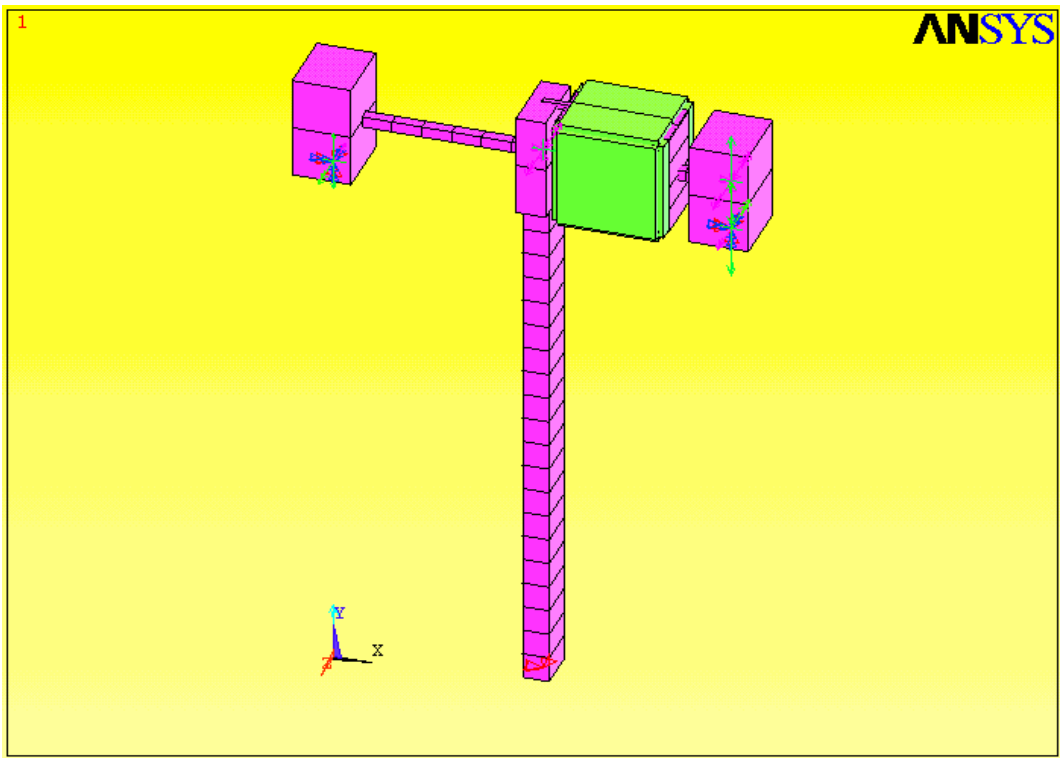

Figure – 6.1 Finite element model of the new analyzer assembly

In this analysis, for the bottommost element of the fixed post the displacement at both ends of the shaft is kept zero on all six degrees of freedom and for the bottom most element of the tangent bar, the displacement on Y and Z direction were kept zero. The coupling condition is used on places where the bearings are attached as because this makes one part free to rotate against another. The red symbol in the Figure – 6.1 represents this condition.

6.3 Computer outputs

After the application of boundary conditions, a modal analysis was performed to determine the lowest six natural frequencies of the modified analyzer assembly. The corresponding modal shapes are shown in Figures – 6.2 to Figure – 6.7.

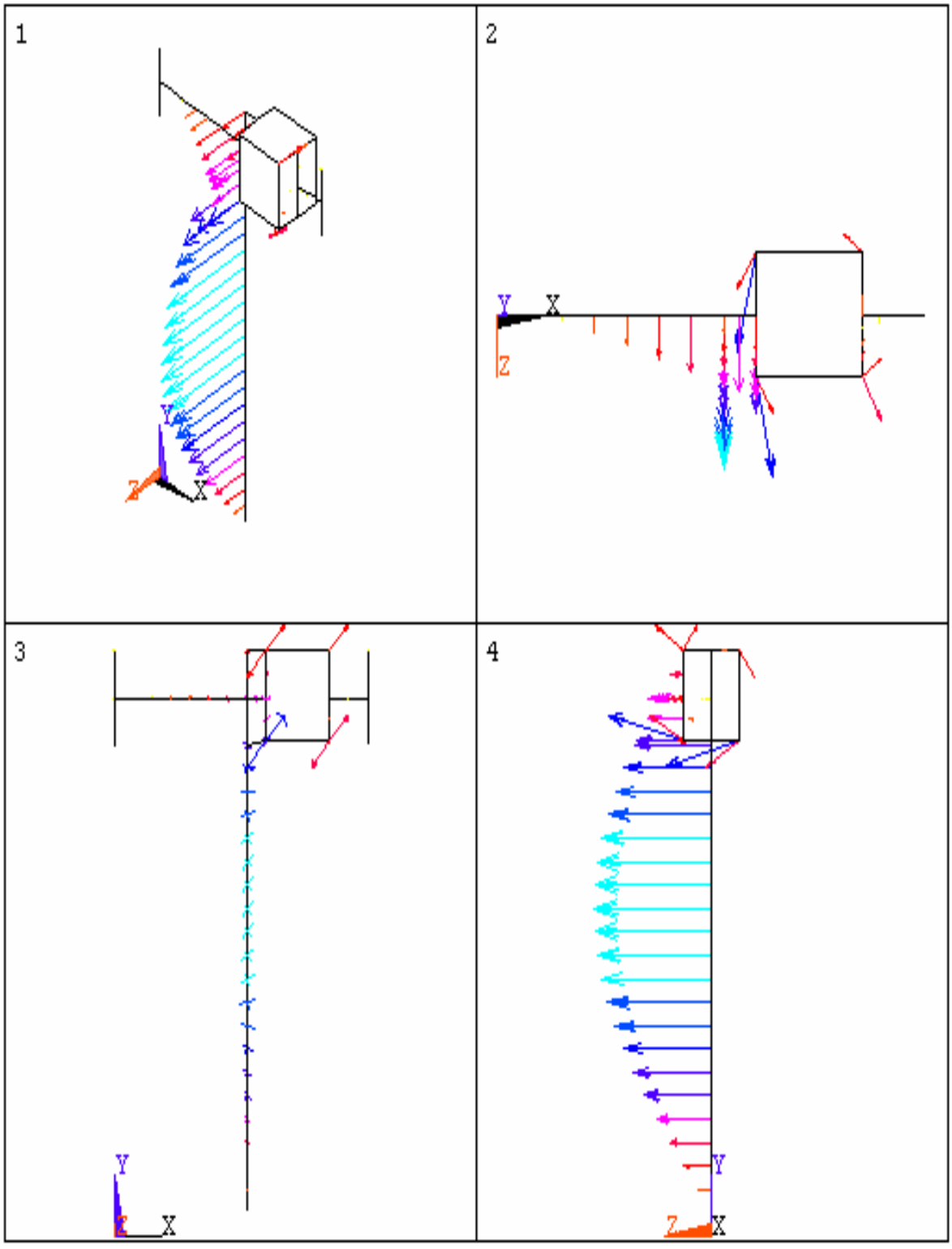

Figure – 6.2 Vibration mode – 1 (Frequency, f_1 = 141.05 Hz)

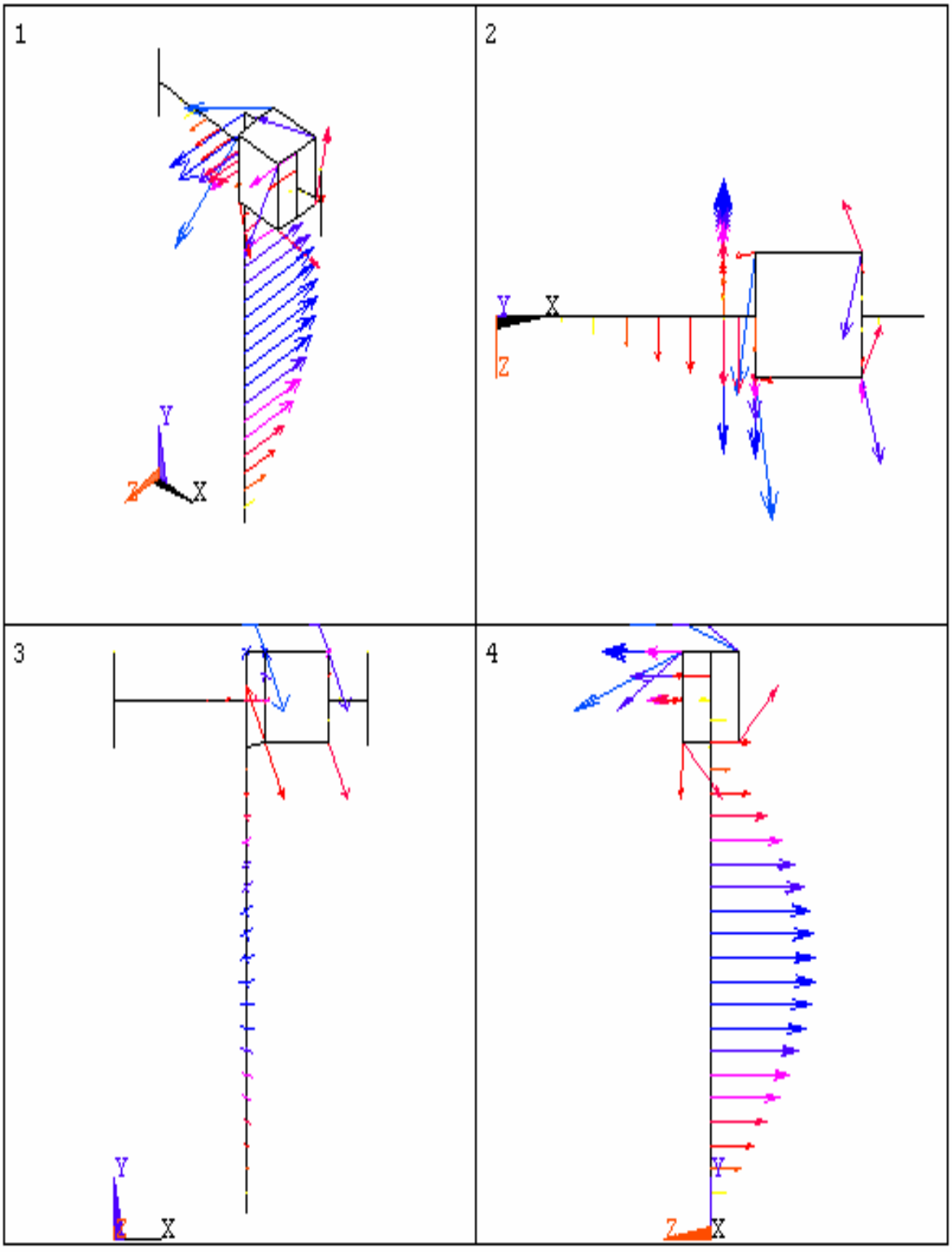

Figure – 6.3 Vibration mode – 2 (Frequency, f_2 = 148.88 Hz)

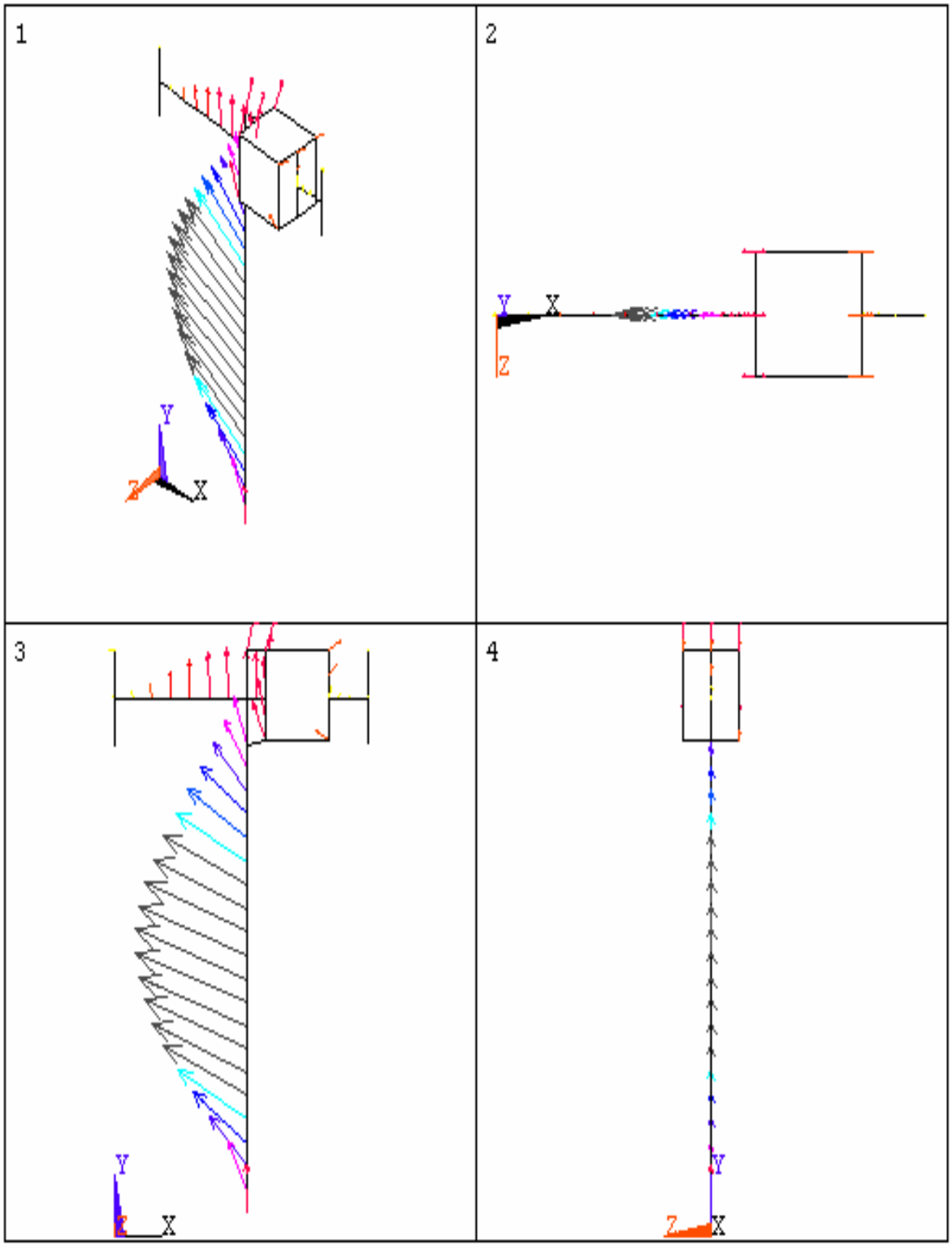

Figure – 6.4 Vibration mode – 3 (Frequency, f_3 = 201.30 Hz)

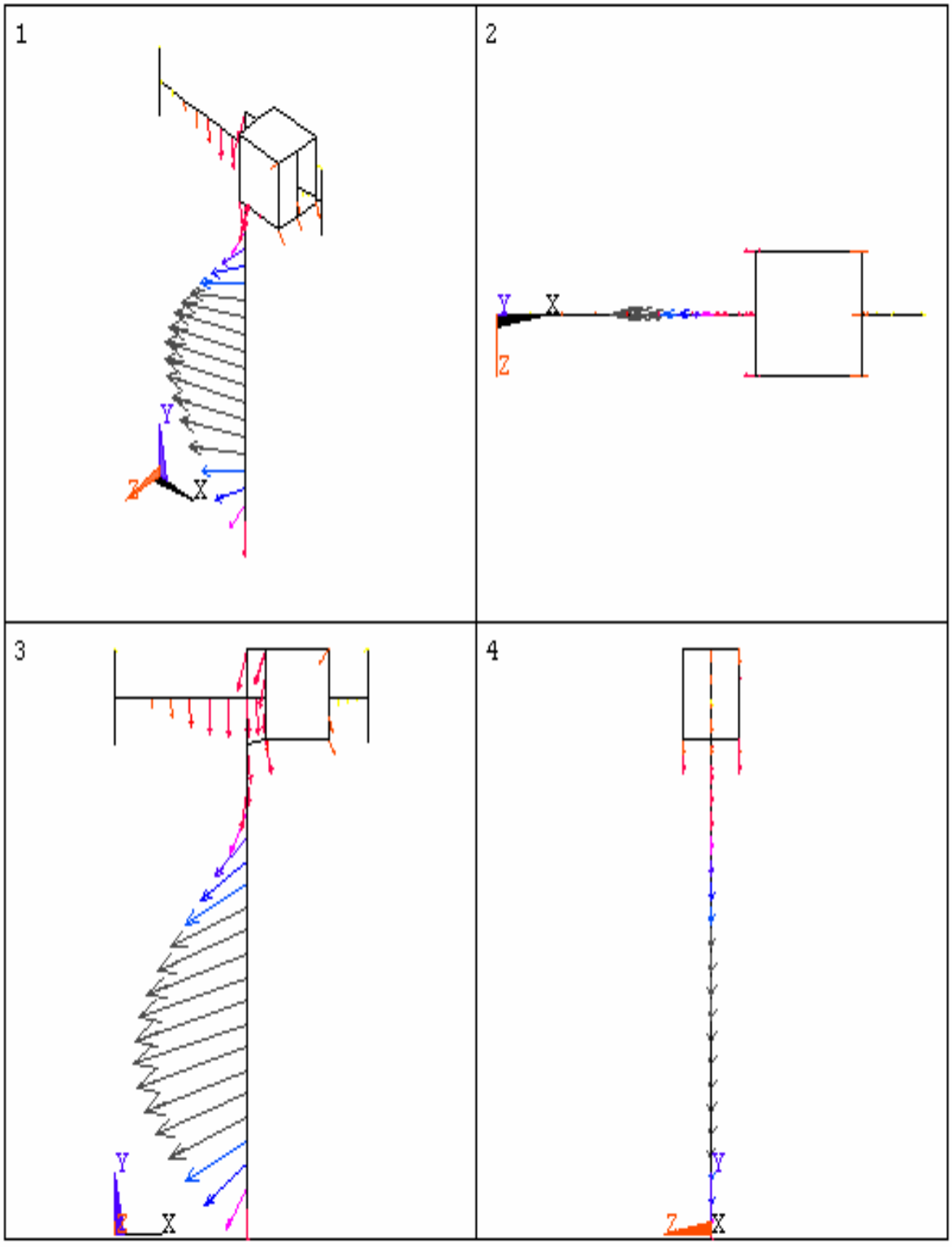

Figure – 6.5 Vibration mode – 4 (Frequency, f_4 = 253.80 Hz)

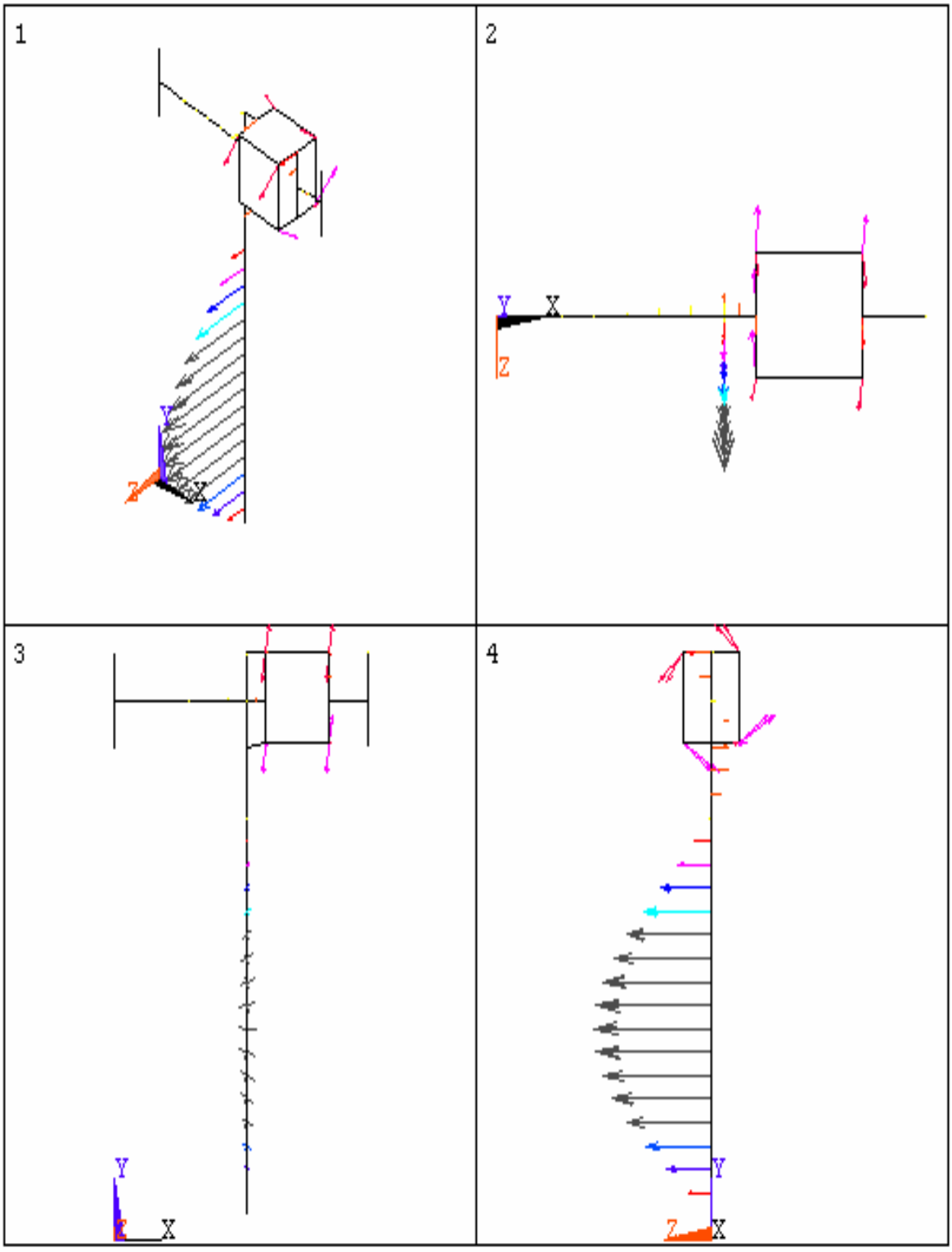

Figure – 6.6 Vibration mode – 5 (Frequency, f_5 = 415.65 Hz)

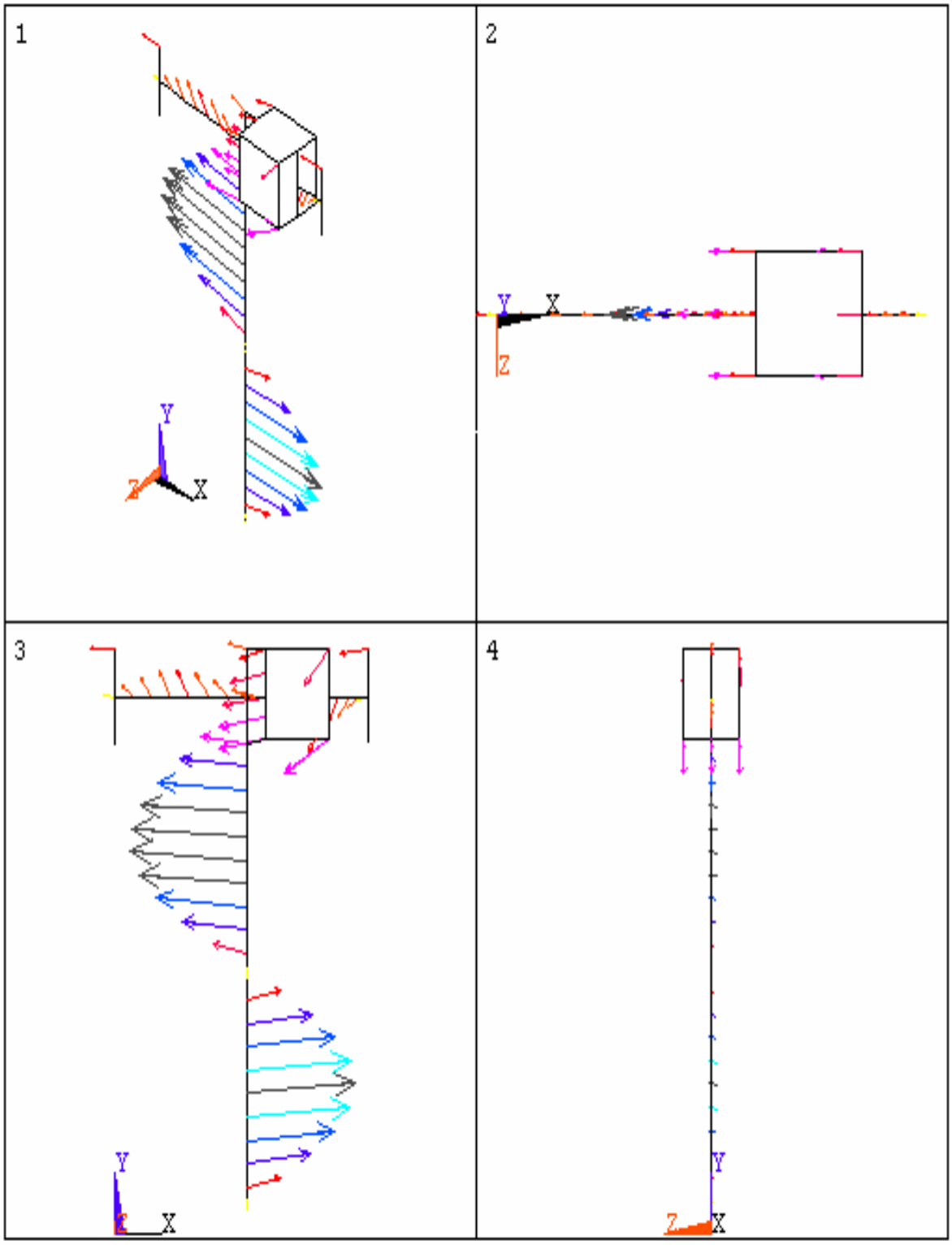

Figure – 6.7 Vibration mode – 6 (Frequency, f_6 = 632.40 Hz)

Table of modal frequencies got from ANSYS are given below in Table – 6.1.

Table – 6.1 Natural frequency values

MODE	FREQUENCY (Hz)
1	141.05
2	148.88
3	201.30
4	253.79
5	415.65
6	632.39

6.4 Results discussion

It was evident from all of the six modes that the vibrations in the new analyzer assembly involve the tangent bar which is 1 m long. As the frequencies of these vibrations are higher, the vibrations will be damped faster and their impact on the system will be less. However, the lowest natural frequency of vibration for the new design (141.05 Hz) is raised approximately eight times higher than the old system (17.894 Hz), which was the main objective of this thesis. Since the stiffness is proportional to the frequency squared (with the mass approximately unchanged), it can be claimed that this system is approximately 64 times stiffer than the old analyzer system. If the natural frequency has to be raised further, either the tangent bar can be made shorter or the stiffness has to be increased.

6.5 Summary

In this chapter, the natural frequency analysis of the new analyzer assembly was done to confirm that the new system is much stiffer and will more probably satisfy the requirements of the

DEI system. The analysis confirmed that the new analyzer assembly is 64 times stiffer than the old system. The next chapter will present the conclusion of this work and the future work which can be done to further reduce the vibrations in the analyzer assembly design.

CHAPTER – 7. CONCLUSION AND FUTURE WORK

7.1 Conclusion

In this thesis, the inability to control, set and fix the angle of the analyzer crystal precisely has been fixed. The results of the study can be summarized as follows:

- The dimensional stability of the system has been increased by raising the lowest natural frequency of the system. This was done by increasing the stiffness of the parts in the DEI analyzer assembly and by decreasing the mass of the parts in the system with use of aluminum for every part (except the crystal and the shaft). The ANSYS simulation results showed that the lowest natural frequency of the new system has been increased approximately by 8 times than the existing system. This new system will satisfy the requirements of the DEI system.
- A pneumatic lock system was designed to automatically make the larger angular adjustments of the analyzer crystal. This automatic lock system should reduce the time to take an image in the DEI system.
- The analyzer crystal was placed in an enclosure which makes it easier to control the temperature of the crystal thermally from the hutch environment. An additional benefit is the protection the enclosure provides for accidental bumping or having things dropped on it during hutch access for setup or sample access.

The vibration analysis in the analyzer assembly was performed by using the modal analysis in ANSYS in Chapter-3. Effective design changes to reduce analyzer assembly oscillations due to random disturbances were proposed in Chapter-4. A double solenoid valve controlled pneumatic

lock system for making larger angular adjustments of the analyzer crystal in the modified DEI assembly was proposed in Chapter-5.

The individual components of the system were specified, fabricated and assembled. After the final assembly tests were completed, the entire system was shipped to Brookhaven National Laboratory's National Synchrotron Light Source to the X15A imaging beamline. This system has been incorporated into a test DEI system using a conventional X-ray tube. This is a temporary arrangement in which a test of the viability of using a DEI system with an X-ray tube for potential clinical applications; specifically, mammography. Once these tests are completed (estimated in July 2007), the analyzer system will become a permanent part of the X15A beamline. At that time, detailed measurements can be done on validating the performance of the analyzer system.

7.2 Future work

The following areas are worthy of further research:

- 1 m long tangent bar can be modified to make the DEI system more compact;
- Incorporating water cooling of the analyzer box and tangent bar to improve thermal stability;
- Extending the present analysis to the DEI monochromator mechanism which would then include the thermal loading of the first crystal with the synchrotron beam;
- Analyze the complete DEI system including the X-ray optical components and the mechanical support system for the object being imaged and detector.

REFERENCES

[1] Hasnah, M., Oltulu, O., Zhong, Z., Chapman, D., "Application of absorption and refraction matching techniques for diffraction enhanced imaging", Review of Scientific Instruments, 73, March 2002.

[2] Guinier A., and Fournet G., Small Angle Scattering of X-rays, John Wiley and Sons, New York, 1995.

[3] Mollenhaeur, J., Aurich, M.E., Zhong, Z., Muelhleman, C., Cole, A.A, Hasnah, M., Oltulu, O., Kuettner, K.E., Margulis, A., and Chapman, D., "Diffraction enhanced X-ray imaging of articular cartilage", Osteoarthritis and Cartilage, 10: 163-171, 2002.

[4] Chapman, L.D., Thomlinson, W., Johnston, R.E., Washburn, D., Pisano, E., Gmur, N., Zhong, Z., Menk, R., Arfelli, F., and Sayers, D., "Diffraction enhanced X-ray imaging", Physics in Medicine and Biology, 42: 2015-2025, 1997.

[5] Zhong, Z., Thomlinson, W., Chapman, D., and Sayers, D., "Implementation of diffraction enhanced imaging at NSLS and APS", Nuclear Instruments and Methods in Physics Research, A450: 556-567, 2000.

[6] Paquin, R. "Dimensional instability." SPIE Proceeding, 1335: 167-174, 1990.

[7] Oltulu, O., "A unified approach to X-ray absorption-refraction-extinction contrast with diffraction enhanced imaging", Ph.D., Illinois Institute of Technology, Chicago, USA, 2003.

[8] Li, J., Zhong, Z., Lidtke, R., Kuettner, K.E, Peterfy, C., Aliyeva, E., and Muehleman, C., "Radiography of soft tissues of the foot and ankle with diffraction enhanced imaging", Journal of Anatomy, 202: 463-470, 2003.

[9] Förster, E., Goetz, K., and Zaumseil, P., "Double Crystal Diffractometry for the Characterization of Targets for Laser Fusion Experiments". Kristall und Technik, 15(8): 937- 945, 1980.

[10] Zachariasen, W.H, Theory of X-ray diffraction in crystals, John Wiley and Sons, New York, 1945.

[11] Johnston, R.E., Washburn, D., Pisano, E., Burns, C., Thomlinson, W.C., Chapman, L.D, Arfelli, F., Gmur, N., Zhong, Z., and Sayers, D., "Mammographic phantom studies with synchrotron radiation", Radiology, 200: 659-653, 1996.

[12] Bender, J.W., and Wahl, R.L., "Work-induced stress and long-term stability in optically polished silicon", SPIE proceeding, 1533: 201-209, 1991.

[13] Roseau, M., Vibrations in Mechanical Systems - Analytical Methods and Applications, Springer-Verlag, Berlin, 1987.

[14] ANSYS 2006, ANSYS release 10.0 documentation preview, Swanson Analysis System Inc., Houston, 2006.

[15] ANSYS 10.0, User's documentation overview, ANSYS Inc., 2006.

[16] Bathe, K. J., Finite Element Procedures in Engineering Analysis, Prentice-Hall Inc., New Jersey, 1982.

[17] SKF, High precision angular contact bearing: User's Guide, SKF USA Inc., Pennsylvania, 2003.

[18] Motosh, N., "Development of design charts for bolts preloaded upto the plastic range", Journal of Engineering for Industries, 98(3): 849–851, August 1976.

[19] Uchino, K., Giniewicz, J.R., Micromechatronics, Marcel Dekker, New York, 2003.

[20] Kasap, S.O., Principles of electrical engineering materials and devices, Irwin McGraw-Hill, Chicago, 1997.

[21] Thorlabs, Multilayer piezo-electric actuators: User's Manual, Thorlabs Inc., New Jersey, 2006.

[22] Norton, R.L., Machine design: an integrated approach, Prentice-Hall Inc., New Jersey, 1996.

[23] Bethke, R.J., and Rediess, D.J., "Modeling and analysis of a pneumatic system," Proceedings of the Twenty-First Annual Pittsburgh Modeling and Simulation Conference, 2397-2402, Pittsburgh, PA., 1990.

[24] FESTO, Festo Inc., 5300 Explorer Drive, Mississauga, ON L4W 5G4, CANADA, [online] edition, 2006. Available from the World Wide Web athttp://catalog.festo.com/enu/asp/start.asp. Cited on 2007-05-06.

[25] NSLS, NSLS aerial view, National Synchrotron Light Source, Brookhaven National Laboratory, P.O. Box 5000, Upton, NY 11973-5000, USA, [Online] edition, 2003. Available from the World Wide Web at http:// www.nsls.bnl.gov/ about/ imagelibrary/ images/hr/NSLS_Aerial_hires.tif. Cited on 2007-05-06.

[26] CLS, CLS images, Canadian Light Source Inc., University of Saskatchewan, 101 Perimeter Road, Saskatoon, SK S7N 0X4, CANADA, [online] edition, 2006. Available from the World Wide Web at http://www.lightsource.ca/files/index.php?id=12. Cited on 2007-05-06.

[27] Nielson, J.A., Mc Morrow D., "Elements of Modern X-ray Physics", John Wiley and Sons, New York, 1937.

[28] Newport, Motorized Actuators: User's guide, Newport Corporation, California, 2006.

[29] Parham, C., Courtesy, School of Medicine and Department of Biomedical Engineering, University of North Carolina, Raleigh, NC, USA. Cited on 2007-05-06.

[30] Chapman, D., Courtesy, Department of Anatomy and Cell Biology, University of Saskatchewan, Saskatoon, SK, CANADA. Cited on 2007-05-06.

[31] Matweb, Aluminum Alloys, Automation Creations Inc., Blacksburg, Virginia, USA, [online] edition, 2006. Available from the World Wide Web at http://www.matweb.com/search/SpecificMaterial.asp?bassnum=MA0001. Cited on 2007-05-06.

[32] Ewins, D.J., Modal Testing: Theory, practice and application, Research studies press ltd., Hertfordshire, 2000.

[33] Kittel, C., Introduction to Solid State Physics, John Wiley and Sons, New York, 1971.

APPENDIX – A. ADDITIONAL MATERIALS

A.1 Formulae used in Chapter – 3

For a cylindrical tube:

Area, $A = \pi \times R^2$

where R is the radius of the cylinder

Moment of area, $I = \frac{\pi}{4}(R_O^4 - R_I^4)$

where R_O is the outer radius of the cylinder and R_I is the inner radius of the cylinder

Geometric torsion, $J_T = \frac{\pi}{2}(R_O^4 - R_I^4)$

For a Hollow rectangular block:

Area, $A = B \times H$

Moment of area, $I = \frac{BH^3}{12} - \frac{bh^3}{12}$

Geometric torsion, $J_T = \frac{4\,((B-T)\times(H-T))^2}{\frac{2((B-T)\times(H-T)}{T}}$

where B – breadth of the outer surface, H – height of the outer surface, b – breadth of the inner surface, h – height of the inner surface and T – thickness

For a Cylinder:

Area, $A = \pi \times R^2$

Moment of area, $I = \frac{\pi}{4}R^4$

Polar moment of inertia, $I = \frac{\pi}{2}R^4$

For a rectangular block:

Area, $A = B \times H$

Moment of area, $I = \frac{BH^3}{12}$

Geometric torsion, $J_T = (0.312) \times B \times H^3$ (if $\frac{\text{longest side}}{\text{shortest side}} \simeq 10$)

Geometric torsion, $J_T = (0.291) \times B \times H^3$ (if $\frac{\text{longest side}}{\text{shortest side}} \simeq 6$)

Table – A.1 Area, Moment of area and Geometric torsion for all the parts

No	Parts	Area(mm) 10^2	I_{xx} (mm^4) 10^6	I_{yy} (mm^4) 10^5	I_{zz} (mm^4) 10^5	Figure
1	Fixed post (bottom)	20.62	3.98	19.88	19.88	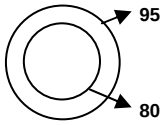
2	Fixed post(top)	13.20	3.88	31.34	21.94	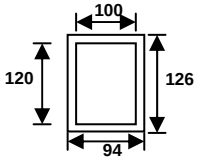
3	Shaft	12.57	0.25	1.26	1.26	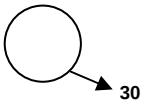
4	Tangent bar (top)	10.20	1.18	19.99	4.61	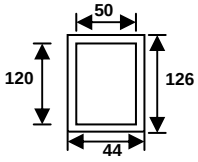
5	Tangent bar (bottom)	6.90	0.49	5.31	2.31	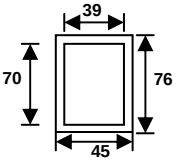
6	Connection assembly	12	3.74	10.00	0.14	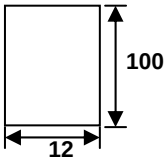
7	Analyzer crystal and support assembly	45.41	38.86	10.94	2.70	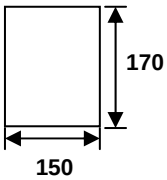

A.2 Centroid calculation for Chapter – 5

Analyzer crystal: (Material-Silicon)

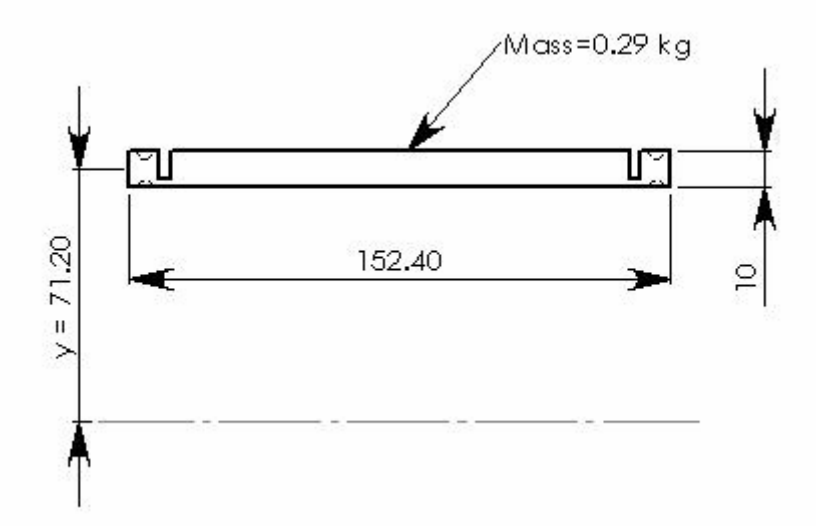

Figure – A.1 Centroid of analyzer crystal [mm]

Volume of the crystal = L×W×H

$= 140 \times 90 \times 10 = 126000\ mm^3 = 126\ cm^3$

Mass = Density (ρ) ×Volume (ν)

$= 2.33\ g/cm^3 \times 126\ cm^3$

Mass of the analyzer crystal = 293.58 grams = 0.293 kg

Centroid of the silicon crystal, $\bar{y} = 71.20$ mm

Therefore, $\bar{y} \times m = 71.2 \times 293.58 = 20.9$ kg.mm

Crystal support plate-1: (Material- Aluminum)

Volume of crystal support plate = $165 \times 100 \times 5 = 82500\ mm^3 = 82.5\ cm^3$

Mass = $\rho \times \nu = 2.6989\ g/cm^3 \times 82.5\ cm^3$

Mass of the support plate = 222.66 grams = 0.22 kg

Centroid of the crystal support plate, $\bar{y} = 63.70$ mm

Therefore, $\bar{y} \times m = 63.7 \times 0.22 = 14.01$ kg.mm

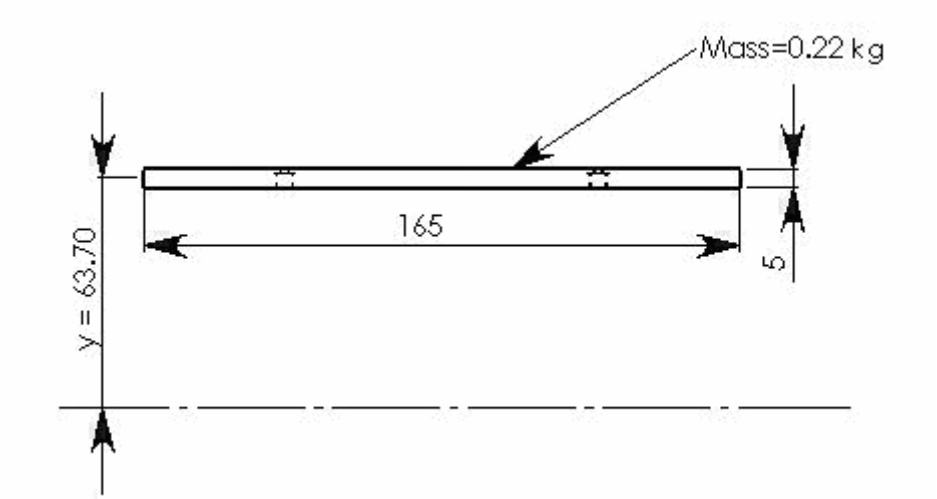

Figure – A.2 Centroid of crystal support plate-1 [mm]

Crystal support plate-2: (Material - Aluminum)

Volume of crystal support plate = 177.8 ×101.6 ×12.7 = 229418.9 mm^3 = 229.419 cm^3

Mass = ρ × ν = 2.6989 g/ cm^3 × 229.42 cm^3

Mass of the crystal support plate = 0.62 kg

Centroid of the crystal support plate, $\bar{y}$ = 30.20 mm

Therefore, $\bar{y}$ × m = 30.2 × 0.62 =18.72 kg.mm

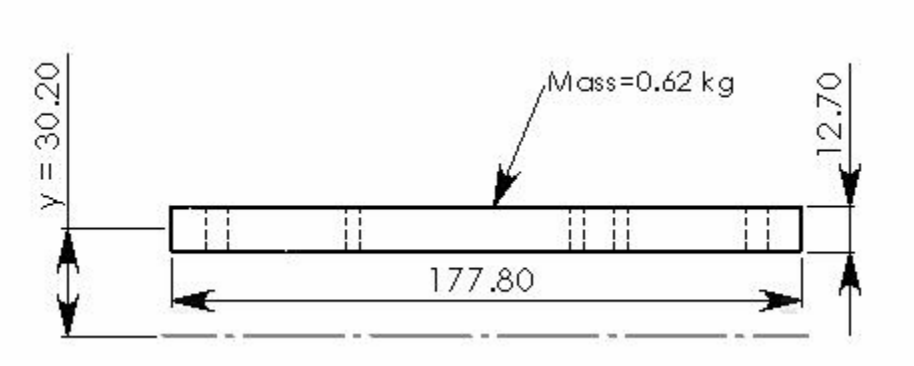

Figure – A.3 Centroid of crystal support plate-2 [mm]

Cross plate (Bottom):

Length- 228.86 mm, Breadth-139.7 mm, Height-12.7 mm

Volume of cross plate = 228.6×139.7×12.7 = 405580 mm^3 = 405.58 cm^3

Mass of cross plate = ρ × ν = 2.6989 g/ cm^3 × 405.58 cm^3 = 1.1 kg

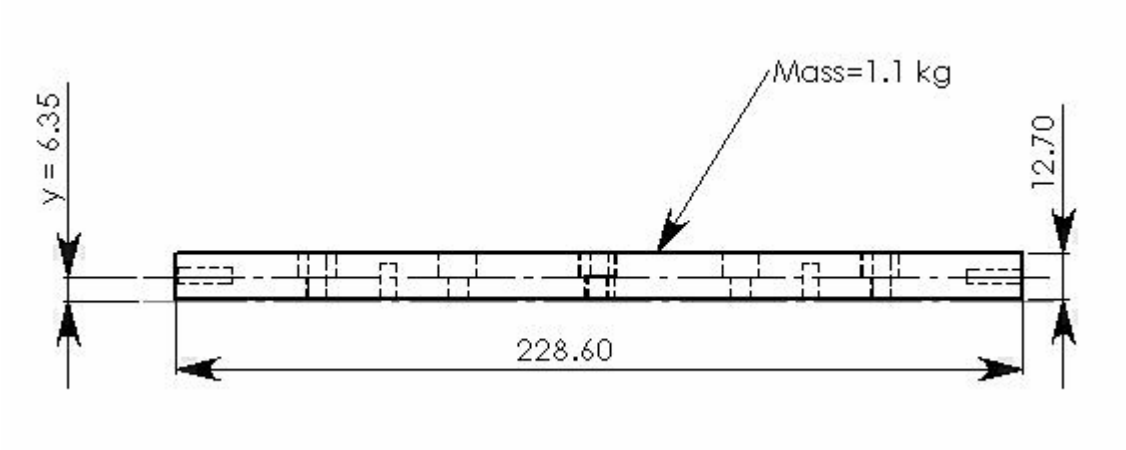

Figure – A.4 Centroid of cross plate (bottom) [mm]

Centroid of cross plate, $\bar{y} = 6.35$ mm

Therefore, $\bar{y} \times m = 6.35 \times 1.09 = 6.979$ kg.mm

Cross plate (Top):

Centroid of cross plate, $\bar{y} = 146.05$ mm

Therefore, $\bar{y} \times m = 146.05 \times 1.1 = 160.51$ kg.mm

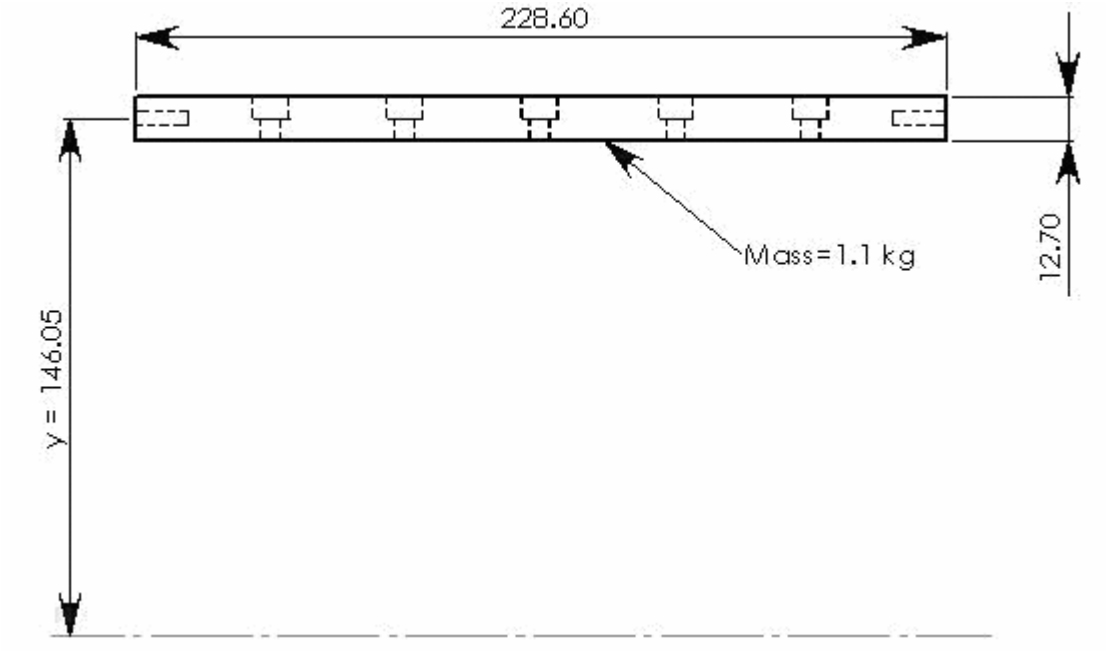

Figure – A.5 Centroid of cross plate (top) [mm]

Faceplate:

Length- 228.86 mm, Breadth-12.67 mm, Height-12.7 mm

Volume of faceplate = (228.6×12.67×12.7) − (203×6.96×1.27) = 188400 mm^3 = 188.4 cm^3

Mass of faceplate = ρ × ν = 2.6989 g/ cm^3 × 188.4 cm^3 = 0.51 kg

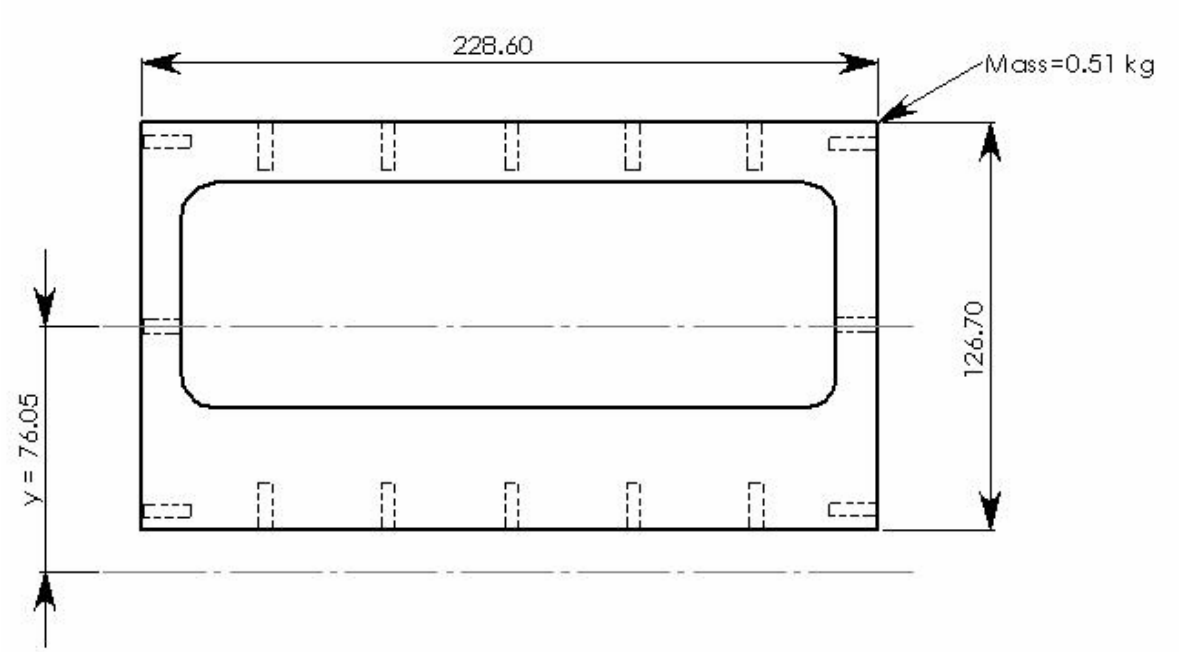

Figure – A.6 Centroid of face plate [mm]

Centroid of face plate, $\bar{y}$ = 76.05 mm

Therefore, $\bar{y}$×m = 76.05×0.51= 38.79 kg.mm

Endplate:

Length- 139.7 mm, Breadth-152.4 mm, Height-12.7 mm

Volume of endplate = 139.7×152.4×12.7 = 270390 mm^3 = 270.39 cm^3

Mass of endplate = 2.6989 g/ cm^3 × 270.39 cm^3 = 0.734 kg

Centroid of endplate, $\bar{y}$ = 76.2 mm

Therefore, $\bar{y}$×m = 76.2×0.734 = 55.93 kg.mm

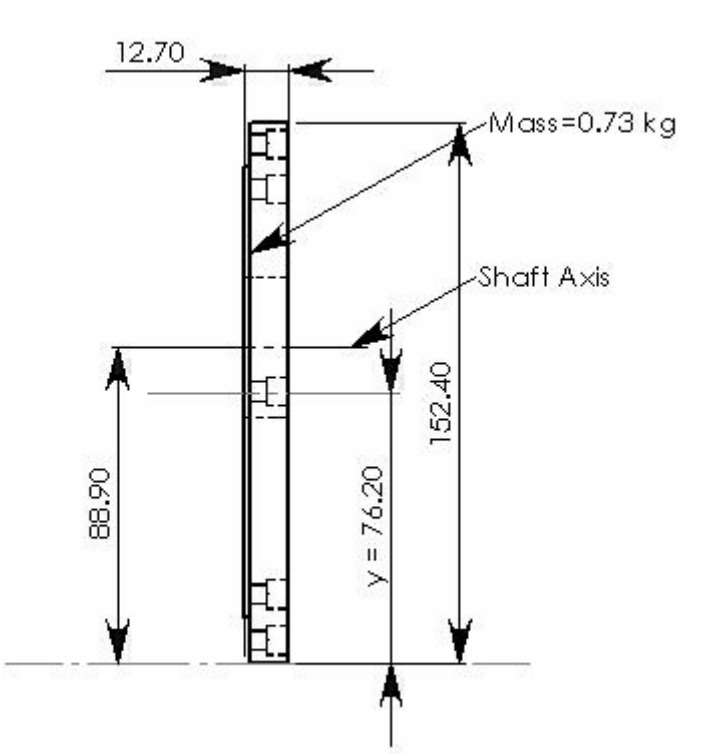

Figure – A.7 Centroid of end plate [mm]

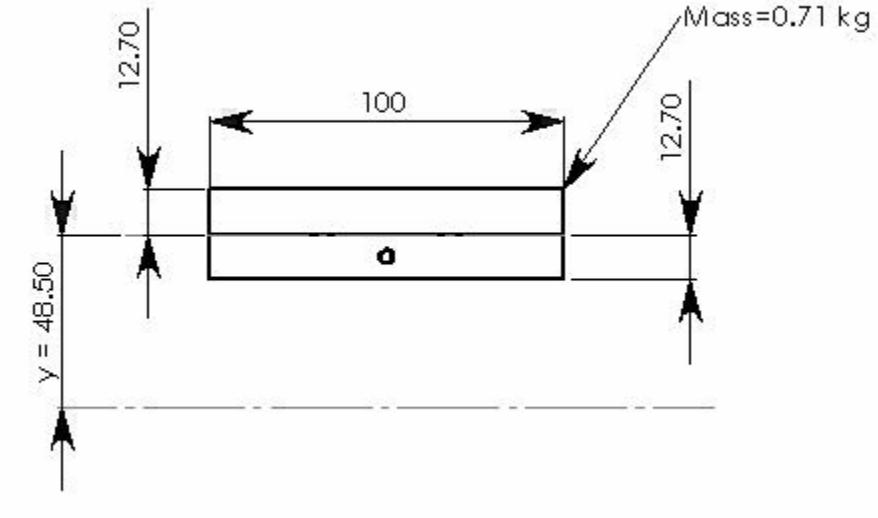

Figure – A.8 Centroid of magnetic kinematic base [mm]

Magnetic kinematic base:

Length- 101.6 mm, Breadth- 101.6 mm, Height - 25.4 mm

Volume of kinematic base = $101.6 \times 101.6 \times 25.4 = 262193.03\ mm^3 = 262.19\ cm^3$

Mass of kinematic base $= 2.6989\ g/\ cm^3 \times 262.19\ cm^3 = 0.71\ kg$

Centroid of kinematic base, $\bar{y} = 48.5\ mm$

Therefore, $\bar{y} \times m = 48.5 \times 0.71 = 34.435\ kg.mm$

Micrometer motor, piezo and spring:

Mass of micrometer motor, piezo and spring = 0.4 kg

Centroid = $\bar{y} = 15.1\ mm$

Therefore, $\bar{y} \times m = 15.1 \times 0.4 = 6.04\ kg.mm$

APPENDIX – B. ANSYS CODES

B.1 ANSYS code used for the natural frequency analysis of old analyzer assembly

This finite element modal analysis was done to find the lowest natural frequency of vibration in the old analyzer assembly.

```
Fini
/clear
/prep7
A=1e-03
pi=3.141592
! Defining Area, Moment of area, Geometric torsion and thickness for all the parts
h1=1000*A                          !height of part 1
ro1=47.5*A                         !outer radius
ri1=40*A                          !inner radius
ap1=pi*(ro1**2-ri1**2)                  !area
Iyy1=(pi*(ro1**4-ri1**4))/4              !moment of area along y
Izz1=(pi*(ro1**4-ri1**4))/4              !moment of area along z
JT1=(pi*(ro1**4-ri1**4))/2               !geometric torsion
t2=3*A                            !thickness
h2=190*A
bo2=100*A                          !maximum breadth of part 2
bi2=94*A                          !minimum breadth
ho2=126*A                          !maximum height
hi2=120*A                          !minimum height
ap2=(bo2*ho2)-(bi2*hi2)
Iyy2=((bo2*(ho2**3))-(bi2*(hi2**3)))/12
Izz2=((ho2*(bo2**3))-(hi2*(bi2**3)))/12
JT2=(4*((bo2+bi2)/2)*((ho2+hi2)/2))/((2*(((bo2+bi2)/2)+((ho2+hi2)/2)))/t2)
h3=406.4*A
ro3=15*A
ap3=pi*(ro3**2)
Iyy3=(pi*(ro3**4))/4
Izz3=(pi*(ro3**4))/4
JT3=(pi*(ro3**4))/2
t4=3*A
h4=190*A
bo4=50*A
bi4=44*A
ho4=126*A
hi4=120*A
ap4=(bo4*ho4)-(bi4*hi4)
Iyy4=((bo4*(ho4**3))-(bi4*(hi4**3)))/12
Izz4=((ho4*(bo4**3))-(hi4*(bi4**3)))/12
JT4=(4*((bo4+bi4)/2)*((ho4+hi4)/2))/((2*(((bo4+bi4)/2)+((ho4+hi4)/2)))/t4)
t5=3*A
```

```
h5=1000*A
bo5=45*A
bi5=39*A
ho5=76*A
hi5=70*A
ap5=(bo5*ho5)-(bi5*hi5)
Iyy5=((bo5*(ho5**3))-(bi5*(hi5**3)))/12
Izz5=((ho5*(bo5**3))-(hi5*(bi5**3)))/12
JT5=(4*((bo5+bi5)/2)*((ho5+hi5)/2))/((2*(((bo5+bi5)/2)+((ho5+hi5)/2)))/t5)
h6=215*A
bo6=12*A
ho6=100*A
ap6=bo6*ho6
Iyy6=(bo6*(ho6**3))/12
Izz6=(ho6*(bo6**3))/12
JT6=0.312*bo6*(ho6**3)
h7=150*A
bo7=26.71*A
ho7=170*A
ap7=bo7*ho7
Iyy7=(bo7*(ho7**3))/12
Izz7=(ho7*(bo7**3))/12
JT7=0.291*bo7*(ho7**3)
h9=50*A
ro9=10*A
ap9=pi*(ro9**2)
Iyy9=(pi*(ro9**4))/4
Izz9=(pi*(ro9**4))/4
JT9=(pi*(ro9**4))/2

!Defining the real constants for the parts
r,1,ap1,Izz1,Iyy1,ro1,ro1,,
rmore,,JT1
r,2,ap2,Izz2,Iyy2,ho2,bo2,,
rmore,,JT2
r,3,ap3,Izz3,Iyy3,ro3,ro3,,
rmore,,JT3
r,4,ap4,Izz4,Iyy4,ho4,bo4,,
rmore,,JT4
r,5,ap5,Izz5,Iyy5,ho5,bo5,,
rmore,,JT5
r,6,ap6,Izz6,Iyy6,ho6,bo6,,
rmore,,JT6
r,7,ap7,Izz7,Iyy7,ho7,bo7,,
rmore,,JT7
r,9,ap9,Izz9,Iyy9,ro9,ro9,,
rmore,,JT9
```

```
!Defining material and element types
!material1
ex,1,70e9      !young's modulus
nuxy,1,0.3     !Poisson's ratio
acel,,9.81       !acceleration
dens,1,2710    !density
!material 2
ex,2,200e9
nuxy,2,0.3
acel,,9.81
dens,2,7800
et,1,beam4   !3-D beam
et,2,shell63
r,8,26.71e-03

!generating nodes
n,1,0,0
n,21,0,h1
fill,1,21,20,2,1
n,22,0,h1+h2
n,23,0,h1+(h2/2)
n,30,h3-(50*A),h1+(h2/2)
fill,23,30,6,24,1
n,200,h3-(50*A),h1+(h2/2)
n,31,h3-(50*A),h1+h2
n,301,h3-(50*A),1142.5e-03
n,32,h3-(50*A),h1
n,52,h3-(50*A),0
fill,32,52,20,33,1
n,54,h3,h1+(h2/2)
fill,30,54,1,53,1
n,300,h3,h1+(h2/2)
n,56,h3,(h1+h2)
fill,54,56,1,55,1
n,58,h3,h1+(7*A)
fill,54,58,1,57,1
n,59,h3,h1+(7*A),bo7/2
n,60,h3+ho7-(6*A),h1+(7*A),bo7/2
n,61,h3+ho7-(6*A),h1+(7*A)
n,62,h3+ho7-(6*A),h1+(7*A),-bo7/2
n,63,h3,h1+(7*A),-bo7/2

!generating elements
e,1,2
mat,1
real,1
egen,20,1,1,1,
mat,1
real,2
```

```
e,21,23
e,23,22
mat,2
real,3
e,23,24
egen,7,1,23,23
mat,1     !specifying the materials for elements
real,4
e,200,301
e,301,31
e,200,32
mat,1
real,5      !specifying the real  constants for the elements
e,32,33
egen,20,1,33,34
mat,2
real,3
e,30,53
e,53,54

mat,1
real,6
e,300,55
!e,54,55
e,55,56
e,300,57
!e,54,57
e,57,58
eplot     !creating an element plot
type,2
mat,1
real,8
e,58,61,60,59
e,58,63,62,61


type,1
real,7
mat,1
e,58,61
e,63,62
e,59,60
/view,1,2,3,4

type,1
mat,2
real,9
e,31,56
e,32,58
```

```
d,1,all,0.0  !displacement is zero at 1 on all axes
d,52,uz,0
d,52,ux,0
cp,1,ux,200,30 !Coupling condition
cp,2,uy,200,30
cp,3,uz,200,30
cp,4,roty,200,30
cp,5,rotz,200,30
cp,6,ux,300,54
cp,7,uy,300,54
cp,8,uz,300,54
cp,9,roty,300,54
cp,10,rotz,300,54

/eshape,1,0     !getting the element shape for all parts
eplot
fini
/solu
solve
finish

/solu   !free vibrations
antype,modal    !modal analysis
modopt,subsp,6 !specifying the subspace iteration method
solve   !6 modes of vibr
finish

!to look at vibration results
/post1
set,list
set,1,1   !mode 1
pldispl,1       !plot of display.
```

B.2 ANSYS code used for the natural frequency analysis of new analyzer assembly

This finite element modal analysis was done to find the lowest natural frequency of vibration in the new analyzer assembly.

```
Fini
/clear
/prep7
A=1e-03
pi=3.141592
! Defining Area, Moment of area, Geometric torsion and thickness for all the parts
h1=1000*A                       !height of part 1
ro1=47.5*A                      !outer radius
ri1=40*A                        !inner radius
ap1=pi*(ro1**2-ri1**2)                  !area
```

```
Iyy1=(pi*(ro1**4-ri1**4))/4              !moment of area along y
Izz1=(pi*(ro1**4-ri1**4))/4              !moment of area along z
JT1=(pi*(ro1**4-ri1**4))/2               !geometric torsion
t2=3*A                                !thickness
h2=190*A
bo2=100*A                               !maximum breadth of part 2
bi2=94*A                               !minimum breadth
ho2=126*A                               !maximum height
hi2=120*A                               !minimum height
ap2=(bo2*ho2)-(bi2*hi2)
Iyy2=((bo2*(ho2**3))-(bi2*(hi2**3)))/12
Izz2=((ho2*(bo2**3))-(hi2*(bi2**3)))/12
JT2=(4*((bo2+bi2)/2)*((ho2+hi2)/2))/((2*(((bo2+bi2)/2)+((ho2+hi2)/2)))/t2)
h3=406.4*A
ro3=20*A
ap3=pi*(ro3**2)
Iyy3=(pi*(ro3**4))/4
Izz3=(pi*(ro3**4))/4
JT3=(pi*(ro3**4))/2
t4=3*A
h4=190*A
bo4=50*A
bi4=44*A
ho4=126*A
hi4=120*A
ap4=(bo4*ho4)-(bi4*hi4)
Iyy4=((bo4*(ho4**3))-(bi4*(hi4**3)))/12
Izz4=((ho4*(bo4**3))-(hi4*(bi4**3)))/12
JT4=(4*((bo4+bi4)/2)*((ho4+hi4)/2))/((2*(((bo4+bi4)/2)+((ho4+hi4)/2)))/t4)
t5=3*A
h5=1000*A
bo5=45*A
bi5=39*A
ho5=76*A
hi5=70*A
ap5=(bo5*ho5)-(bi5*hi5)
Iyy5=((bo5*(ho5**3))-(bi5*(hi5**3)))/12
Izz5=((ho5*(bo5**3))-(hi5*(bi5**3)))/12
JT5=(4*((bo5+bi5)/2)*((ho5+hi5)/2))/((2*(((bo5+bi5)/2)+((ho5+hi5)/2)))/t5)
h6=215*A
bo6=24*A
ho6=100*A
ap6=bo6*ho6
Iyy6=(bo6*(ho6**3))/12
Izz6=(ho6*(bo6**3))/12
JT6=0.312*bo6*(ho6**3)
h7=140*A
bo7=150*A
ho7=170*A
```

```
ap7=bo7*ho7
Iyy7=(bo7*(ho7**3))/12
Izz7=(ho7*(bo7**3))/12
JT7=0.291*bo7*(ho7**3)
h9=50*A
ro9=10*A
ap9=pi*(ro9**2)
Iyy9=(pi*(ro9**4))/4
Izz9=(pi*(ro9**4))/4
JT9=(pi*(ro9**4))/2

r,1,ap1,Izz1,Iyy1,ro1,ro1,,
rmore,,JT1
r,2,ap2,Izz2,Iyy2,ho2,bo2,,
rmore,,JT2
r,3,ap3,Izz3,Iyy3,ro3,ro3,,
rmore,,JT3
r,4,ap4,Izz4,Iyy4,ho4,bo4,,
rmore,,JT4
r,5,ap5,Izz5,Iyy5,ho5,bo5,,
rmore,,JT5
r,6,ap6,Izz6,Iyy6,ho6,bo6,,
rmore,,JT6
r,7,ap7,Izz7,Iyy7,ho7,bo7,,
rmore,,JT7
r,9,ap9,Izz9,Iyy9,ro9,ro9,,
rmore,,JT9

!Defining material and element types
!material1
ex,1,70e9      !young's modulus
nuxy,1,0.3     !Poisson's ratio
acel,,9.81       !acceleration
dens,1,2710    !density
!material 2
ex,2,200e9
nuxy,2,0.3
acel,,9.81
dens,2,7800
et,1,beam4   !3-D beam
et,2,shell63
r,8,20e-03

!generating nodes

n,1,0,h1
n,2,0,h1+h2
n,3,0,h1+(h2/2)
n,10,h3-(50*A),h1+(h2/2)
```

```
fill,3,10,6,4,1
n,200,h3-(50*A),h1+(h2/2)
n,11,h3-(50*A),h1+h2
n,12,h3-(50*A),h1
n,32,h3-(50*A),0
fill,12,32,20,13,1
n,34,h3,h1+(h2/2)
n,300,h3,h1+(h2/2)
fill,10,34,1,33,1
n,36,h3,(h1+h2)
fill,34,36,1,35,1
n,38,h3,h1+(7*A)
fill,34,38,1,37,1
n,39,h3,h1+(7*A),bo7/2
n,40,h3+ho7,h1+(7*A),bo7/2
n,41,h3+ho7,h1+(7*A)
n,42,h3+ho7,h1+(7*A),-bo7/2
n,43,h3,h1+(7*A),-bo7/2
n,45,h3+ho7,h1+(h2/2)
n,201,676.4*A,h1+(h2/2)
fill,41,45,1,44,1
n,47,h3+ho7,h1+h2
fill,45,47,1,46,1
n,51,676.4*A,h1+(h2/2)
fill,45,51,3,48,1
n,52,676.4*A,h1
n,53,676.4*A,h1+h2
n,203,h3,h1+h2,bo7/2
n,204,h3+ho7,h1+h2,bo7/2
n,205,h3+ho7,h1+h2,-bo7/2
n,206,h3,h1+h2,-bo7/2

!generating elements
mat,1
real,2
e,1,3
e,3,2
mat,2
real,3
e,3,4
egen,7,1,3,3
mat,1
real,4
e,200,11
e,200,12
mat,1
real,5
e,12,13
egen,20,1,12,12
```

```
mat,2
real,3
e,10,33
e,33,34
en,33,33,300
mat,1
real,6
e,34,35
e,35,36
e,34,37
e,37,38
eplot
type,2
mat,1
real,8
e,38,41,40,39
e,38,43,42,41
type,1
mat,1
real,6
e,41,44
e,44,45
e,45,46
e,46,47
mat,2
real,3
e,45,48
e,48,49
e,49,50
e,50,51
mat,1
real,2
e,201,53
e,201,52
mat,1
real,9
e,11,36
e,12,38
type,2
mat,1
real,8
e,36,47,204,203
e,36,47,205,206
e,36,38,39,203
e,36,38,43,206
e,47,41,42,205
e,47,41,40,204
e,203,204,40,39
e,206,205,42,43
```

```
d,1,all,0.0  !displacement is zero at 1 on all axes
d,52,all,0.0
d,32,uz,0
d,32,ux,0
cp,1,ux,200,10
cp,2,uy,200,10
cp,3,uz,200,10
cp,4,roty,200,10
cp,5,rotz,200,10
cp,6,ux,201,51
cp,7,uy,201,51
cp,8,uz,201,51
cp,9,roty,201,51
cp,10,rotz,201,51
/eshape,1,0
eplot
fini
/solu
solve
finish

/solu   !free vibrations
antype,modal
modopt,subsp,6
solve   !6 modes of vibr
finish

!to look at vibration results
/post1
set,list
set,1,1   !mode 1
pldispl,1.
```

B.3 Code for display of four views

```
! Set screen to show four standard views:
! User may want to set /DSCALE to the same value in all windows
/WIN,1,LTOP           ! Window 1 left top
/WIN,2,RTOP           ! Window 2 right top
/WIN,3,LBOT           ! Window 3 left bottom
/WIN,4,RBOT           ! Window 4 right bottom
/WIN,5,OFF           ! Turn off Window 5
/VIEW,1,1,1,1         ! Window 1 ISO (isometric projection) view
/VUP,1,Y             ! Reference orientation
/VIEW,2,0,1,0         ! Window 2 top (plan) view
/VUP,2,Y             ! Reference orientation
/VIEW,3,0,0,1         ! Window 3 front (front elevation) view
/VUP,3,Y             ! Reference orientation
```

```
/VIEW,4,1,0,0          ! Window 4 right (side elevation) view
/VUP,4,Y              ! Reference orientation
/AUTO,ALL              ! Fit all windows
/PLOPTS,INFO,1         ! Include information column
/PLOPTS,LEG2,0         ! Don't include view information
/TYPE,ALL,2            ! Centroid sort, better print that Z-buffer
/CPLANE,0              ! Cutting plane
/graphics,full         ! NOT PowerGraphics (fewer facets?)
pldispl,1,1,1,1        ! Window 1 ISO (isometric projection) view
/VUP,1,Y              ! Reference orientation
/VIEW,2,0,1,0          ! Window 2 top (plan) view
/VUP,2,Y              ! Reference orientation
/VIEW,3,0,0,1          ! Window 3 front (front elevation) view
/VUP,3,Y              ! Reference orientation
/VIEW,4,1,0,0          ! Window 4 right (side elevation) view
/VUP,4,Y              ! Reference orientation
/AUTO,ALL              ! Fit all windows
/PLOPTS,INFO,1         ! Include information column
/PLOPTS,LEG2,0         ! Don't include view information
/TYPE,ALL,2            ! Centroid sort, better print that Z-buffer
/CPLANE,0              ! Cutting plane
/graphics,full         ! NOT PowerGraphics (fewer facets?)
pldispl,1


!To return to the main menu use the following command
! Set screen to show one front view in Window 1
/WIN,1,SQUA            ! Full square Window 1
/WIN,1,ON              ! Turn on  Window 1
/WIN,2,OFF             ! Turn off Window 2
/WIN,3,OFF             ! Turn off Window 3
/WIN,4,OFF             ! Turn off Window 4
/WIN,5,OFF             ! Turn off Window 5
/PLOPTS,INFO,1         ! Info on for right column
/PLOPTS,LEG2,0         ! Don't show the view information
/VIEW,1,0,0,1          ! Front (front elevation) view
/VUP,1,Y              ! Reference orientation
/TYPE,ALL,2            ! Centroidal sort, better print than Z-buffer
/CPLANE,0              ! Cutting plane
/graphics,full         ! Not PowerGraphics (fewer facets?)
pldispl,1
################################################################################
```

APPENDIX – C. DETAILED DRAWINGS

ALL DIMENSIONS IN MILLIMETERS

SCALE – 1: 2

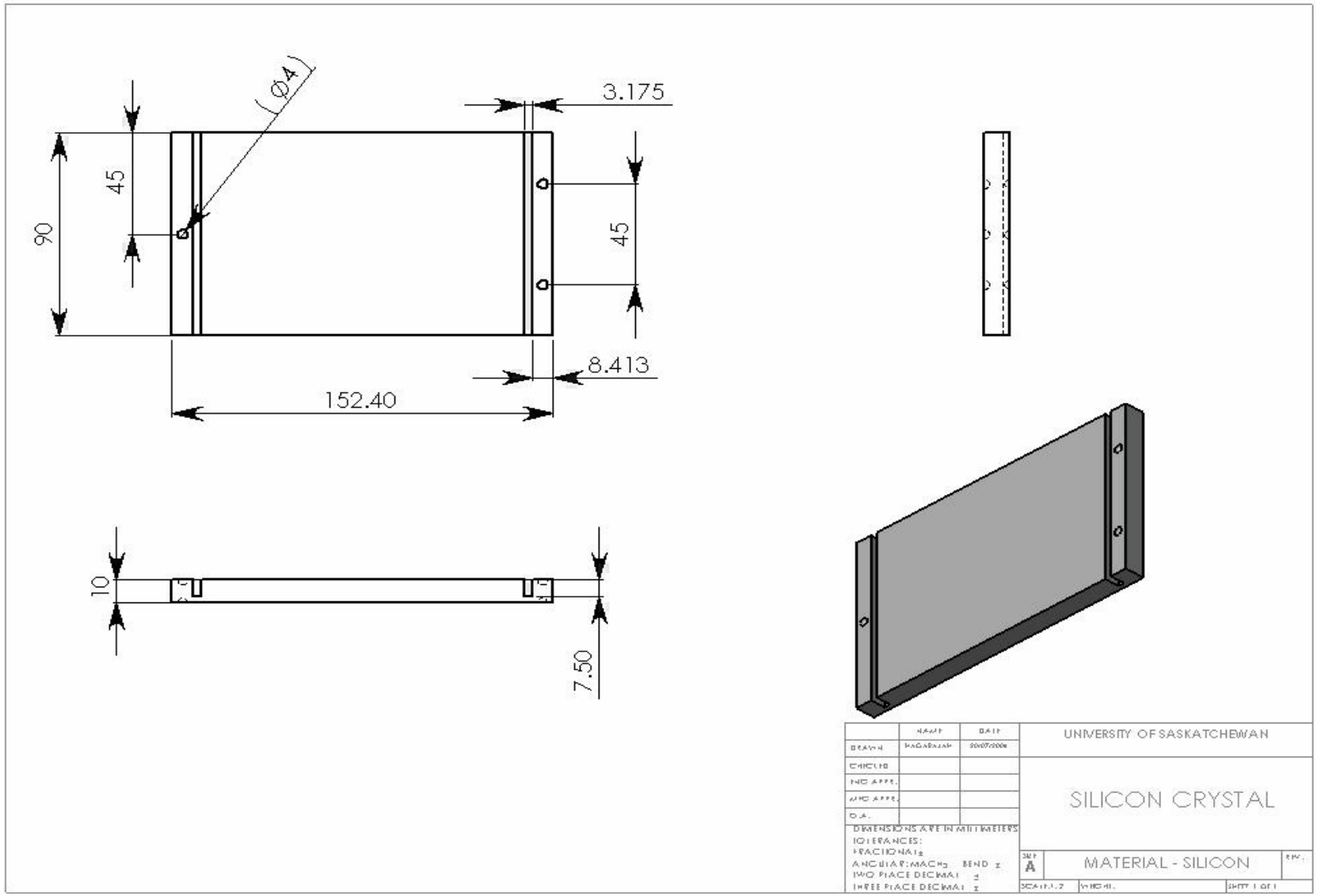

Figure – C.1 Silicon analyzer crystal

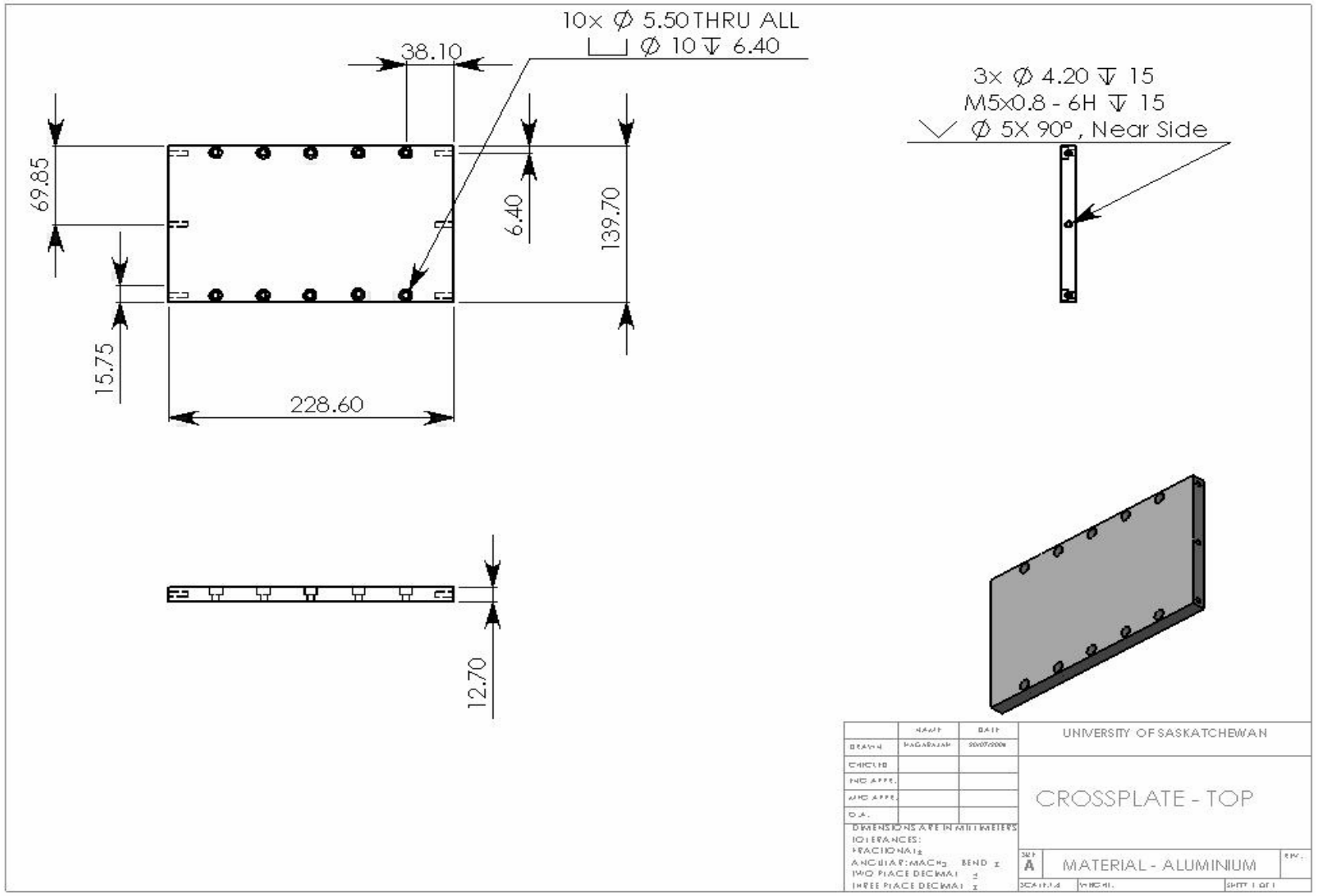

Figure – C.2 Cross plate (top)

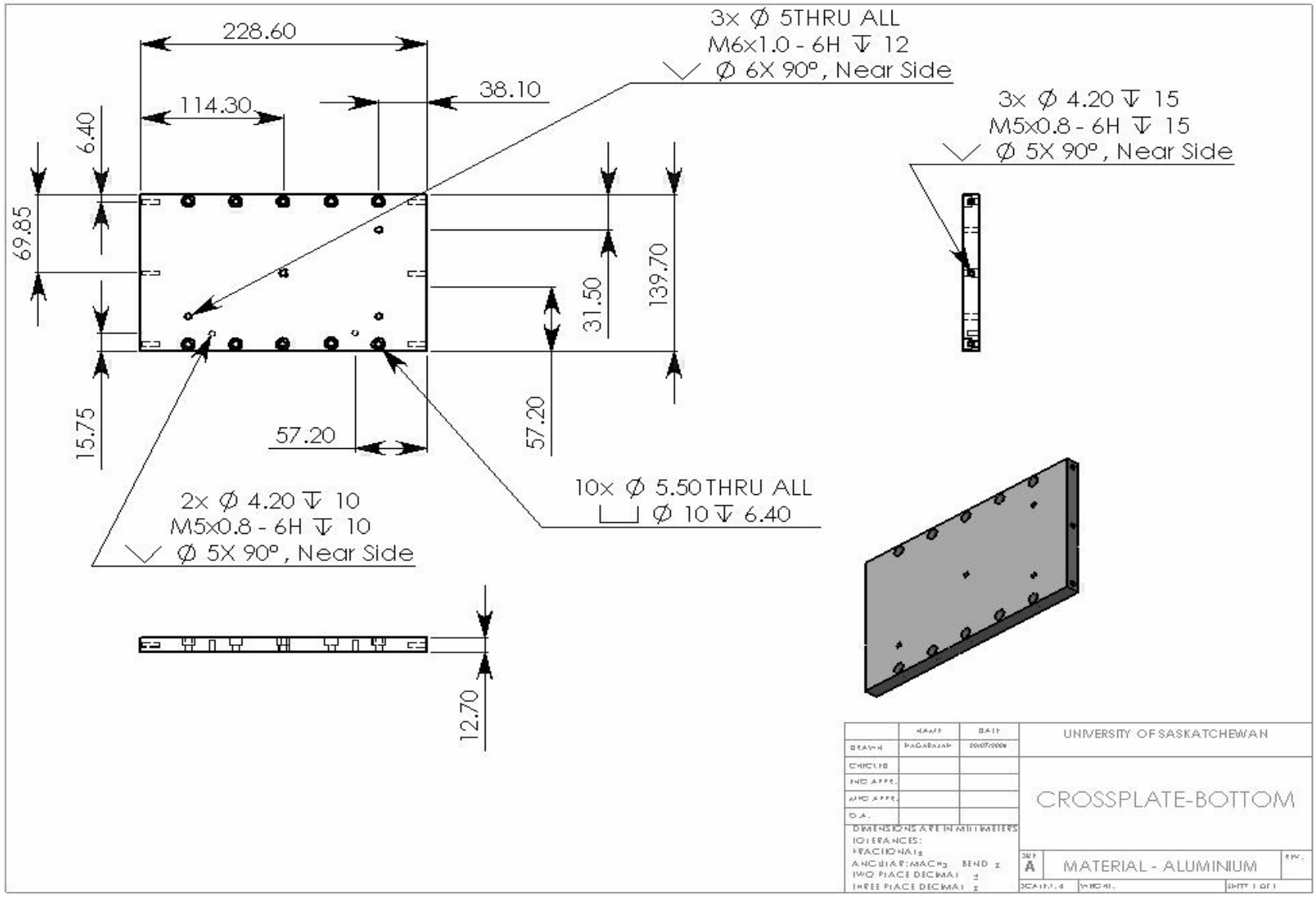

Figure – C.3 Cross plate (bottom)

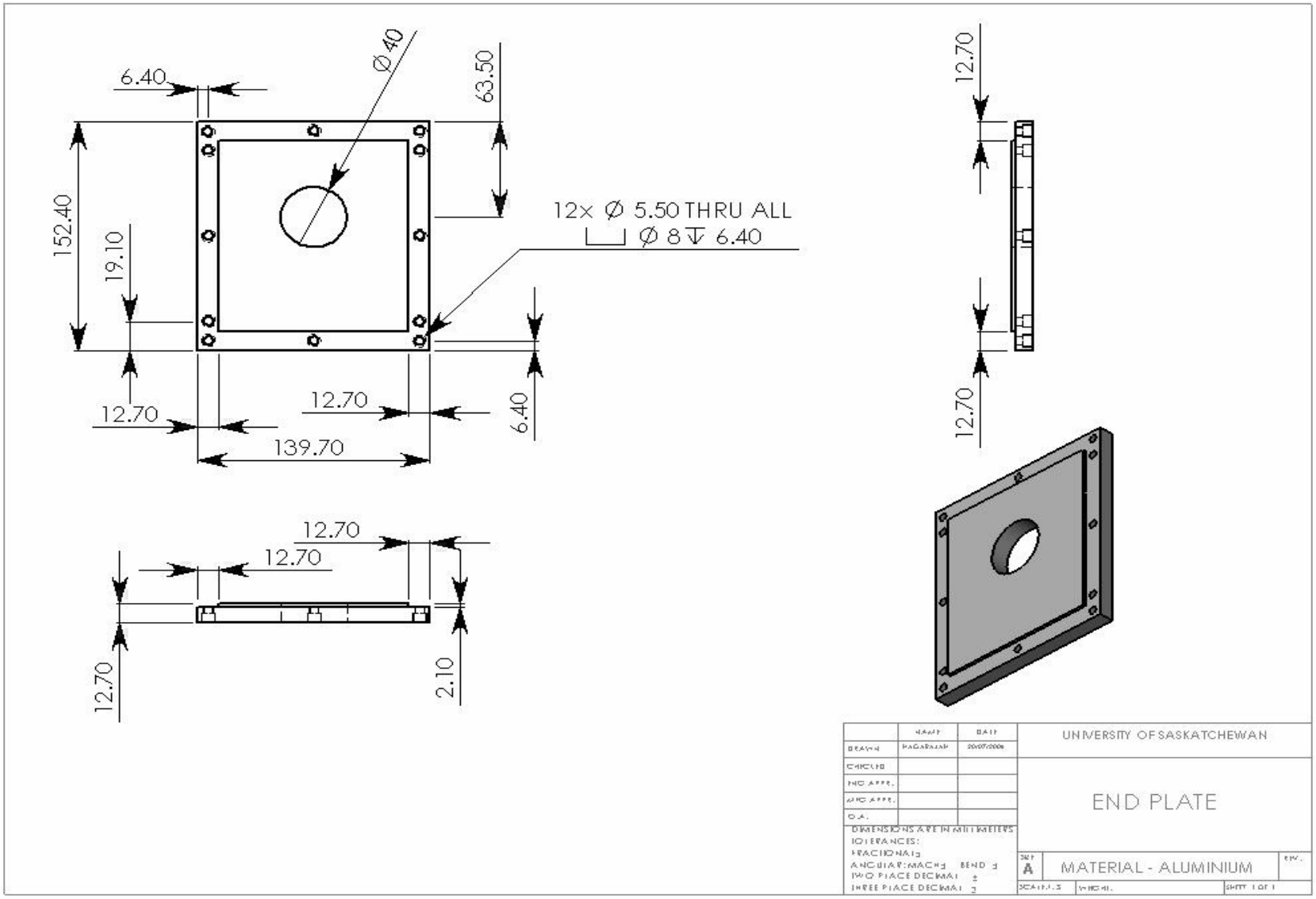

Figure – C.4 End plate

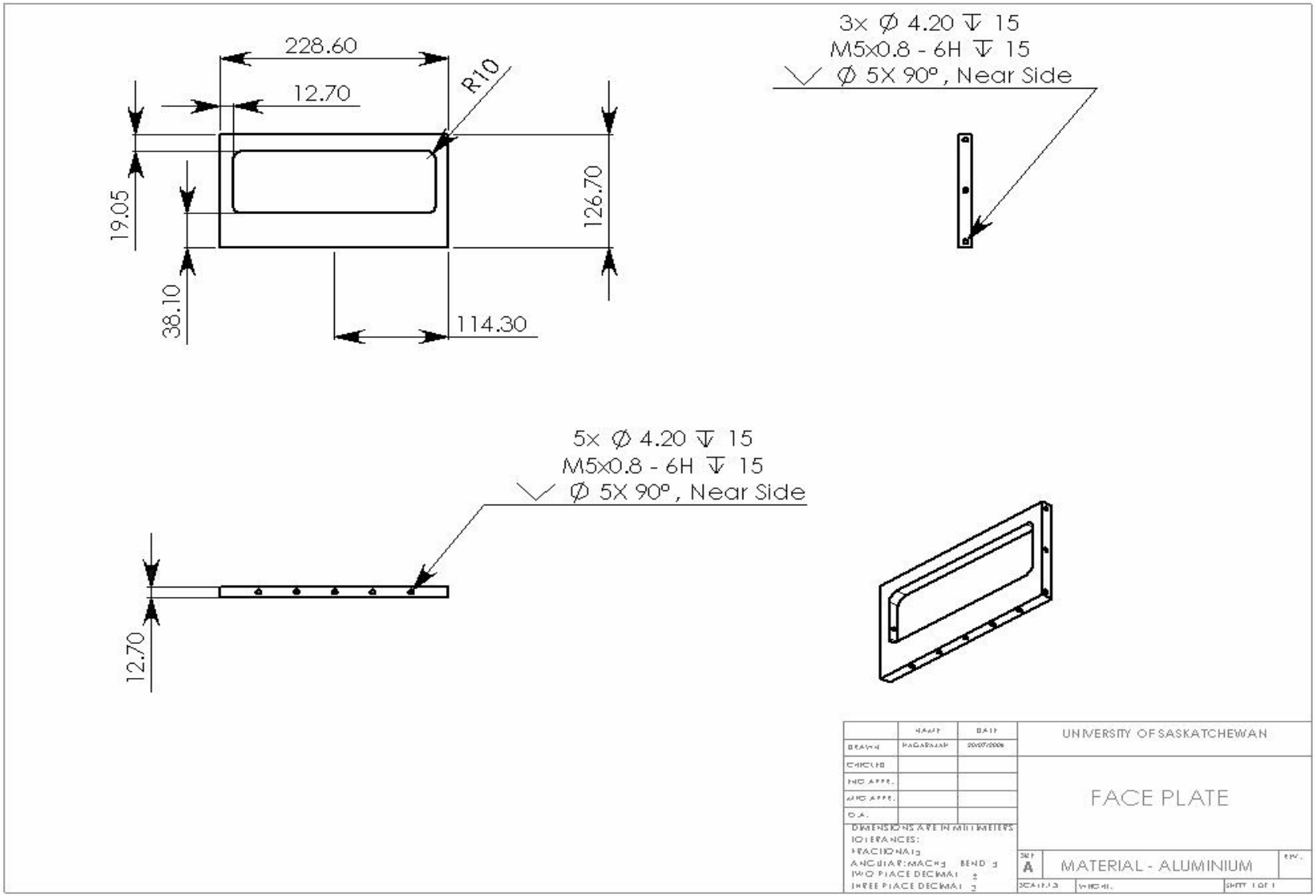

Figure – C.5 Face plate

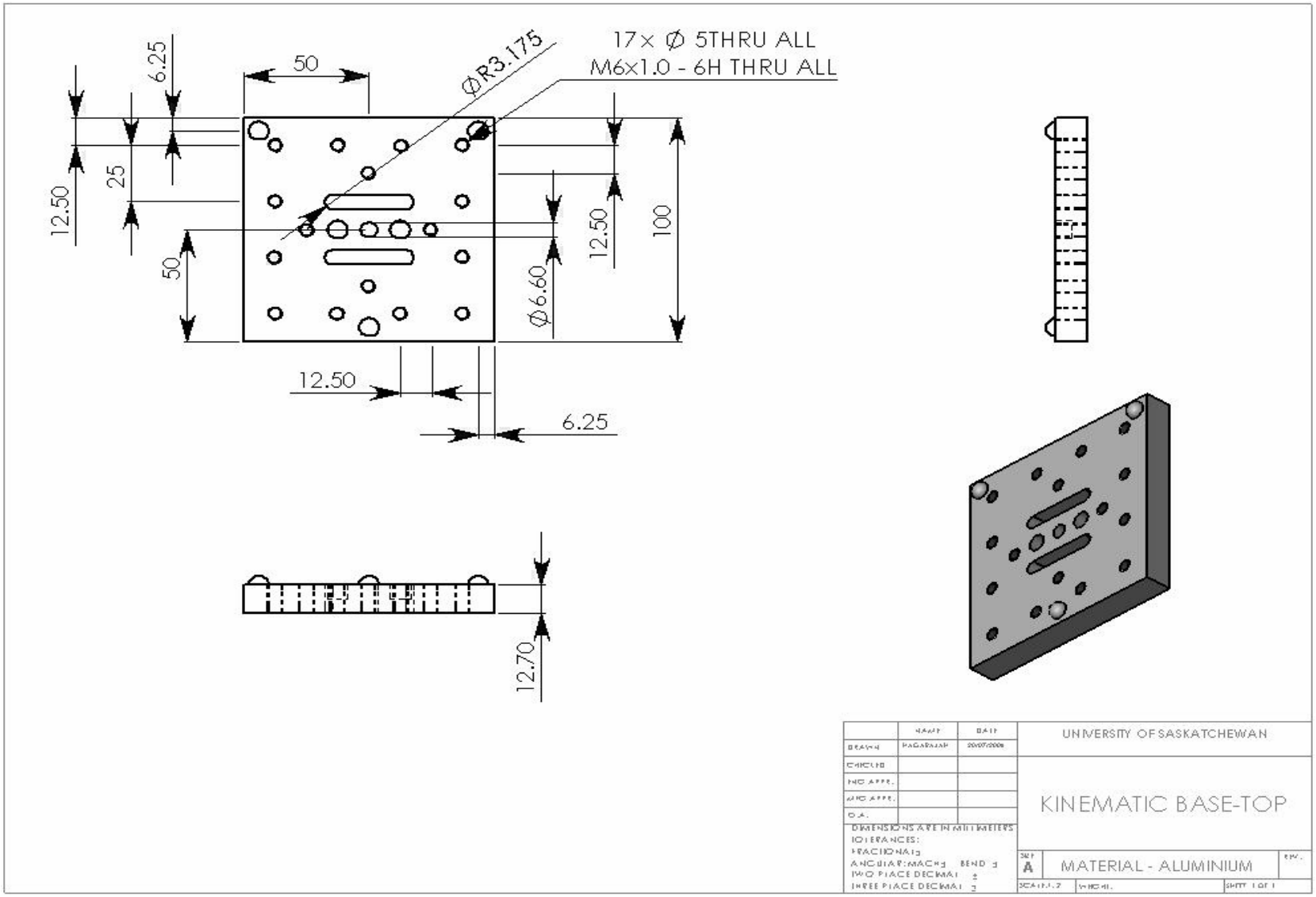

Figure – C.6 Magnetic kinematic base (top)

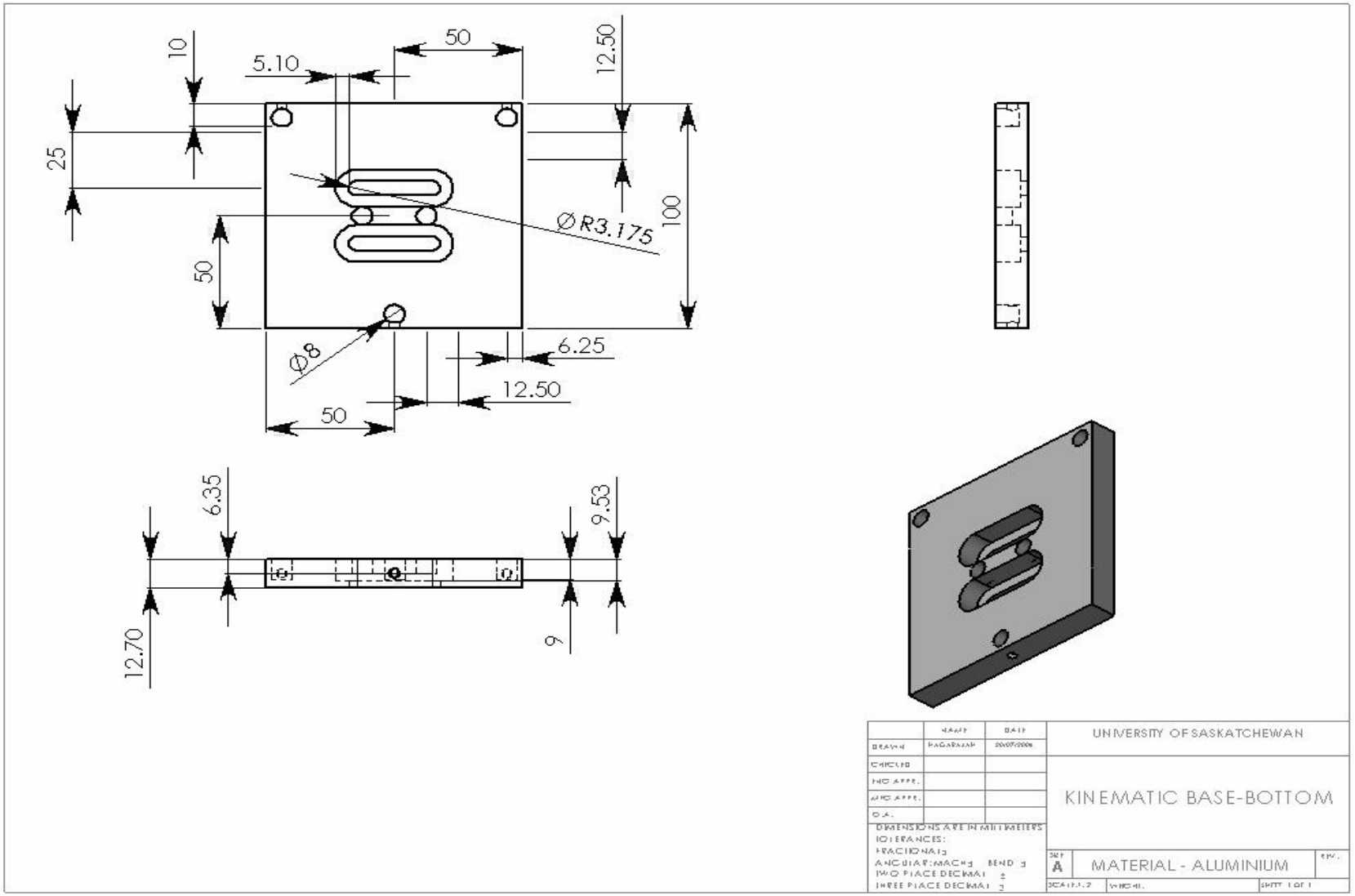

Figure – C.7 Magnetic kinematic base (bottom)

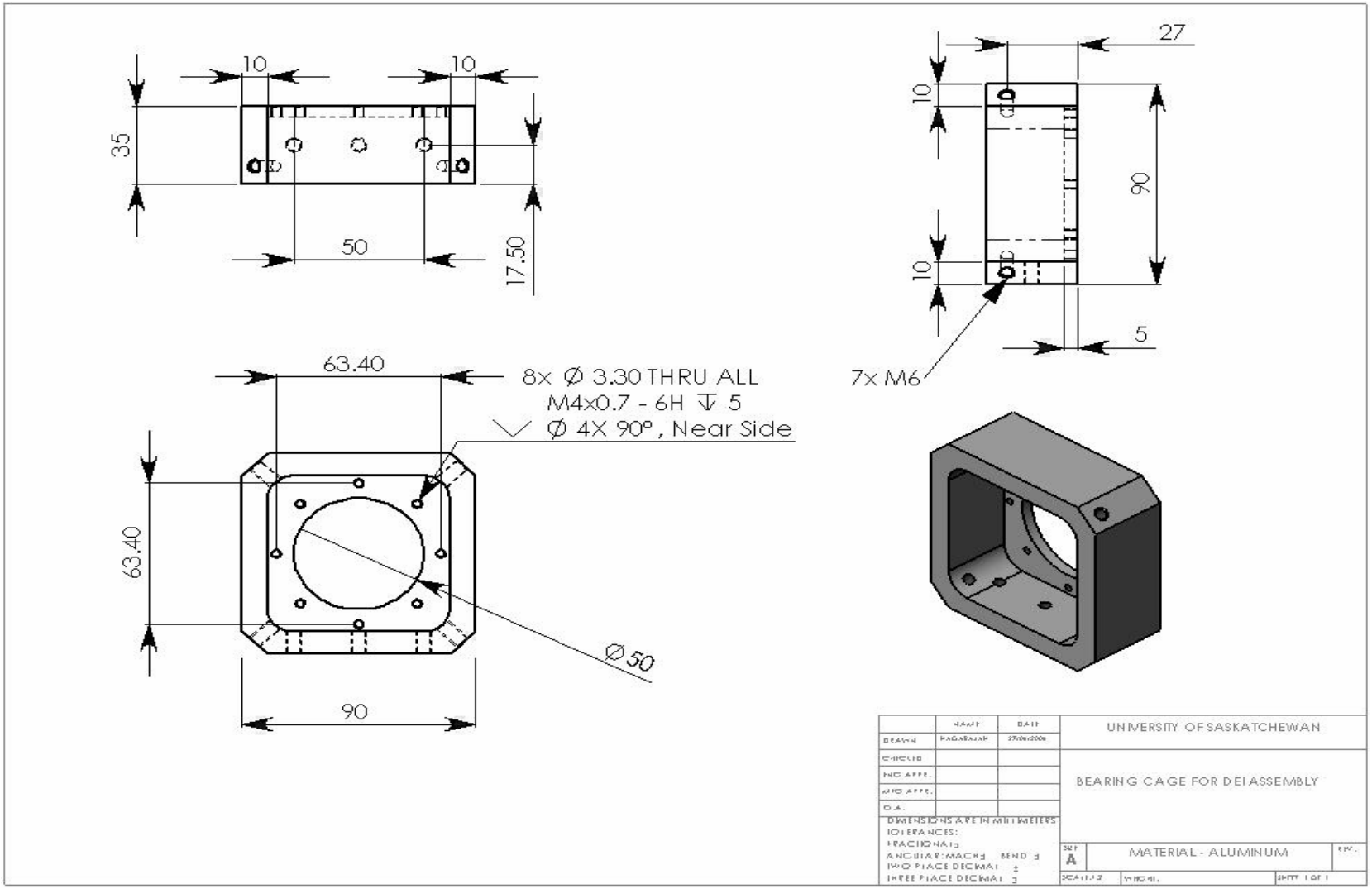

Figure – C.8 Bearing cage for DEI assembly

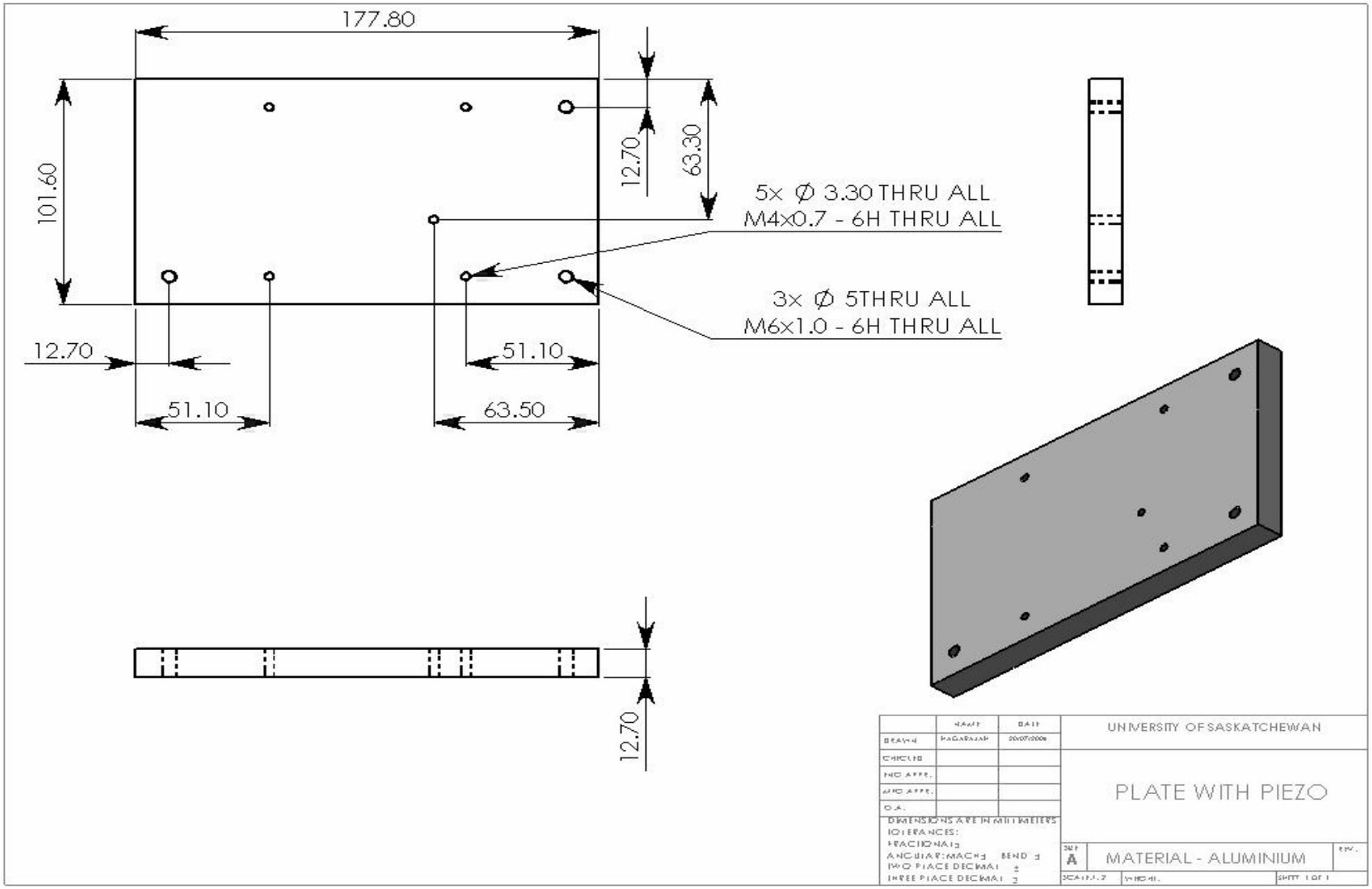

Figure – C.9 Plate with piezo-electric actuators

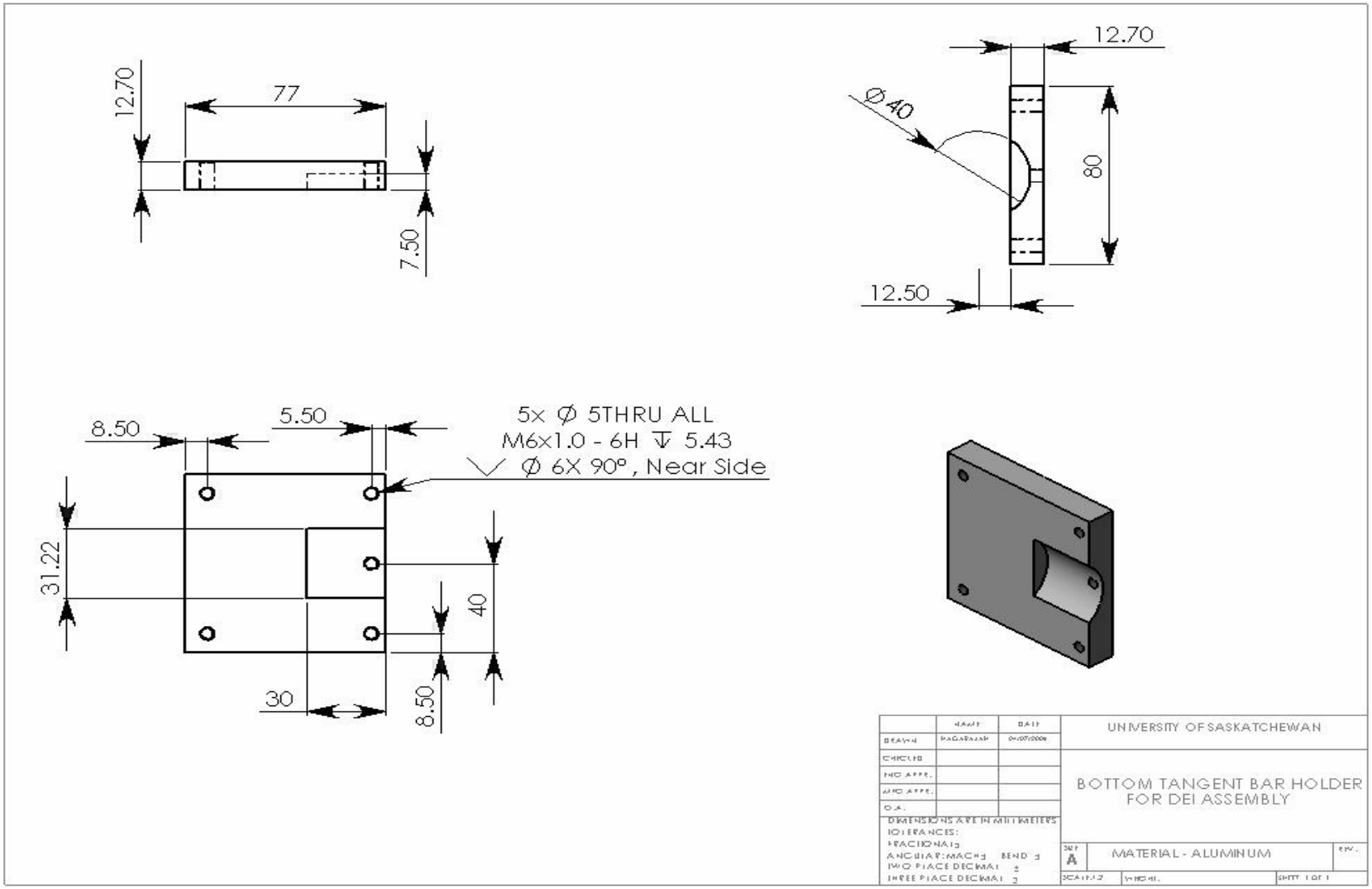

Figure – C.10 Bottom tangent bar holder for DEI assembly

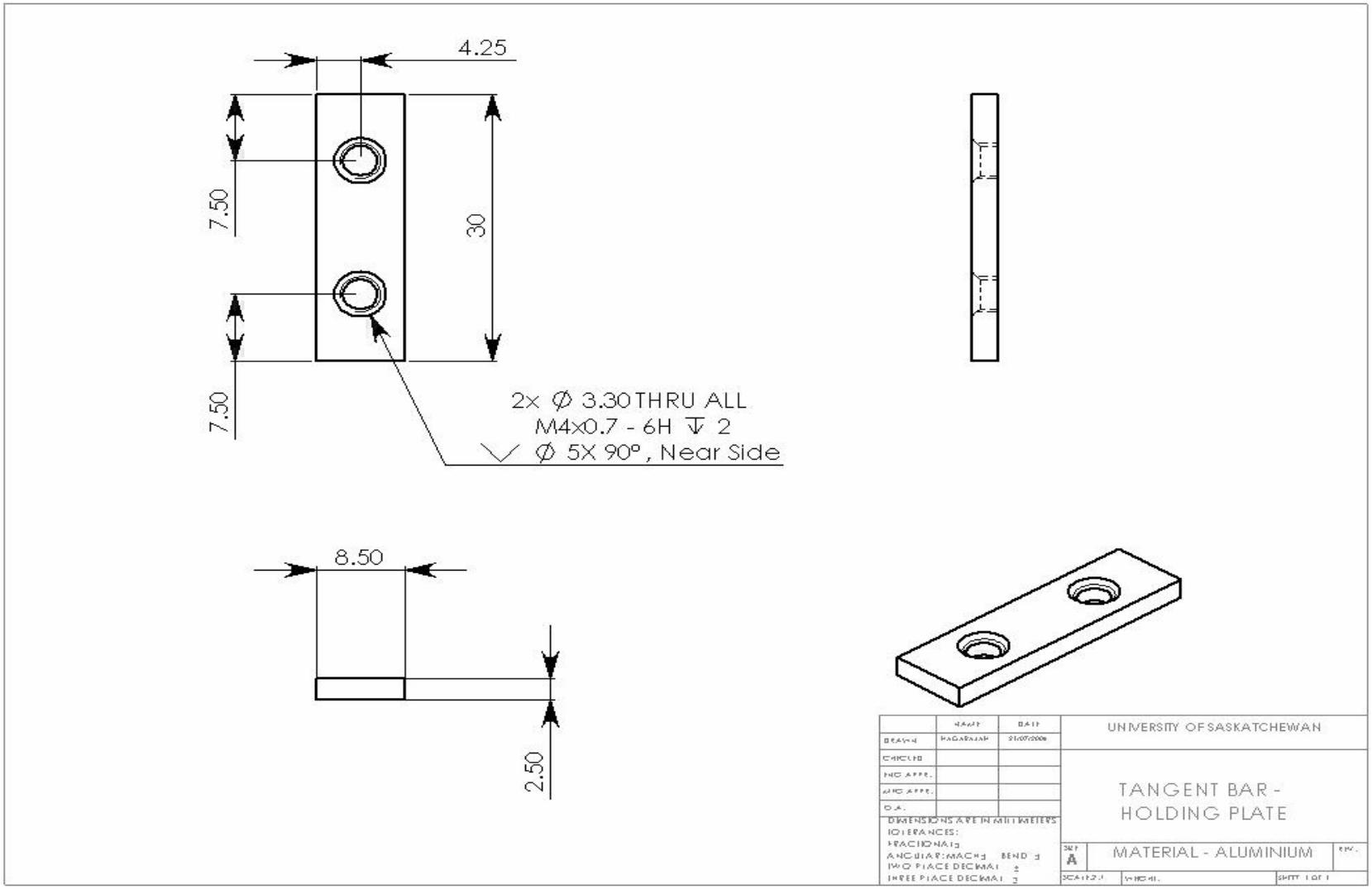

Figure – C.11 Tangent bar holding plate

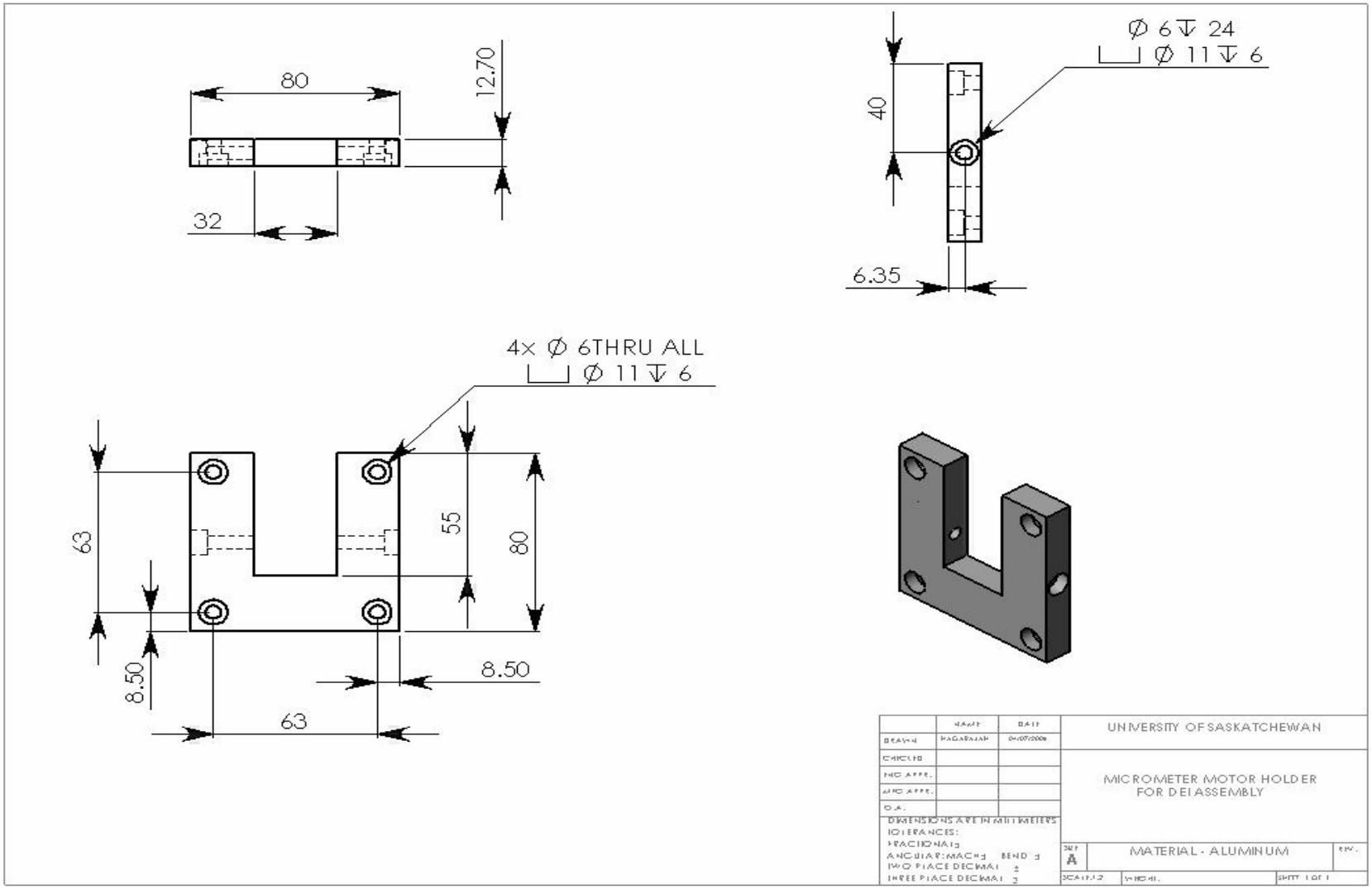

Figure – C.12 Motorized linear actuator holder

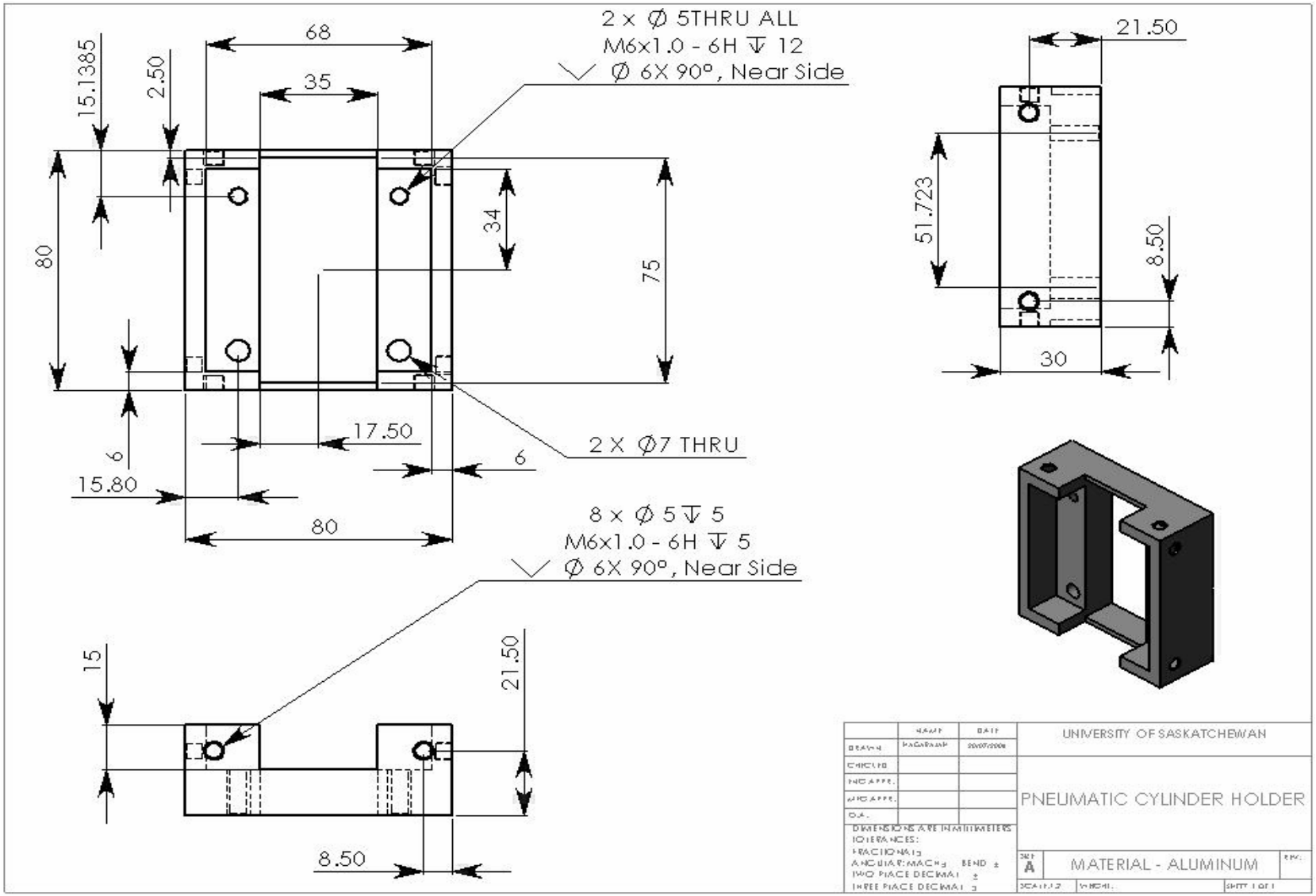

Figure – C.13 Pneumatic cylinder holder

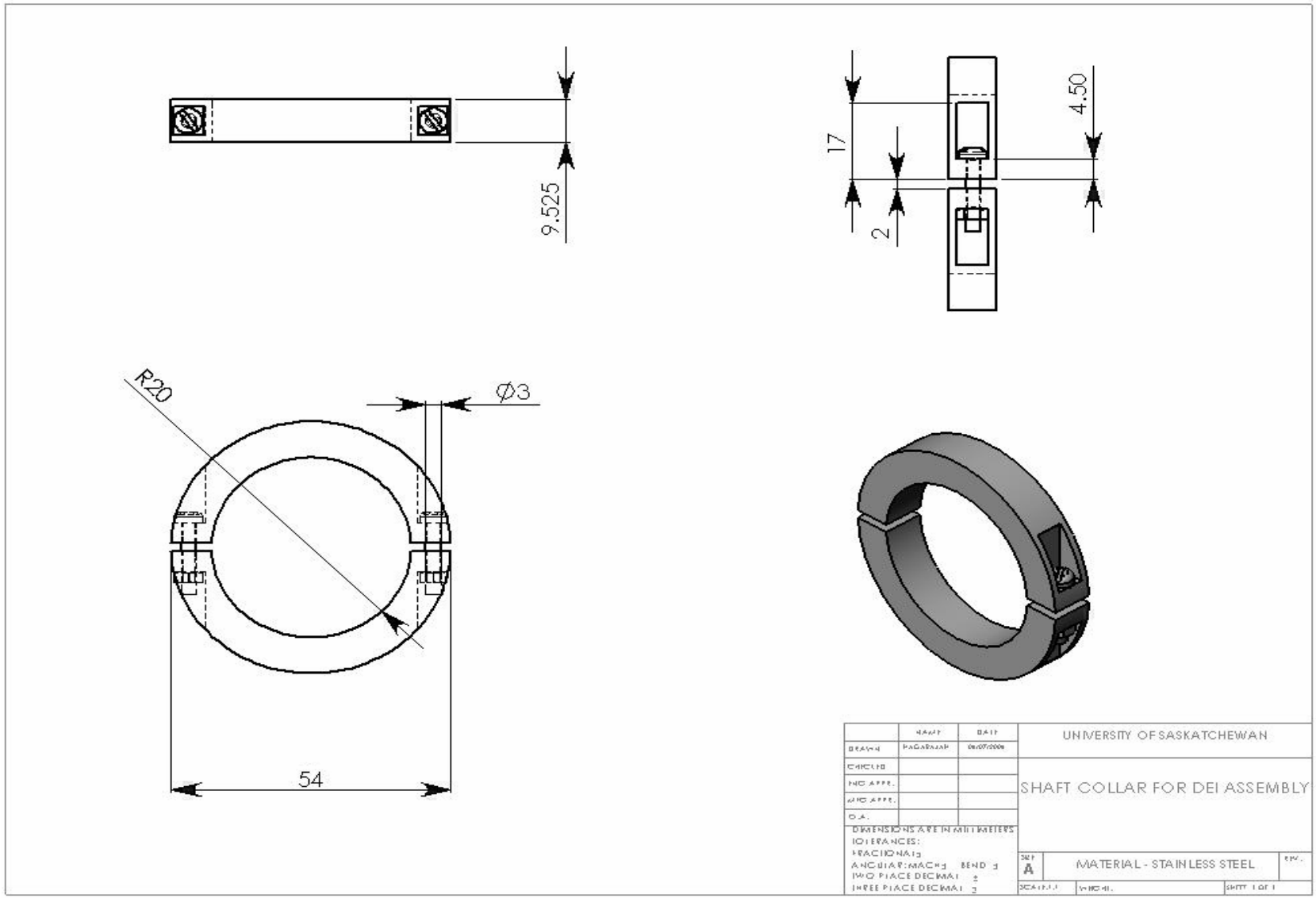

Figure – C.14 Shaft collar for DEI assembly

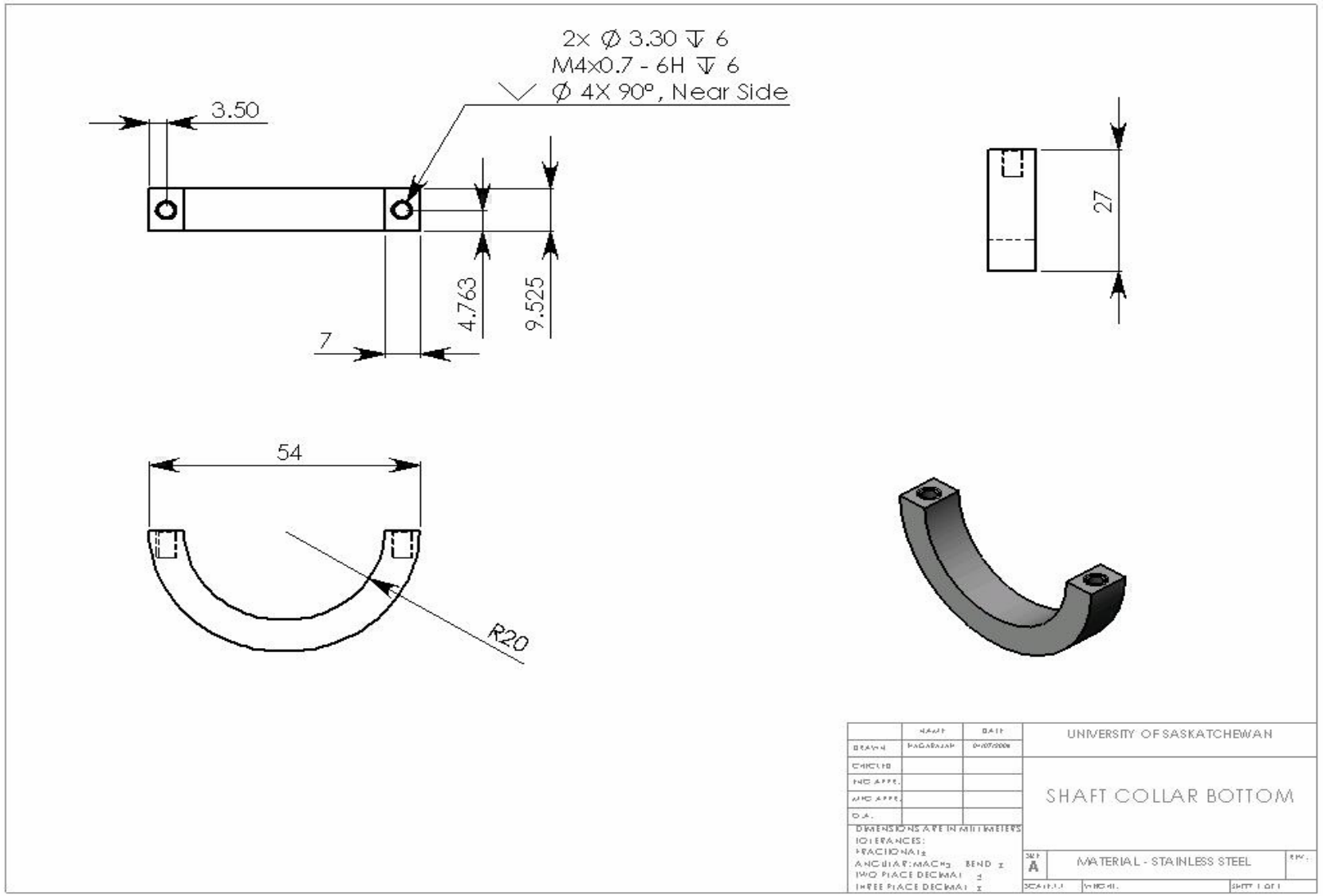

Figure – C.15 Shaft collar bottom

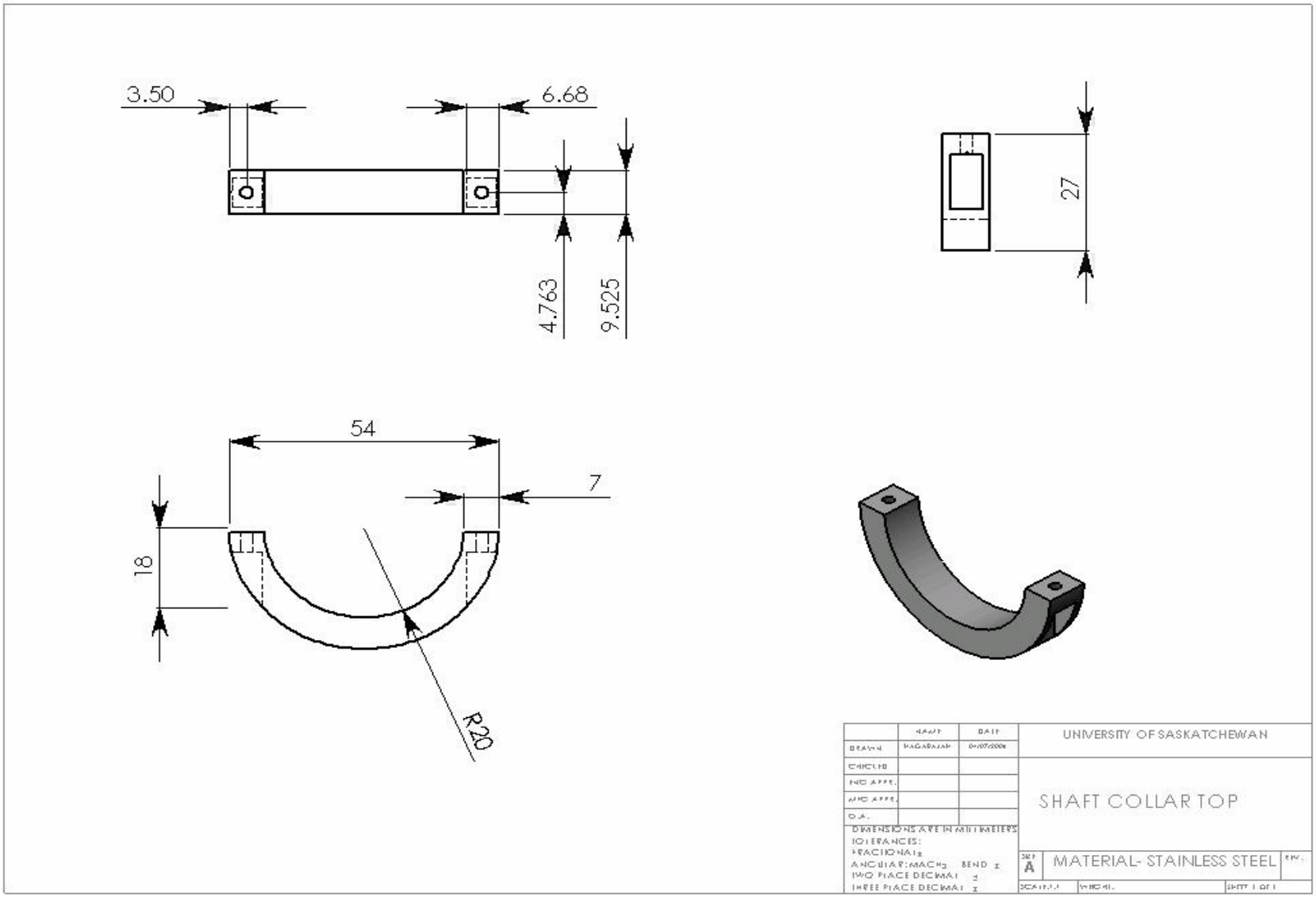

Figure – C.16 Shaft collar top

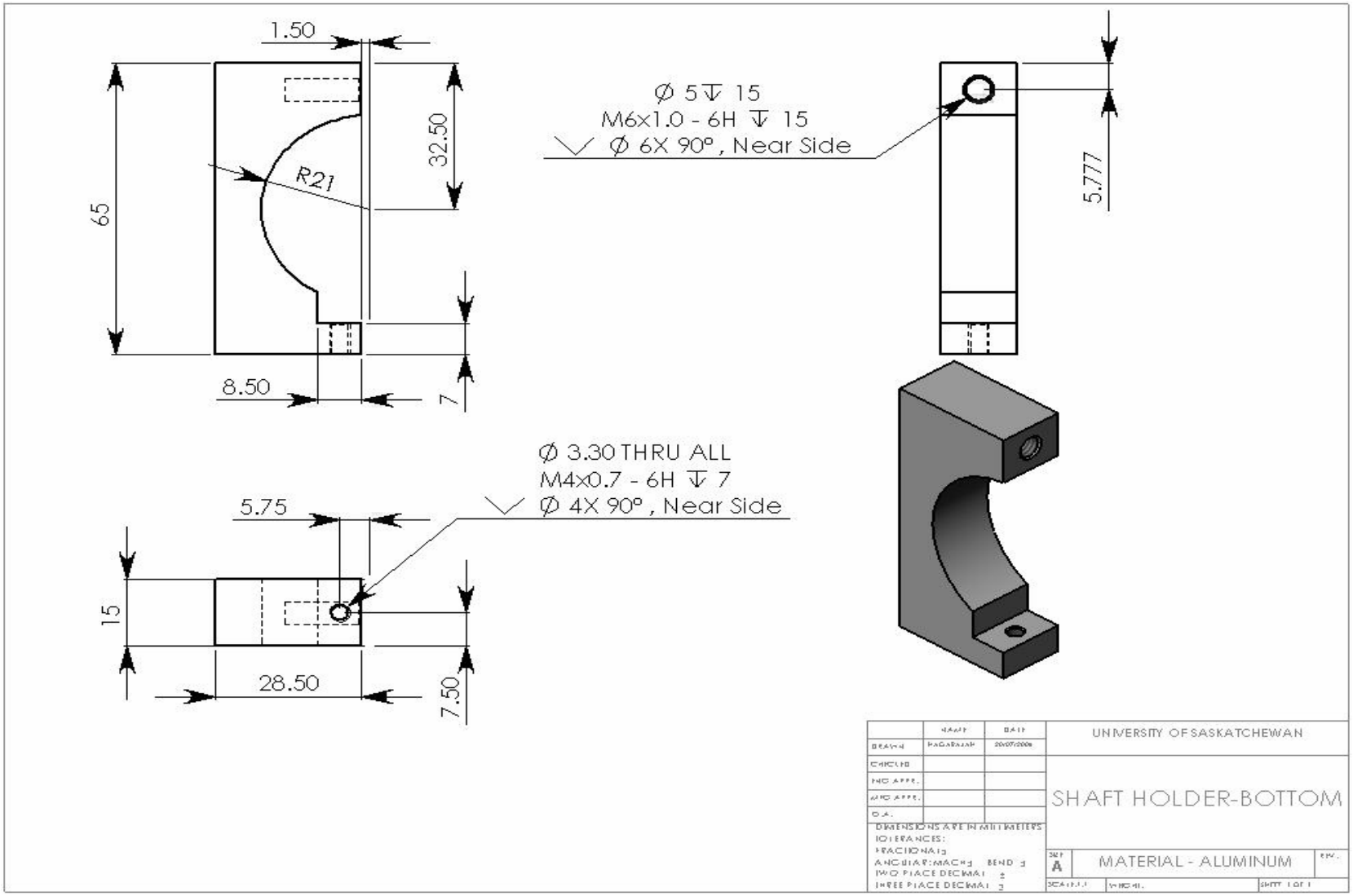

Figure – C.17 Shaft holder bottom

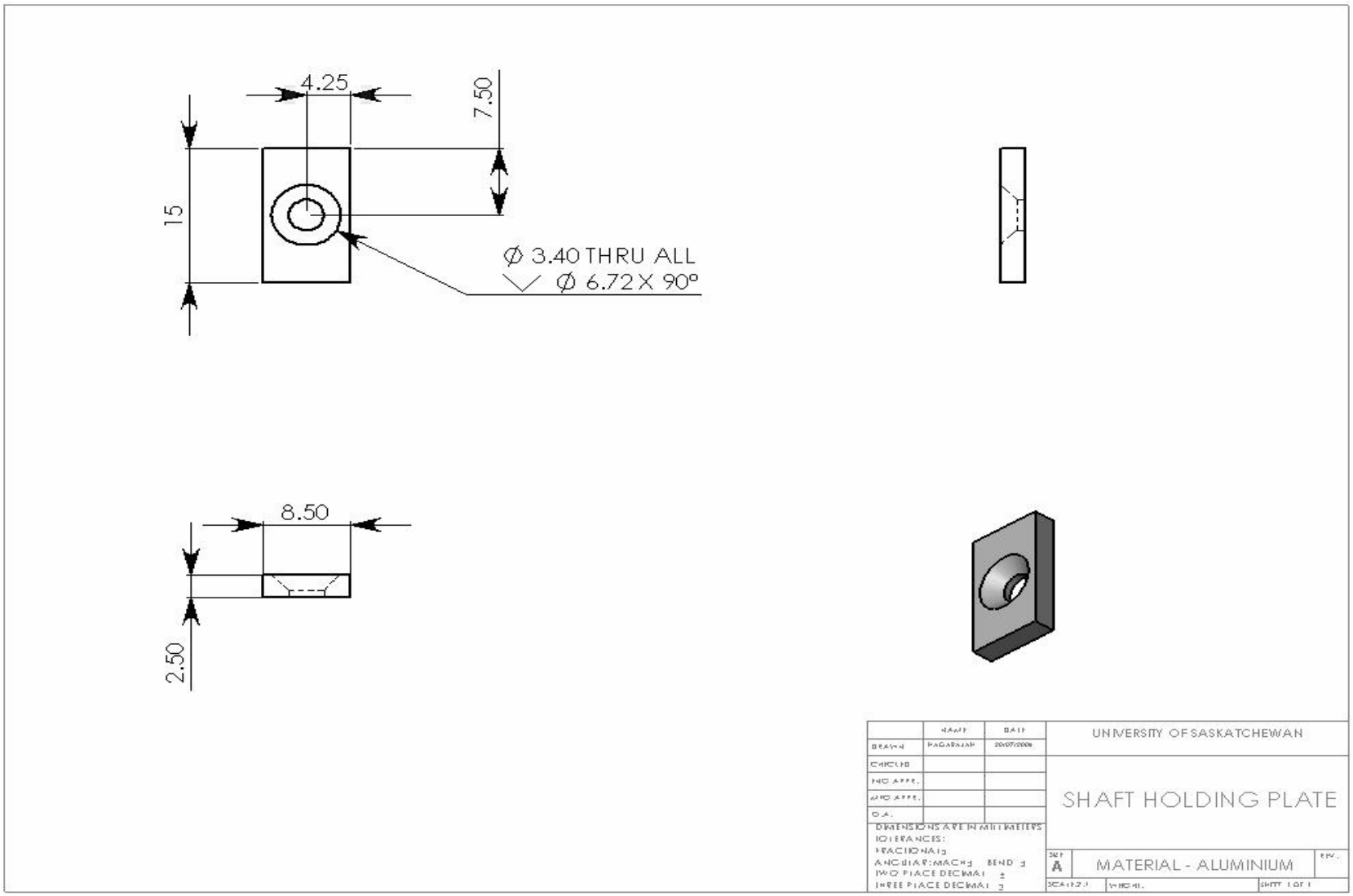

Figure – C.18 Shaft holding plate

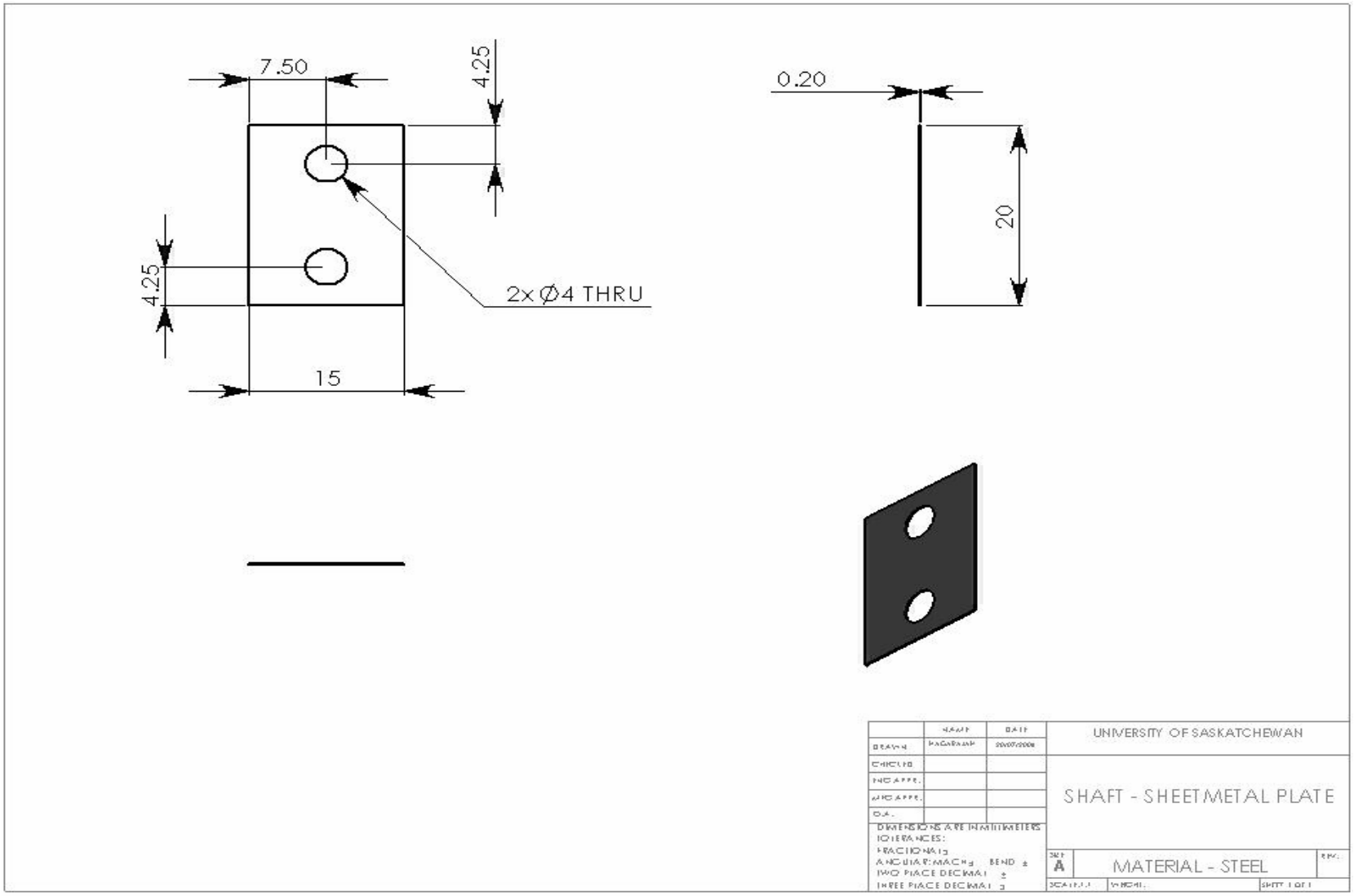

Figure – C.19 Sheet metal plate for shaft holder

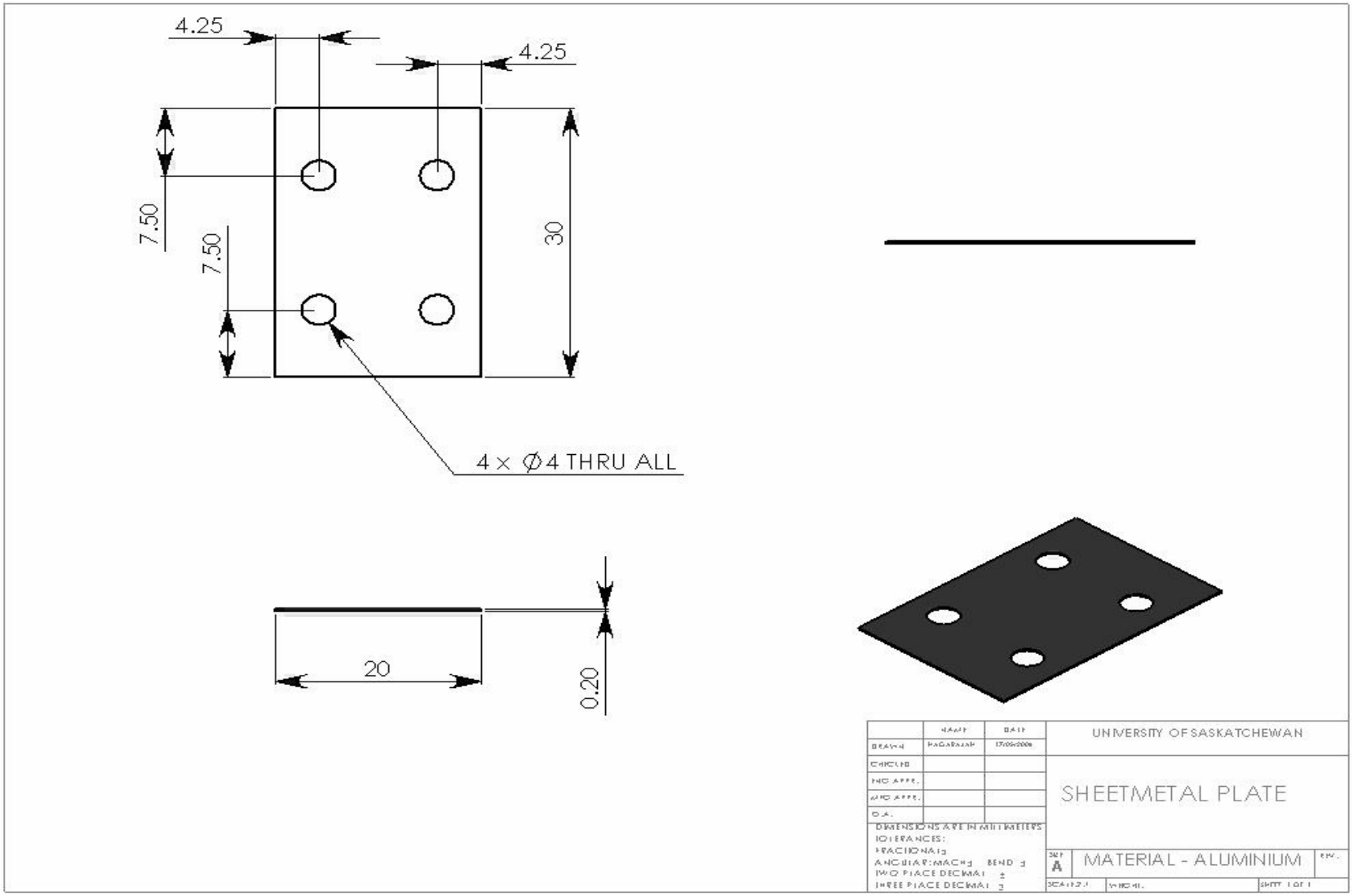

Figure – C.20 Sheet metal plate for tangent bar holder

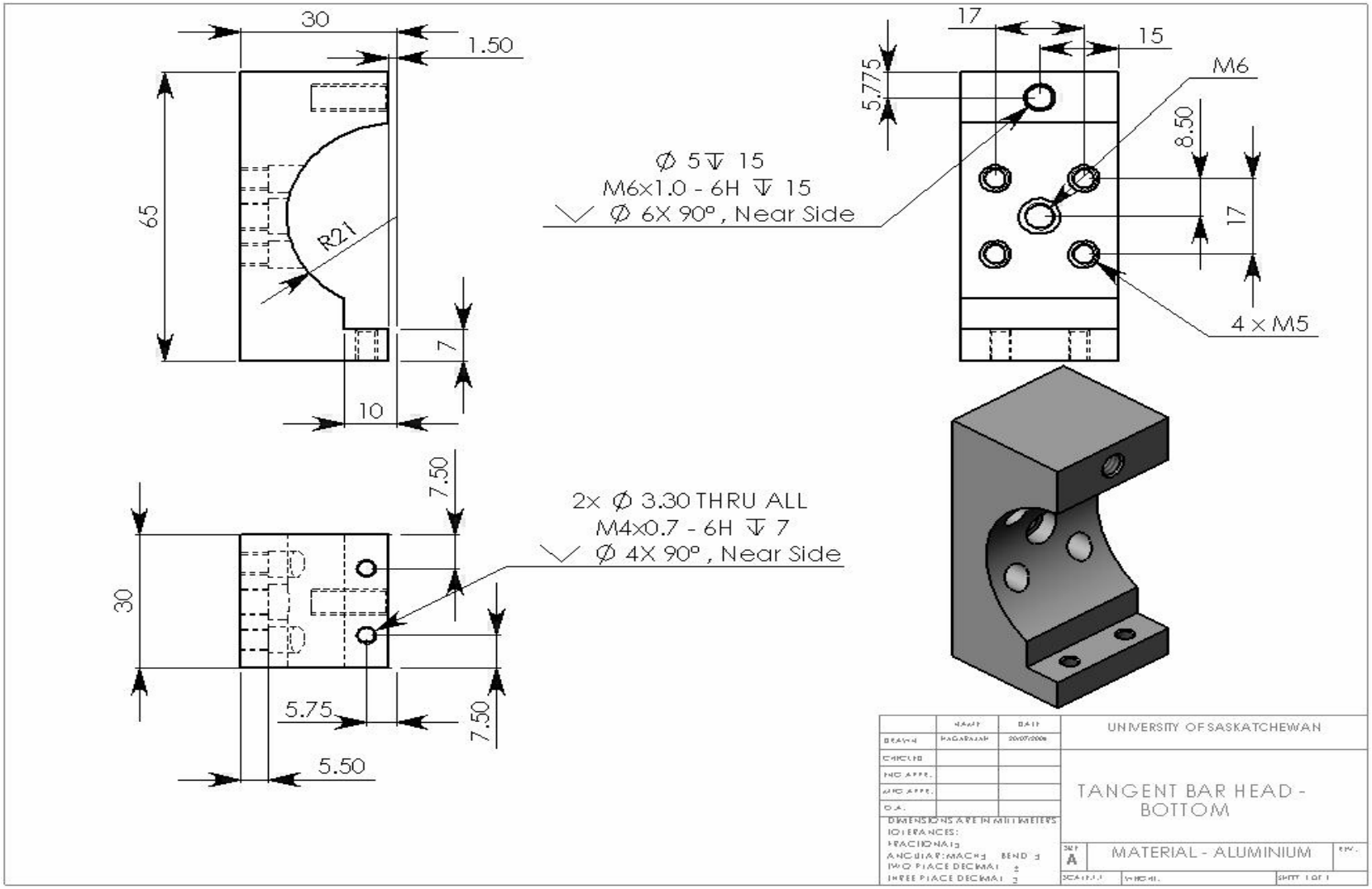

Figure – C.21 Tangent bar head (bottom)

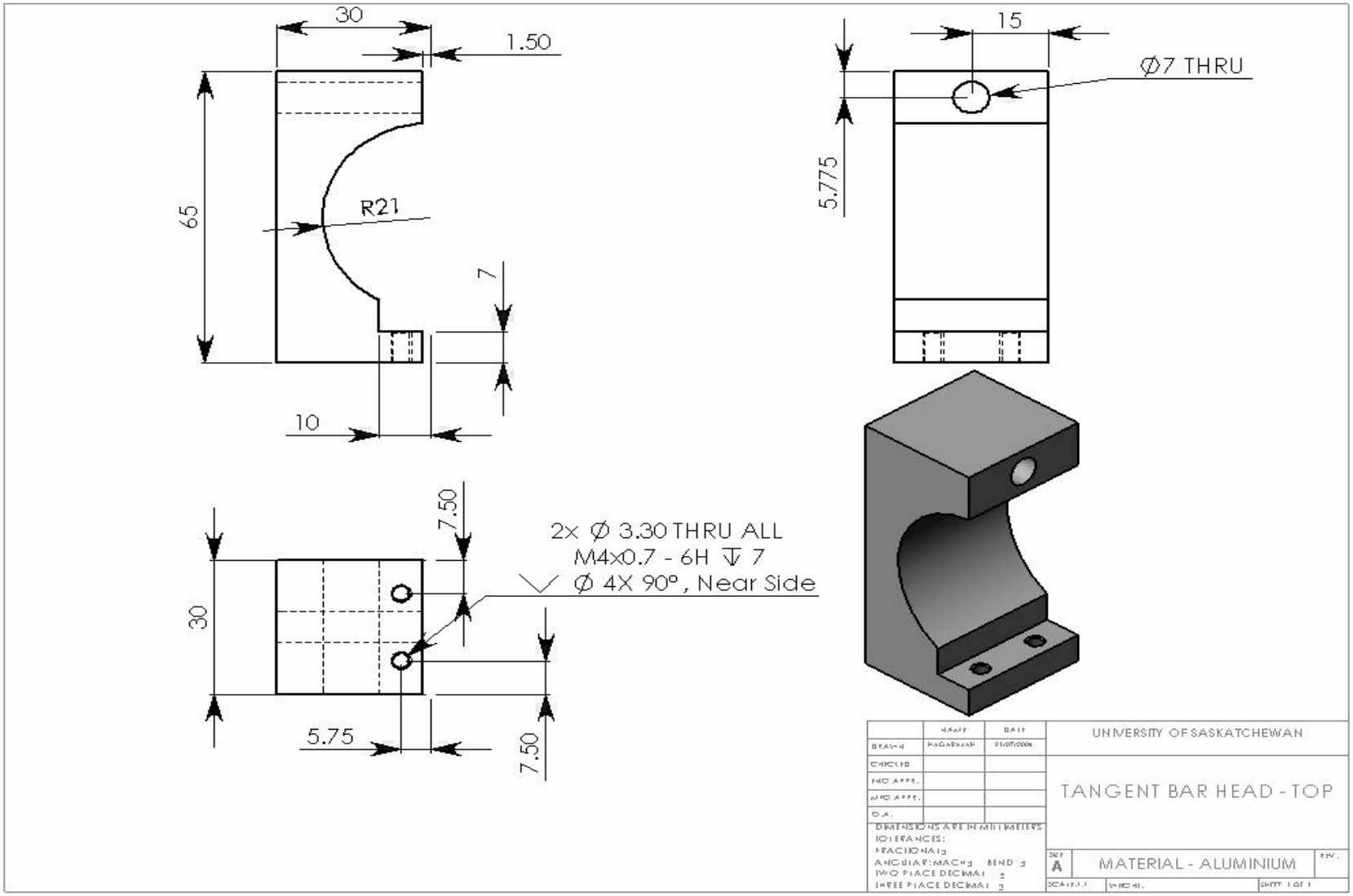

Figure – C.22 Tangent bar head (top)